EVALUATING THE CLIMATIC AND ENERGY BALANCE CONTROLS ON SNOW ACCUMULATION AND MELT IN MOUNTAIN SNOWPACKS

by

KEITH STEVEN JENNINGS

B.S., University of Vermont, 2005

M.S., Oregon State University, 2014

A dissertation submitted to the

Faculty of the Graduate School of the

University of Colorado in partial fulfillment

of the requirement for the degree of

Doctor of Philosophy

Department of Geography

2018

This dissertation entitled:

Evaluating the Climatic and Energy Balance Controls on Snow Accumulation and Melt in Mountain Snowpacks

written by Keith Steven Jennings

has been approved for the Department of Geography

_____

Dr. Noah Molotch, committee chair

_____

Dr. Peter Blanken

_____

Dr. Ben Livneh

_____

Dr. Mark Raleigh

_____

Dr. Thomas Painter

Date_____

The final copy of this dissertation has been examined by the signatories, and we find that both the content and the form meet acceptable presentation standards of scholarly work in the above mentioned discipline.

Jennings, Keith Steven (PhD, Geography)

Evaluating the Climatic and Energy Balance Controls on Snow Accumulation and Melt in Mountain Snowpacks

Dissertation directed by Associate Professor Noah Molotch

Abstract

Snow is indispensible to the water resources and economy of the western United States, making it essential to accurately predict snowmelt volume, timing, and rate. However, uncertainties in snowpack processes, the effects of climate change, and spatial variability in precipitation phase partitioning all complicate efforts to simulate snow accumulation and melt. With those three issues in mind, this work clarifies seasonal snow cover evolution in a changing climate by utilizing ground observations and validated output from a physics-based snow model.

The first project focuses on how snowpacks develop cold content, the internal energy deficit that must be satisfied before snowmelt can begin. Previously it was unknown whether cold content developed primarily through meteorological or energy balance processes. Using snow pit data and model output, I show that new snowfall exerts the primary control on cold content development in the snowpacks at an alpine and subalpine site in the Colorado Rocky Mountains. Additionally, model output indicates that cold content damps snowmelt rate and delays snowmelt onset at time scales one month and shorter, but has little correlation to those quantities at seasonal time scales.

The second project evaluates the physical processes controlling the response of the alpine and subalpine snowpacks to increases in air temperature and changes to precipitation total and seasonality. The increased sensitivity of the subalpine snowpack to climate warming is primarily a result of decreases to snowpack cold content and increases in positive energy fluxes. As opposed to the differential response to warming, the two snowpacks exhibited fairly consistent

responses to changes in total precipitation with later melt onset and faster snowmelt rates being associated with increased precipitation. Changes to precipitation seasonality had a near-negligible impact on snow cover properties at both sites.

The final project expands on the spatial scope of the first two by simulating snow accumulation and melt at sites in the western United States that span a climatic gradient from warm maritime to cold continental. Previous research had shown spatial variability in rain-snow partitioning, but little was known about how this variability affected snow model simulations. The results from this project indicate that the selection of a method to partition rain and snow leads to the greatest divergence in seasonal snow cover evolution at the lower elevation maritime sites. Peak snow water equivalent and snowmelt timing simulated by the different methods varied by several hundred millimeters and over one month, respectively, at the warmest sites, and typically less than 20 mm and one week at the two coldest sites. Overall, this dissertation highlights how snow models and ground observations can be used to better understand snow accumulation and melt processes in a changing climate.

Acknowledgments

In 2011 I told the woman who would become my wife that I wanted to go back to school. I don't think either of us expected that decision to turn into a 6-year journey from North Carolina to Oregon to Colorado. No matter what has happened, Marley has been by my side and I will be forever grateful to her. Without her there'd be no dissertation and no degree. Most importantly, there'd be no Oscar Fox, the most wonderful little human anyone could hope to call their son.

I am also inexpressibly thankful for my parents who have done everything in their power (for 33 years now) to support and encourage me. Whether I was bike racing in Europe or going back to school, I knew that they would be there for me no matter the outcome.

No dissertation would be possible without an advisor and I've been lucky to call Noah Molotch just that. Of the many sacrifices he's made for his students, perhaps none has been so great as reading this document with a single space after each period instead of his preferred two.

I am also thankful for my committee: Ben Livneh, Mark Raleigh, Tom Painter, and Peter Blanken. You have invested countless hours into my studies and helped me take my admittedly rough ideas and turn them into something useful.

I'm indebted to the Mountain Hydrology Group, as well. The group's camaraderie was a big reason why I came to CU Boulder. There have been some miserable days in the field and some brilliant ones. No matter the weather, we've been there for one another.

I'm also a big proponent of having friends outside of the academic sphere and I have been blessed by having the unwavering support of some of the most compassionate and interesting people in Boulder, some of whom I have known for over 15 years now. There is no problem a bike ride with your best friends in the mountains can't solve.

Contents

Tables

Figures

Chapter 1

1 Introduction

1.1 Motivation

Snowmelt serves as a critical water resource for nearly 2 billion people globally (Barnett et al., 2005; Mankin et al., 2015). Mountain snowpacks function as *in situ* reservoirs, storing water during the winter months when human and environmental demand are low and then releasing it in spring and summer as demand increases (Viviroli et al., 2007). In the western United States, greater than 50% of streamflow in a given year is derived from mountain snowmelt (Li et al., 2017; United States Geological Survey, 2005), providing approximately 60 million people with the water they need for domestic use, irrigated agriculture, and industrial purposes (Bales et al., 2006). In financial terms, snow provides more than a $1 trillion benefit to the economy of the western United States through its streamflow, reservoir, and recreation services (Sturm et al., 2017).

In addition to satisfying human demand, snow serves a myriad of other hydrologic, ecologic, cryospheric, and climatic roles. From the beginning of the snow accumulation season in the fall and winter, through the melt period in spring and summer, snow fundamentally alters its surroundings. For one, snow cover is an efficient insulator, keeping the ground temperature warmer than it would be in the absence of snow (Groffman et al., 2001). In general, the insulating properties of snow reach a maximum at a snow depth near 50 cm (Slater et al., 2017), below which diurnal soil temperature ranges are typically low (Burns et al., 2014; Jennings et al., 2018a). Snow cover therefore affects microbial respiration rates as well as carbon dioxide fluxes from the land surface to the atmosphere (Blanken et al., 2009; Brooks and Williams, 1999; Monson et al., 2006). Snow cover also exerts a strong control on land surface albedo given its

high reflectivity relative to that of bare ground. In this context, seasonal snow cover at the mid- and high-latitudes influences the global climate system by reflecting a high proportion of incoming solar radiation to space (Flanner et al., 2011; Groisman et al., 1994).

As the snow season progresses towards spring and summer, insolation increases and air temperature warms, the snow cover evolves and snowmelt begins. The onset of snowmelt is associated with increases in soil moisture (Harpold and Molotch, 2015) as well as with the uptake of carbon by vegetation (Blanken et al., 2009; Winchell et al., 2016) and landscape greening (Knowles et al., 2018; Trujillo et al., 2012). The spring snowmelt pulse also drives increases in streamflow (Cayan and Peterson, 1989), shaping the annual hydrograph and peak flow timing in snow-dominated basins (Berghuijs et al., 2016). In turn, both aquatic fauna and streamside vegetation are adapted to the annual snowmelt freshet (Lytle and Poff, 2004). Thus, the availability of meltwater in terms of both timing and volume are critical to humans, ecosystems, and global hydroclimate.

1.2 General background material

The rate and timing of snowmelt are controlled by the snowpack energy balance. Throughout this dissertation, it will take the following form:

$$\frac{dU}{dt} + Q_M = Q_{SW} + Q_{LW} + Q_H + Q_{LE} + Q_G + Q_R \qquad (1.1)$$

where $\frac{dU}{dt}$ is the simulated rate of change in internal snowpack energy, Q_M is the energy available for melt once the snowpack becomes isothermal, Q_{SW} is net shortwave radiation, Q_{LW} is net longwave radiation, Q_H is sensible heat flux, Q_{LE} is latent heat flux, Q_G is ground heat flux, and Q_R is the heat advected by precipitation (all W m^{-2}). Together, Q_{SW} and Q_{LW} comprise the radiative fluxes, while Q_H and Q_{LE} represent the turbulent fluxes. Fluxes are positive when they

are directed towards the snowpack (i.e., the snowpack's internal temperature rises) and negative when they are directed away from the snowpack (i.e., the snowpack's internal temperature decreases).

In order to simulate seasonal snow cover evolution, computer models use various formulations and abstractions of the snowpack energy balance. This ranges from simple temperature index models where air temperature is used as a proxy for the radiative fluxes, to complex, physics-based snow models that provide a full treatment of the snowpack energy balance. While temperature index models can accurately simulate snow water equivalent, model parameters (e.g., the degree day factor that relates air temperature to melt) are often not transferrable in space and time (Hock, 2003). Thus, such models are often calibrated for a specific location and time of year and offer limited information about physical snowpack processes. To that end, more advanced models leverage known physical relationships that are transferrable in space and time. That means well validated physics-based models can be used to evaluate snowpack processes in different areas, a changing climate, and throughout the snow cover season.

However, despite their considerable utility, physics-based models are not without their drawbacks. Although models that better represent physical processes typically outperform simplified models, model comparison work consistently shows that no model performs best in all locations at all times (Essery et al., 2013; Etchevers et al., 2004; Rutter et al., 2009). In addition to the uncertainty introduced by model structure and physics, errors in forcing data can cause divergence in simulated snow cover evolution (Lapo et al., 2015; Raleigh et al., 2016, 2015). In that context, it is essential to have proper validation data for various snow cover properties. For example, Lapo et al. (2015) showed that modeled snow water equivalent (SWE) and energy

balance partitioning between the turbulent and radiative fluxes are improved when validation is performed on more than one snow cover metric. Thus, it is essential that model physics accurately represent snowpack processes, that meteorological observations be quality controlled, and that model output be validated to the greatest extent possible.

1.3 Project introductions

The three projects within this dissertation utilize various permutations of the advanced, physics-based SNOWPACK model (Bartelt and Lehning, 2002; Lehning et al., 2002b, 2002a), which was forced with quality controlled meteorological observations and validated on multiple snowpack measurements. With the importance of snow cover and snowmelt to the economy and hydroclimate of the western United States in mind, the overarching goal was to improve understanding of how snow cover evolves through the accumulation and melt seasons. The research presented herein can be broadly divided into two categories: 1) Evaluation of snowpack processes in historic and future climates, and 2) A critical examination of how precipitation phase affects simulated snow cover evolution.

The first two projects focus on the Niwot Ridge Long Term Ecological Research (LTER) site, which has hourly meteorological and snow pit observations dating back to 1990 and 1995, respectively. Project 1 uses both observational and simulation data to investigate how the snowpack acquires energy deficits, a previously unknown process. Project 2 then leverages the baseline simulations from Project 1 to evaluate the differential response of the snowpack at the Niwot Ridge LTER alpine and subalpine sites to changes in climate. Finally, Project 3 expands the spatial scope to include sites that span a climatic gradient across the western Unites States in order to analyze how the choice of a precipitation phase method leads to uncertainty in simulated snow cover evolution.

1.3.1 Project 1 (Chapter 2): Observations and simulations of the seasonal evolution of snowpack cold content and its relation to snowmelt and the snowpack energy budget

Equation 1.1 shows that $\frac{dU}{dt}$ and Q_M are balanced by the fluxes to and from the snowpack. Critically, little to no energy goes towards Q_M until the snowpack warms from sub-freezing to an isothermal 0°C. If the snowpack is not isothermal, then surface melt can be refrozen in the colder lower layers of the snowpack. First principles therefore dictate that snowmelt onset and rate should at least be partially controlled by the internal energy of the snowpack. Despite this fundamental physical relationship, little research has been done on how cold content (i.e., the snowpack's energy deficit) develops in seasonal snowpacks. This is likely due to the fact that cold content is a linear function of snowpack mass and depth-weighted mean temperature, and that measurements of the latter are rare relative to those of the former. Thus, it remained unknown whether snowpacks developed energy deficits through meteorological (e.g., air temperature and snowfall) or energy balance processes.

Chapter 2 uses observational snow pit and meteorological data as well as validated output from the SNOWPACK model to quantify how new snowfall and negative energy fluxes contribute to cold content development at an alpine and subalpine site at the Niwot Ridge LTER. At the two sites, new snowfall was the dominant pathway for cold content development, while negative energy fluxes—primarily Q_{LW} and Q_{LE}—contributed a lesser amount of cold content on a daily basis. In the alpine, snowfall was responsible for 84.4% of simulated cold content gains and 73.0% in the subalpine. These results were somewhat surprising given the high potential of the snowpack energy balance to drive snowpack cooling at both sites through high wind speeds, cold air temperatures, and low relative humidity (i.e., low atmospheric emissivity). Results from Project 1 also showed that cold content magnitude exerted little control on snowmelt rate and

timing at seasonal time scales. However, non-zero cold content values did delay snowmelt onset and damp snowmelt rates at daily to monthly time scales, suggesting that observations or simulations of cold content have more predictive capacity over shorter time periods (Jennings et al., 2018a).

1.3.2 Project 2 (Chapter 3): Evaluating the differential response of an alpine and subalpine snowpack to changes in climate

The hydrologic landscape of the western United States is changing, particularly in areas reliant on snowmelt-derived streamflow. Recent estimates attribute approximately 50% or greater of the observed change to anthropogenic climate warming (Abatzoglou, 2011; Barnett et al., 2008; Pederson et al., 2013), which has been expressed as an increased fraction of precipitation falling as rain versus snow (Knowles et al., 2006), decreased snow accumulation and earlier snowmelt (Clow, 2010; Harpold et al., 2012; Mote et al., 2005; Pederson et al., 2013, 2011b; Regonda et al., 2005), earlier streamflow timing (Cayan et al., 2001; Clow, 2010; Regonda et al., 2005; Stewart et al., 2005), and reduced streamflow volume (Barnhart et al., 2016; Berghuijs et al., 2014). Most work has ascribed the majority of these impacts to increased surface air temperatures, with little effect resulting from precipitation changes (Hamlet et al., 2005; Kapnick and Hall, 2012; Mote et al., 2018; Pederson et al., 2013; Sospedra-Alfonso et al., 2015). Continued climate warming—a near certainty in most climate simulations—is predicted to exacerbate and protract these impacts, as well as expand their spatial extent (Barnett and Pierce, 2009; Christensen et al., 2004; Klos et al., 2014; Nolin and Daly, 2006; Stewart et al., 2004a). Increased warming is also predicted to restrict the ability of snow-dominated basins to provide reliable water deliveries in the future (Barnett and Pierce, 2009; Christensen et al., 2004; Mankin et al., 2015).

Although the warming has occurred throughout the western United States, mountain snowpacks have exhibited a spatially variable response to air temperature increases. In general, areas at middle elevations with winter air temperatures near -5° to 0 °C have been most sensitive to warming (Kapnick and Hall, 2012; Knowles et al., 2006; Mote et al., 2018) and are expected to remain so with continued warming (Klos et al., 2014; Musselman et al., 2017b). However, the relationships between sensitivity and elevation and air temperature are empirical, meaning there is a need to investigate the physical processes behind the variable response. For this work, the Niwot Ridge LTER again offered an ideal study site as the alpine and subalpine locations span the divide of areas that should be hypothetically less and more sensitive, respectively, to the impacts of climate warming. Project 2 uses the baseline model runs from Project 1 with warming uniformly applied via a delta-change approach in 0.5°C increments from +0.5°C to +4.0°C. For the warming scenarios, atmospheric emissivity was held constant, and incoming longwave radiation was increased through the effect of air temperature on the calculation of atmospheric longwave emission using the Stefan-Boltzmann equation. Our results showed the higher, colder alpine site was less sensitive to future warming in terms of snow accumulation and melt due to three physical reasons: 1) Snowfall fraction decreased less rapidly with warming than in the subalpine; 2) Significant cold content was still added to the alpine snowpack throughout the snow season, preventing mid-winter melt events; 3) Changes to snowmelt rate were not significant because increases to the turbulent fluxes balanced decreases in the radiative fluxes with earlier melt onset.

While continued warming is a near certainty in the western United States, the changes that may occur to total precipitation and precipitation seasonality are less certain (Easterling et al., 2017; IPCC, 2013). Previous work has shown that changes to precipitation can mitigate warming

effects on snow accumulation, so Project 2 also evaluates the impacts of precipitation changes. The delta-change approach was again used for total precipitation, with changes to the baseline applied in 5% increments from -20% to + 20%. Precipitation seasonality was shifted between winter and spring in 10% increments from -30% (spring becomes wetter) to +30% (winter becomes wetter) while keeping total precipitation constant. As opposed to the differential response to warming, changes to total precipitation led to relatively consistent results at the alpine and subalpine sites with later melt onset and faster snowmelt rates being associated with increased precipitation. Changes to precipitation seasonality had a near-negligible impact on snow cover properties at both sites.

1.3.3 Project 3 (Chapter 4): The sensitivity of modeled snow accumulation and melt to precipitation phase methods across a climatic gradient in the western United States

The results from Project 2 showed that declines in snowfall fraction were significant at both the alpine and subalpine sites with future warming. These sites are not unique in that one of the more pronounced effects of climate warming has been a shift from snow to rain in cold and temperate regions across the globe (Knowles et al., 2006; Trenberth, 2011). It is predicted that this trend will continue with future warming due to the strong temperature dependency of precipitation phase (Bintanja and Andry, 2017; Klos et al., 2014; O'Gorman, 2014). Although the shift from snow to rain is exceedingly probable, the fact that the temperature at which rain and snow fall in roughly equal probability varies spatially is often overlooked. Jennings et al. (2018b) showed that snow is more probable at higher temperatures in continental areas than in maritime areas, yet precipitation phase partitioning is often simulated using a spatially uniform air temperature threshold. This same work also showed that the choice of a precipitation phase method (e.g., the air temperature threshold or range used to discriminate between solid and liquid precipitation) introduces significant uncertainty to annual snowfall frequency. Concerningly, the mountainous

areas with the greatest sensitivity, such as California's Sierra Nevada, are indispensable to regional water resources. This is worrisome because work using land surface models and spatially uniform thresholds is progressing rapidly, while little work has been done critically examining how the precipitation phase predicted by different methods propagates into other changes in model simulations.

We therefore have the problem of a snow-to-rain shift occurring with climate warming but simultaneously knowing little about how precipitation phase methods affect snowpack simulations in historic or future climates. To that end, recent research has called into question the simplistic way by which many land surface and hydrologic models partition rainfall and snowfall (Feiccabrino et al., 2015; A. A. Harpold et al., 2017c). Previous work on the topic has shown precipitation phase method can cause uncertainty in simulated SWE and snow cover duration (Fassnacht and Soulis, 2002; Harder and Pomeroy, 2014; Mizukami et al., 2013), but those projects focused on either a single site or a small selection of sites with similar climatic characteristics. Meanwhile, Raleigh et al. (2016) and Harpold et al. (2017a) both indicated that the selection of a precipitation phase method leads to a spatially variable response in annual snowfall fraction. Thus, besides uncertainty in snowfall fraction, it is unknown how a selection of precipitation phase methods would affect simulated snow cover evolution across a climatic gradient like the one expressed by the seasonal snow classes of the western United States.

Project 3 remedies this shortcoming by simulating 8 years of snow cover using 12 different precipitation phase methods at 11 sites, representing warm maritime to cold continental climatic conditions. The three sites with average winter air temperatures less than -5°C expressed minimal sensitivity to the different methods, suggesting that method selection matters little at cold, high-elevation sites where the vast majority of annual precipitation falls as snow.

Conversely, at the warmer sites, precipitation phase method selection introduced significant uncertainty with ranges in annual snowfall fraction exceeding 30% and relative differences between minimum and maximum snowfall fraction approaching 100%. This significant uncertainty propagated into sensitivity in simulated snow cover evolution with peak SWE ranges approaching 500 mm and snow cover duration ranges nearing one month or more. Overall, sites with warmer winter and spring temperatures and greater precipitation were most sensitive in terms of the variability in snow cover evolution. This work has implications for simulations of past, present, and future hydroclimatic conditions given the wide ranges in snow cover properties produced by the different methods. Variability in simulated peak SWE caused by precipitation phase method selection could degrade the estimates of water stored in mountain snowpacks, while uncertainty in snow cover duration would affect calculations of land surface albedo and the earth's energy balance.

Chapter 2

2 Observations and simulations of the seasonal evolution of snowpack cold content and its relation to snowmelt and the snowpack energy budget

Chapter 2 was originally published in *The Cryosphere* with contributions from my co-authors Timothy Kittel and Noah Molotch:

Jennings, K.S., Kittel, T.G. and Molotch, N.P., 2018. Observations and simulations of the seasonal evolution of snowpack cold content and its relation to snowmelt and the snowpack energy budget. *The Cryosphere*, *12*(5), p.1595. https://doi.org/10.5194/tc-12-1595-2018.

Abstract

Cold content is a measure of a snowpack's energy deficit and is a linear function of snowpack mass and temperature. Positive energy fluxes into a snowpack must first satisfy the remaining energy deficit before snowmelt runoff begins, making cold content a key component of the snowpack energy budget. Nevertheless, uncertainty surrounds cold content development and its relationship to snowmelt, likely because of a lack of direct observations. This work clarifies the controls exerted by air temperature, precipitation, and negative energy fluxes on cold content development and quantifies the relationship between cold content and snowmelt timing and rate at daily to seasonal time scales. The analysis presented herein leverages a unique long-term snow pit record along with validated output from the SNOWPACK model forced with 23 water years (1991–2013) of quality controlled, infilled hourly meteorological data from an alpine and subalpine site in the Colorado Rocky Mountains. The results indicated that new precipitation

exerted the primary control on cold content development at our two sites with snowfall responsible for 84.4% and 73.0% of simulated daily gains in the alpine and subalpine, respectively. A negative surface energy balance—primarily driven by sublimation and longwave radiation emission from the snowpack—during days without snowfall provided a secondary pathway for cold content development, and was responsible for the remaining 15.6% and 27.0% of cold content additions. Non-zero cold content values were associated with reduced snowmelt rates and delayed snowmelt onset at daily to sub-seasonal time scales, while peak cold content magnitude had no significant relationship to seasonal snowmelt timing. These results suggest that the information provided by cold content observations and/or simulations is most relevant to snowmelt processes at shorter time scales, and may help water resource managers to better predict melt onset and rate.

2.1 Introduction

Cold content is a key component of the snowpack energy budget as it represents the internal energy deficit that must be overcome before snowmelt runoff can begin. It is a linear function of snowpack temperature and snow water equivalent (SWE), whereby colder snowpacks with greater SWE have increased energy deficits. Until cold content is satisfied, positive energy fluxes go towards raising the internal snowpack temperature to an isothermal 0°C and any surface melt that is produced may be refrozen in the colder lower layers of the snowpack. In this regard, cold content influences the timing and rate of snowmelt runoff, which is of critical importance to various ecohydrologic and cryospheric processes, including: streamflow generation (Barnhart et al., 2016; Regonda et al., 2005), water resources availability (Barnett et al., 2005; Christensen et al., 2004; Mankin et al., 2015; Stewart, 2009), water uptake by vegetation (Winchell et al., 2016), soil moisture (Harpold and Molotch, 2015), flooding

(Jennings and Jones, 2015; Kampf and Lefsky, 2016), and land surface albedo (Déry and Brown, 2007), among others.

Cold content can be estimated using at least one of three primary methods: 1) As an empirical function of air temperature (e.g., Anderson, 1976; DeWalle and Rango, 2008; Seligman et al., 2014; United States Army Corps of Engineers, 1956); 2) As a function of precipitation and air temperature (e.g., Cherkauer et al., 2003; Lehning et al., 2002b; Wigmosta et al., 1994) or wet bulb temperature (Anderson, 1968) during precipitation; and 3) As a residual of the snowpack energy balance (e,g., Andreadis et al., 2009; Cline, 1997; Lehning et al., 2002b; Marks and Winstral, 2001). In general, simple temperature-index models employ method 1, while both 2 and 3 are utilized in physics-based snow models. These methods suggest that cold content develops through both meteorological and energy balance processes, but few direct comparisons to observed cold content exist. This is likely due to the inherent difficulty in measuring cold content, which requires either time-intensive snow pits or co-located snow depth, density, and temperature measurements (Burns et al., 2014; Helgason and Pomeroy, 2011; Marks et al., 1992; Molotch et al., 2016). The lack of validation data introduces significant uncertainty into the dominant process by which cold content develops. Thus, it is not known whether cold content development is primarily a function of air temperature (method 1), snowfall (method 2), or a negative surface energy balance (method 3).

Early work from California's Sierra Nevada mountains indicated cold content developed in the snowpack mainly through a negative surface energy balance. The reported monthly change in snowpack internal energy (i.e., change in cold content) ranged from -34 to -61 W m^{-2} from November through April at an exposed site and -8 to -66 W m^{-2} from November through February at a sheltered site (Marks and Dozier, 1992). However, such negative fluxes would

result in physically unrealistic internal snowpack temperature changes. Even persistent slightly negative flux values, as reported elsewhere in the literature (Armstrong and Brun, 2008), would result in implausibly low snowpack temperatures. It can be inferred that any process producing anomalously low snowpack temperatures either misidentifies or overestimates the importance of a particular meteorological or energy balance mechanism.

Furthermore, the degree to which wintertime cold content magnitude controls snowmelt timing and rate at daily to seasonal timescales is relatively uncertain. Work from the southwestern United States suggests increased cold content may delay seasonal melt timing (Molotch et al., 2009) and the inclusion of cold content generally improves meltwater outflow predictions in point and distributed snowmelt models of varying degrees of physical complexity (Bengtsson, 1982a; Jepsen et al., 2012; Livneh et al., 2010; Mosier et al., 2016; Obled and Rosse, 1977). However, two empirical studies indicated the energy required to satisfy cold content may be relatively small in comparison to the energy required to melt enough snow to fulfill the irreducible water content of an already isothermal snowpack (Bengtsson, 1982a; Seligman et al., 2014).

Given the above unknowns, we aim to improve understanding of the processes controlling cold content development and the relationship between cold content and snowmelt timing and rate at a continental, mid-latitude alpine and subalpine site in the Colorado Rocky Mountains. Our research utilizes observations from a long-term snow pit record and simulation output from a physics-based snow model forced with a quality controlled, serially complete meteorological dataset. Analyses performed on the observations and simulation data are focused on answering the following research questions:

1. What are the meteorological and energy balance controls on cold content development at an alpine and subalpine site in the Colorado Rocky Mountains?
2. How does cold content affect snowmelt timing and rate on seasonal, sub-seasonal, and daily time scales?

2.2 Study site and snow pit and forcing data

The Niwot Ridge Long Term Ecological Research site (LTER) is located on the eastern slope of the Continental Divide in the Rocky Mountains of Colorado, USA (Fig. 2.1). The entirety of the LTER is situated above 3000 m with treeline occurring at approximately 3400 m (Williams et al., 1998). Dominant vegetation in the subalpine is lodgepole pine, aspen, Engelmann spruce, subalpine fir, and limber pine (Burns et al., 2014). The alpine is characterized by several tundra vegetation communities of grasses, forbs, and shrubs, whose distribution is linked to patterns of snow depth and soil moisture (Walker et al., 1993, 1994).

There are multiple meteorological stations within the boundaries of the Niwot Ridge LTER, but this work focuses on the two sites with long-term snow pit records: alpine (3528 m) and subalpine (3022 m), named Saddle and C1, respectively (Fig. 2.1). We employed an additional high alpine station (D1, 3739 m) in the meteorological data infilling procedure (Appendices 2.1 and 2.2), but did not perform model simulations there due to a lack of snow pit validation data. From 2008 to 2012, annual precipitation in the alpine and subalpine averaged 1071 mm and 752 mm, respectively (Knowles et al., 2015) and the ratio between above- and below-treeline precipitation varies annually as a function of upper-air flow regimes (Kittel et al., 2015). The majority of annual precipitation is snow, with estimates of the proportion of snowfall ranging from 63% to 80% of total precipitation in the subalpine and alpine (Caine, 1996; Knowles et al., 2015). Over our study period, December, January, February mean air temperature

was -10.3°C in the alpine and -6.2°C in the subalpine. Dominant wind direction was westerly, but the subalpine site also experienced easterly flow during intermittent upslope events (Blanken et al., 2009; Burns et al., 2014). Elevated wind speeds in the alpine, averaging 10 m s^{-1} to 13 m s^{-1} in winter, exert a primary control on patterns of snow erosion and deposition with snow depth being highly variable as a result (Erickson et al., 2005; Jepsen et al., 2012; Litaor et al., 2008). Snow depths in the alpine can range from 0 m over wind-scoured tundra to upwards of 5 m in drifts on the lee side of terrain features or in gullies. Additionally, blowing snow occurs frequently during winter months in the alpine due to high winds, reaching a maximum in January (Berg, 1986).

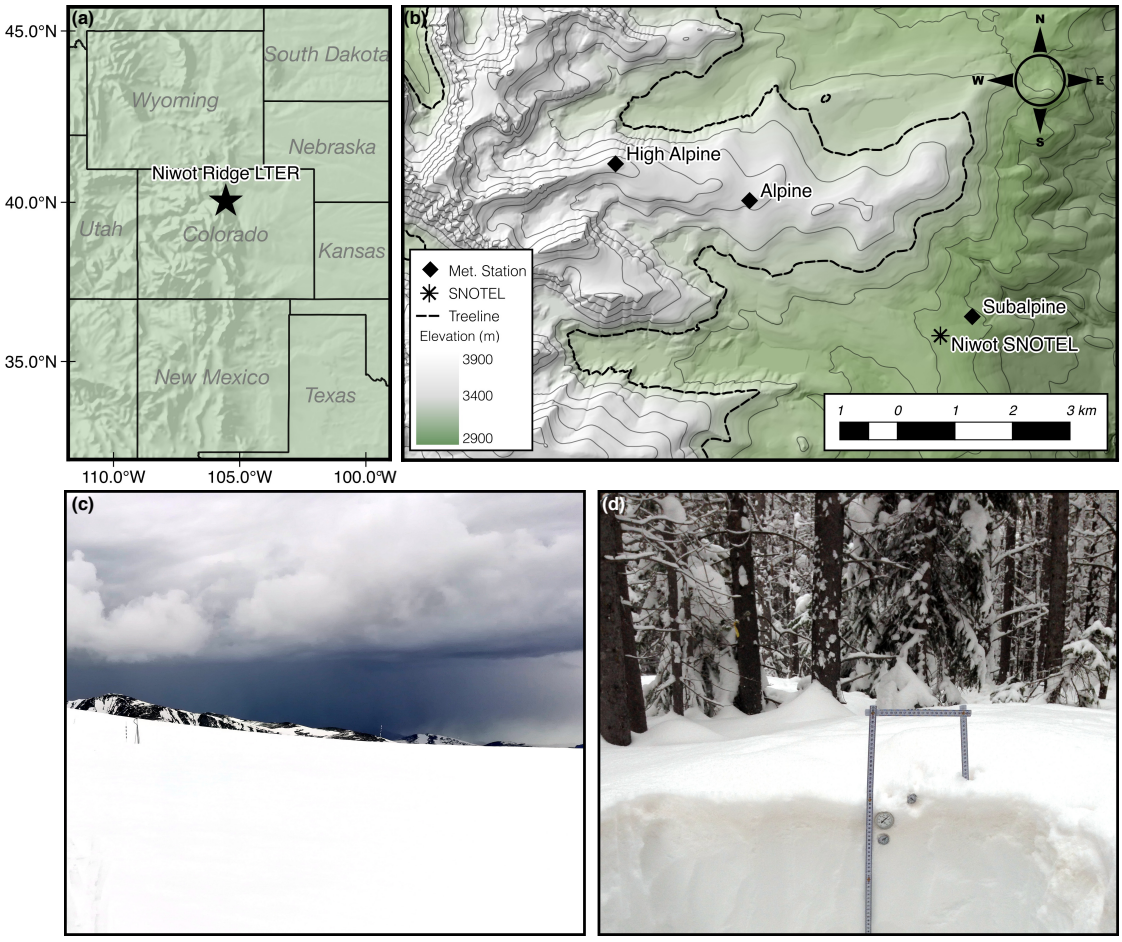

Figure 2.1. The location of the Niwot Ridge LTER within the western United States (a) and a topographical map showing the meteorological stations and snow pit sites. The dashed line in the LTER inset (b) represents approximate treeline (3400 m) and the thin, solid lines are 100 m contours. The snow study focused on the

alpine (c) and subalpine sites (d), the two locations which have co-located snow pit observations and meteorological stations. The high alpine site was used as an additional station in the meteorological data infilling protocol and the Niwot SNOTEL was used for model validation.

Regular snow pit measurements began in 1995 in the alpine and 2007 in the subalpine, and were taken at weekly to monthly intervals from the middle of January through the end of May in most snow seasons (Williams, 2016). A total of 292 alpine and 147 subalpine snow pit records were used in this study (Appendix 2.3). The alpine snow pit represents conditions typical of the above-treeline snowpack as it is not in an area of pronounced snow erosion or deposition. The subalpine snow pit is located in a stand of lodgepole pine, typical of vegetation conditions in the below-treeline areas. Measurement protocol follows Williams et al. (1999): Snow density is measured for each 10 cm layer using a wedge-shaped 1 L density cutter (10 cm × 10 cm × 20 cm) and snow temperature is recorded every 10 cm with dial-stem thermometers. Snow pit measurements enable per-layer and depth-weighted calculations of SWE and cold content:

$$SWE = \frac{\rho_s}{\rho_w} d_s \tag{2.1}$$

$$CC = c_i \rho_s d_s (T_s - T_m) \tag{2.2}$$

where ρ_s and ρ_w are the density of snow and liquid water, respectively (kg m^{-3}), d_s is snow depth (m), CC is cold content (MJ m^{-2}), c_i is the specific heat of ice (2.1 × 10^{-3} MJ kg^{-1} °C^{-1}), T_s is the snow temperature (°C), and T_m is the melting temperature of snow (0°C). Snow pit analyses focused on water years (WY, 1 October from the previous calendar year through 30 September) 2007 through 2013, the period for which overlapping snow pit data were available. The full period of record in the alpine (WY1995–WY2013) was used for model validation.

Hourly meteorological data have been collected at the LTER since 1990, but the record suffers from quality control issues and periods of missing data. Recent research has shown the quality of snow model output depends on having accurate forcing data (e.g., Förster et al., 2014; Lapo et al., 2015; Raleigh et al., 2015, 2016; Schmucki et al., 2014). Measurements were

therefore subjected to an extensive quality control and infilling protocol (Appendices 2.1 and 2.2) to produce a serially complete, hourly dataset with observations of air temperature, relative humidity, incoming solar radiation, wind speed, and precipitation. The dataset also includes hourly estimates of downwelling longwave radiation based on air temperature, relative humidity, and incoming solar radiation using the methods of Angström (1915), Crawford and Duchon (1999) and Dilley and O'Brien (1998) as described in Flerchinger et al. (2009).

2.3 Methodology

Observations from the Niwot Ridge LTER snow pit record and validated output data from physics-based snow model simulations were employed to answer the two research questions. We assessed the meteorological controls on cold content development using measurements of cumulative precipitation and the cumulative mean of air temperature for the full period of record at both sites. We focused the analysis on snow pit observations and simulations between 1 December and the date of peak cold content, the main period of cold content development. We then tested whether persistent large negative energy fluxes could be responsible for cold content development by calculating the rate of change in internal energy between pit observations and using the snow model simulations to calculate the snowpack energy budget. Model output was also used to assess the effect of cold content magnitude and timing on snowmelt rate and timing at daily to seasonal time scales. Additionally, we note that in this paper an "increase" or "gain" in cold content refers to the value increasing in absolute magnitude (becoming more negative i.e., the energy deficit increases). A "decrease" or "loss" of cold content occurs when the value becomes less negative and approaches 0 MJ m^{-2}.

2.3.1 Snow pit analysis

Mean characteristics of and differences between the alpine and subalpine snow pits were quantified using data from WY2007–WY2013, the seven years for which there were overlapping observations. To assess the control each meteorological quantity exerted on cold content, we used the cumulative mean of air temperature and cumulative precipitation between 1 December and the date of snow pit observation as the independent variables with observed cold content acting as the dependent variable in ordinary least squares regression. The strength of the relationship was quantified using the coefficient of determination, r^2, while the p-value of the regression slope indicated statistical significance. Additionally, in order to evaluate whether large persistent negative energy balances were consistent with patterns of cold content development, we calculated the rate of change in internal energy between snow pit observations:

$$\frac{dU}{dt}_{pit} = \frac{\Delta CC}{(86{,}400\ \Delta t)} \tag{2.3}$$

where $\frac{dU}{dt}_{pit}$ is the pit-observed rate of change in internal energy (W m^{-2}), ΔCC is the change in cold content (J m^{-2}) between snow pit observations, 86,400 is the conversion factor between days and seconds (s d^{-1}), and Δt is the number of days between snow pit observations (d). Snow pit cold content in this context integrates the effects of incoming and outgoing fluxes, plus the cold content added by precipitation, by providing a measure of the change in the internal energy of the snowpack independent of any surface flux measurements or estimations.

2.3.2 Snow model simulations

2.3.2.1 Model description

In order to evaluate cold content development processes at a finer temporal resolution and quantify components of the energy budget, we employed the complex, physics-based, multi-

layer, one-dimensional SNOWPACK model (Bartelt and Lehning, 2002; Lehning et al., 2002b, 2002a). This model was selected because previous studies have shown complex, multi-layer models more accurately partition the snowpack energy budget and better represent internal processes (Blöschl and Kirnbauer, 1991; Boone and Etchevers, 2001; Essery et al., 2013; Etchevers et al., 2004). Additionally, SNOWPACK was utilized in previous work to simulate the snowpack energy budget at the Niwot Ridge LTER (Meromy et al., 2015) and it has been validated in the Rocky Mountains of Montana (Lundy et al., 2001). SNOWPACK is forced with air temperature, relative humidity, wind speed, incoming solar radiation, incoming longwave radiation, and precipitation at an hourly or higher temporal resolution. The model discretizes the snowpack into a variable number of layers that change with the addition of new snow, mass loss through snowmelt and sublimation, and densification via compaction. Each layer is composed of water in liquid, solid, and gas phases, all of which are assumed to have the same temperature. SNOWPACK is governed by four differential equations that account for the conservation of energy, mass, and momentum. Explicit routines are included for heat transfer, water transport, and phase changes. In addition, the model features quasi-physical estimations of snow microstructure and snow grain metamorphism. These properties, in turn, control the rate of heat conduction and settling within the snowpack. SNOWPACK also models the penetration of shortwave radiation and wind pumping in the upper layers of the snowpack.

We increased the standard SNOWPACK rain-snow air temperature threshold from 1.2°C to 2.5°C to better represent precipitation phase partitioning at our high-elevation continental sites. In general, the Rocky Mountains have some of the warmest rain-snow air temperature thresholds in the Northern Hemisphere (Jennings et al., 2018b). To test the effect of our threshold selection, we compared the mean annual snow frequency using the 2.5°C threshold

(alpine = 76.4%; subalpine = 61.5%) to a bivariate binary logistic regression phase prediction model (alpine = 76.7%; subalpine = 62.8%). This model predicts precipitation phase as a function of relative humidity and air temperature, and it was shown to be the best precipitation phase method in a Northern Hemisphere comparison (Jennings et al., 2018b).

The bulk Richardson number stability correction was used for computing turbulent fluxes in both the alpine and subalpine. Although Monin-Obukhov similarity theory options were available, these stability corrections generally performed worse relative to the bulk Richardson number in our preliminary simulations as well as in the work of others (Essery et al., 2013). Ground heat flux was simulated using the SNOWPACK-default constant soil surface temperature of 0.0°C because no long-term soil surface temperature data were available.

Additionally, the SNOWPACK canopy module was activated for the subalpine site given its location in a stand of lodgepole pine. Parameters for the canopy module were calibrated using a series of 100 Monte Carlo simulations with parameter ranges bounded by representative estimates of leaf area index, vegetation height, direct canopy throughfall, and wind speed reduction (Table 2.1). Modeled SWE in the subalpine proved most sensitive to the wind speed reduction parameter, likely due to the siting of the anemometer as noted in Appendix 2.1. Using un-corrected observed wind speed as a model input led to a physically unrealistic amount of snow sublimation.

Table 2.1. Calibrated SNOWPACK canopy module parameters for the subalpine site.

	LAI	Vegetation height (m)	Canopy direct throughfall	Wind scaling factor
Parameter value	3.7	7.3	0.25	0.44

2.3.2.2 Model simulations, validation, and analysis

SNOWPACK simulations were performed in the alpine and subalpine for WY1991–WY2013 and forced with the quality controlled, infilled hourly meteorological data detailed in Appendix 2.1. This time range included the lowest (WY2002: 178 mm) and second highest (WY1996: 523 mm) peak SWE observations in the period of record (WY1981–WY2017) at the Niwot Snowpack Telemetry (SNOTEL) station (3020 m), which is located within the Niwot Ridge LTER boundary, less than 1 km from the subalpine snow pit and meteorological tower. Thus, the analysis covered a wide range of feasible snowpack conditions, from pronounced snow drought to peak SWE values greater than 150% of average, according to the SNOTEL observations.

To ensure the simulation output was suitable for in-depth analysis, we validated model SWE, snowpack temperature, and cold content values on the snow pit observations. We pursued this multi-validation approach because our work focuses on the internal energy of the snowpack and recent research has shown the output from snow model simulations (e.g., energy balance partitioning, SWE) is more reliable when several variables are used in model evaluation (Lapo et al., 2015). Modeled subalpine SWE estimates were also evaluated using observed SWE at the Niwot SNOTEL site. For each quantity of interest, we assessed model performance using the coefficient of determination and mean bias. To improve model output, we corrected precipitation measurements relative to snow pit and SNOTEL SWE observations (Appendix 2.1) and optimized the canopy parameters for subalpine simulations (Sect. 2.3.2.1). Additionally, there were several times per winter when the simulated cold content spiked rapidly down (ΔCC < -0.3 MJ m^{-2} h^{-1}), then back up. These data points, which represented less than 0.2% of the simulation hours, were filtered from the analysis.

We then used the validated output from SNOWPACK to quantify the controls on cold content development and snowmelt processes at a finer temporal resolution than the weekly to

monthly snow pit observations. To evaluate the meteorological processes controlling cold content development, we used the same methods employed in the snow pit observations outlined above (Sect. 2.3.1). Additionally, we quantified the contributions of the simulated snowpack energy balance to cold content development:

$$\frac{dU}{dt} + Q_M = Q_{SW} + Q_{LW} + Q_H + Q_{LE} + Q_G + Q_R \quad (2.4)$$

where $\frac{dU}{dt}$ is the simulated rate of change in internal snowpack energy, Q_M is the energy available for melt (once cold content equals 0.0 MJ m^{-2}), Q_{SW} is net shortwave radiation, Q_{LW} is net longwave radiation, Q_H is sensible heat flux, Q_{LE} is latent heat flux, Q_G is ground heat flux, and Q_R is the heat advected by precipitation (all W m^{-2}). This work focuses primarily on Q_{SW}, Q_{LW}, Q_H, Q_{LE}, and Q_G, which we will refer to as Q_{net} throughout the remainder of this paper. Q_R is typically negligible because significant rain-on-snow events are rare at the Niwot Ridge LTER.

Simulation results were also used to quantify the control cold content exerts on snowmelt timing and rate at multiple time scales. At the seasonal time scale, we set snowmelt onset to correspond to the date of peak SWE and snowmelt rate to the ablation slope, which is the average daily snowmelt rate between the date of peak SWE and the date at which SWE first equals 0 mm (e.g., Barnhart et al., 2016; Trujillo and Molotch, 2014). At sub-seasonal time scales, we calculated snowmelt timing and rate in time windows from 1 d to 30 d, with a corresponding cold content value at day zero. Finally, we used the cold content at 6AM local time (CC_{6AM}) to evaluate the effect of cold content on snowmelt timing and rate at daily time scales. For the sub-seasonal and daily time scales above, we set snowmelt timing to be the first instance of simulated snowmelt runoff and snowmelt rate to be the mean rate for the time window.

2.4 Results

2.4.1 Snow pit observations of cold content

Snow pit observations showed daily and peak annual snowpack cold content were consistently greater in the alpine than subalpine (Fig. 2.2). From WY2007–WY2013, mean peak cold content was 2.6 times greater in the alpine than subalpine, while mean peak SWE was 2.1 times greater in the alpine (Table 2.2). On average, peak cold content and peak SWE, respectively, occurred 33 d and 10 d later in the alpine than subalpine. The average temporal gap between peak cold content and peak SWE was also 23 d shorter in the alpine, indicating greater energy exchange between the snow and atmosphere at this site during the main time of snowpack ripening. Mean $\frac{dU}{dt}_{pit}$ for this period, as estimated using Eq. 2.3, was 1.2 W m^{-2} and 0.4 W m^{-2} in the alpine and subalpine, respectively.

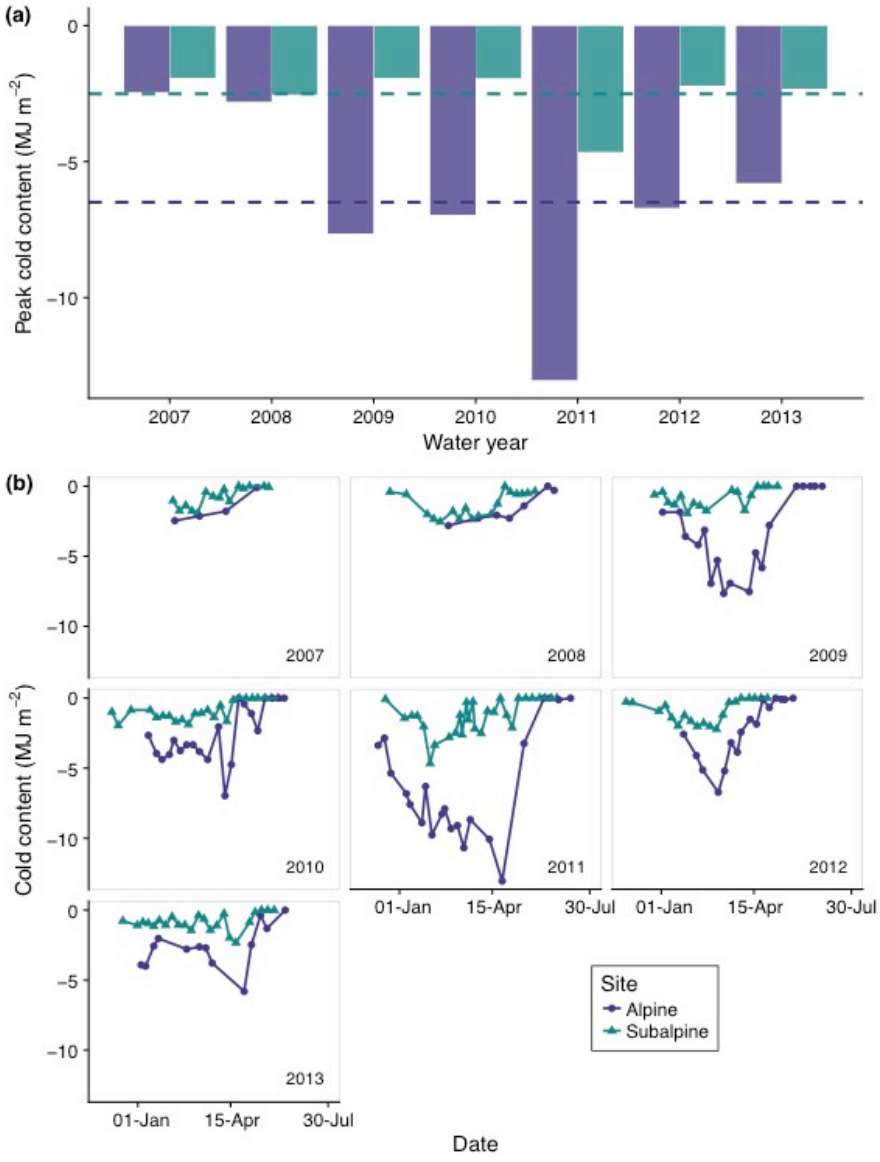

Figure 2.2. Peak annual cold content (a) and individual snow pit observations of cold content (b) for the alpine and subalpine from WY2007–WY2013. The dashed horizontal lines in (a) represent the mean peak annual cold content values for the two sites.

Table 2.2. Mean quantities for the alpine and subalpine snow pits from WY2007–WY2013

Site	Peak CC (MJ m^{-2})	Peak SWE (mm)	Date of Peak CC	Date of Peak SWE
Alpine	-6.5	843	19-March	6-May
Subalpine	-2.5	395	14-February	26-April

From 1 December to the date of snow pit observation, increased cumulative precipitation was associated with increased cold content at both sites (Fig. 2.3). Cumulative precipitation

explained 55% and 17% of the variance in cold content in the alpine and subalpine, respectively. The relationship was statistically significant at the 99% level at both sites despite the low coefficient of determination in the subalpine. Conversely, the cumulative mean of air temperature had no statistically significant relationship to snowpack cold content, explaining less than 1% of the variance at both sites (not shown). Although there may be snowpack energy losses during periods of low air temperature, these results indicate that, of the two meteorological quantities evaluated here, snowfall exerts the primary control on cold content development. This is likely due to the higher variability of winter precipitation, the coefficient of variation of which is 2.9 and 2.7 times greater than that of air temperature in the alpine and subalpine, respectively. Furthermore, the difference in r^2 values between the two sites suggests that precipitation plays a more important role in the alpine than subalpine in terms of cold content development.

Snow pit observations were also used to calculate $\frac{dU}{dt}_{pit}$ by quantifying the change in cold content between two points in time (Eq. 2.3). During periods of SWE accumulation, $\frac{dU}{dt}_{pit}$ was typically near 0.0 W m^{-2} (Fig. 2.4a), indicating a large negative energy balance was not responsible for cold content development at our two sites. The average flux in the alpine (-0.8 W m^{-2}) was greater in magnitude during this period than in the subalpine (-0.4 W m^{-2}), and both distributions were left-skewed as the energy balance was typically negative from snowfall- and/or flux-driven cold content increases. Changing the analysis to snow pit observations when melt occurred (Fig. 2.4b) led to a pronounced right-skew in the flux distribution with values again of a higher magnitude in the alpine. Thus, we found no evidence for highly negative internal energy changes at our sites with $\frac{dU}{dt}_{pit}$ values only being large in magnitude during snowmelt.

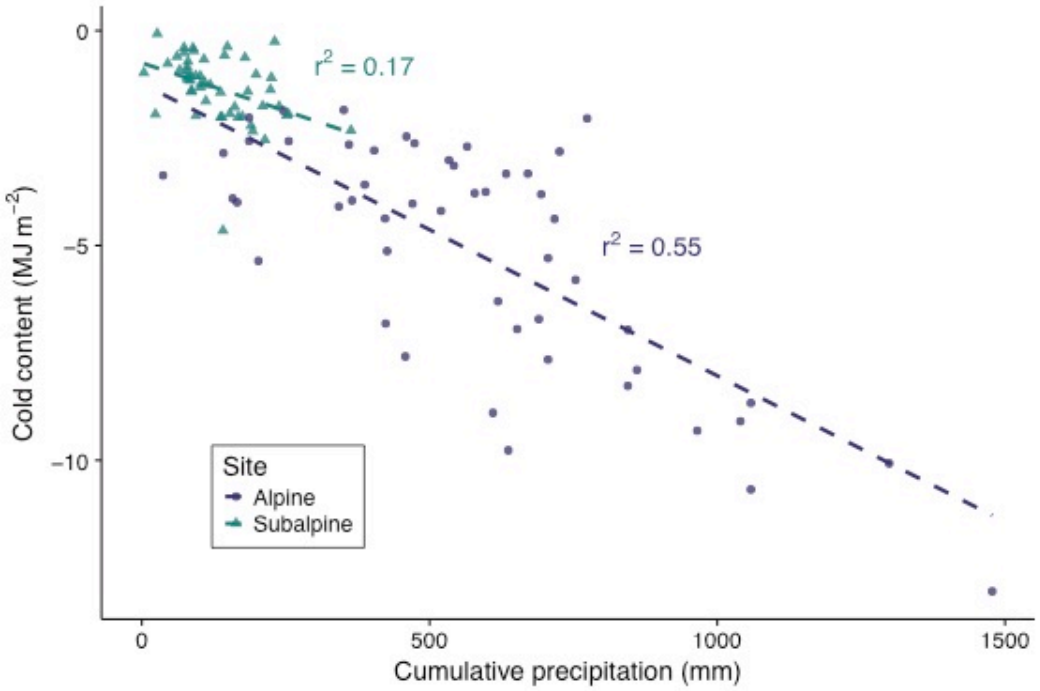

Figure 2.3. Cold content plotted against cumulative precipitation from 1 December to the date of snow pit observation for the alpine and subalpine for the snow season up to and including the date of peak cold content from WY2007–WY2013. The dashed lines of best fit were calculated using ordinary least squares linear regression.

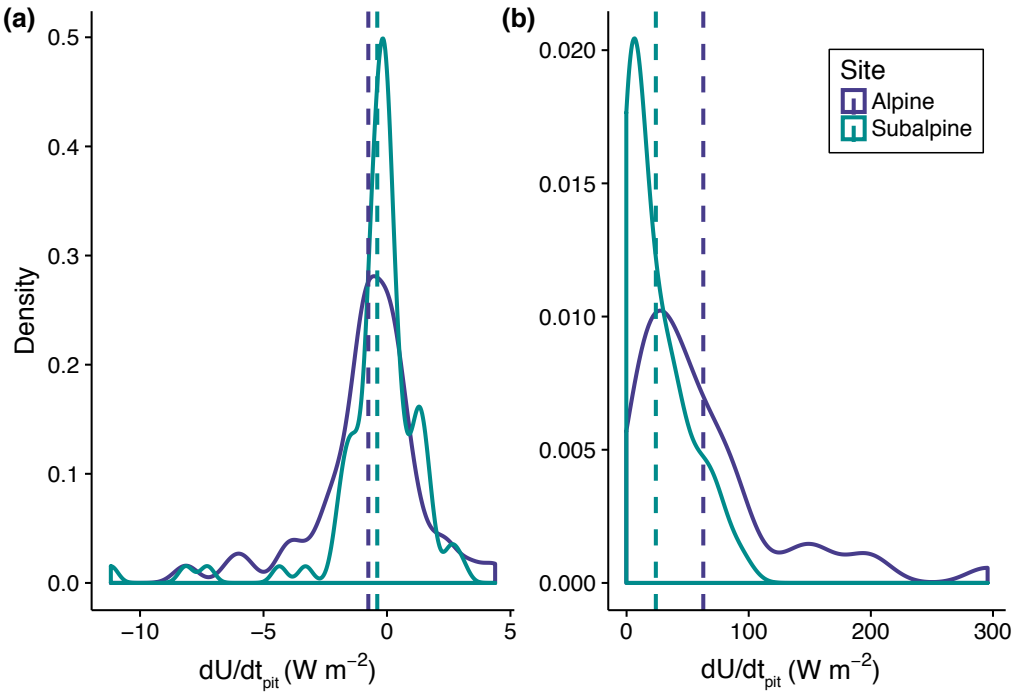

Figure 2.4. Kernel density estimates of $\frac{dU}{dt_{pit}}$ distributions as calculated from snow pit observations for periods with SWE gain (a) and loss (b) in the alpine and subalpine for WY2007–WY2013. The dashed vertical lines represent the mean $\frac{dU}{dt_{pit}}$ for the alpine (a = -0.8 W m^{-2}; b = 62.8 W m^{-2}) and subalpine (a = -0.4 W m^{-2}; b = 23.9 W m^{-2}).

2.4.2 Model SWE, snowpack temperature, and cold content validation

SNOWPACK simulations reproduced observed snow pit SWE patterns at both sites, with a higher coefficient of determination and lower bias in the subalpine than alpine (Fig. 2.5a,b; Table 2.3). Subalpine simulations were also in line with daily SWE observations from the Niwot SNOTEL (Table 2.3). Simulated depth-weighted snowpack temperature had a slight warm bias of 1.1°C in the alpine and 0.6°C in the subalpine (Fig. 2.5c,d, Table 2.3), while cold content was overpredicted in the alpine and underpredicted in the subalpine (Fig. 2.5e,f, Table 2.3). In this regard, simulated cold content errors integrated the SWE and snowpack temperature biases. Overprediction in the alpine was a result of the positive SWE bias having a greater effect on simulated cold content than the warm temperature bias. Conversely, underprediction of snowpack cold content in the subalpine was primarily due to the warm temperature bias.

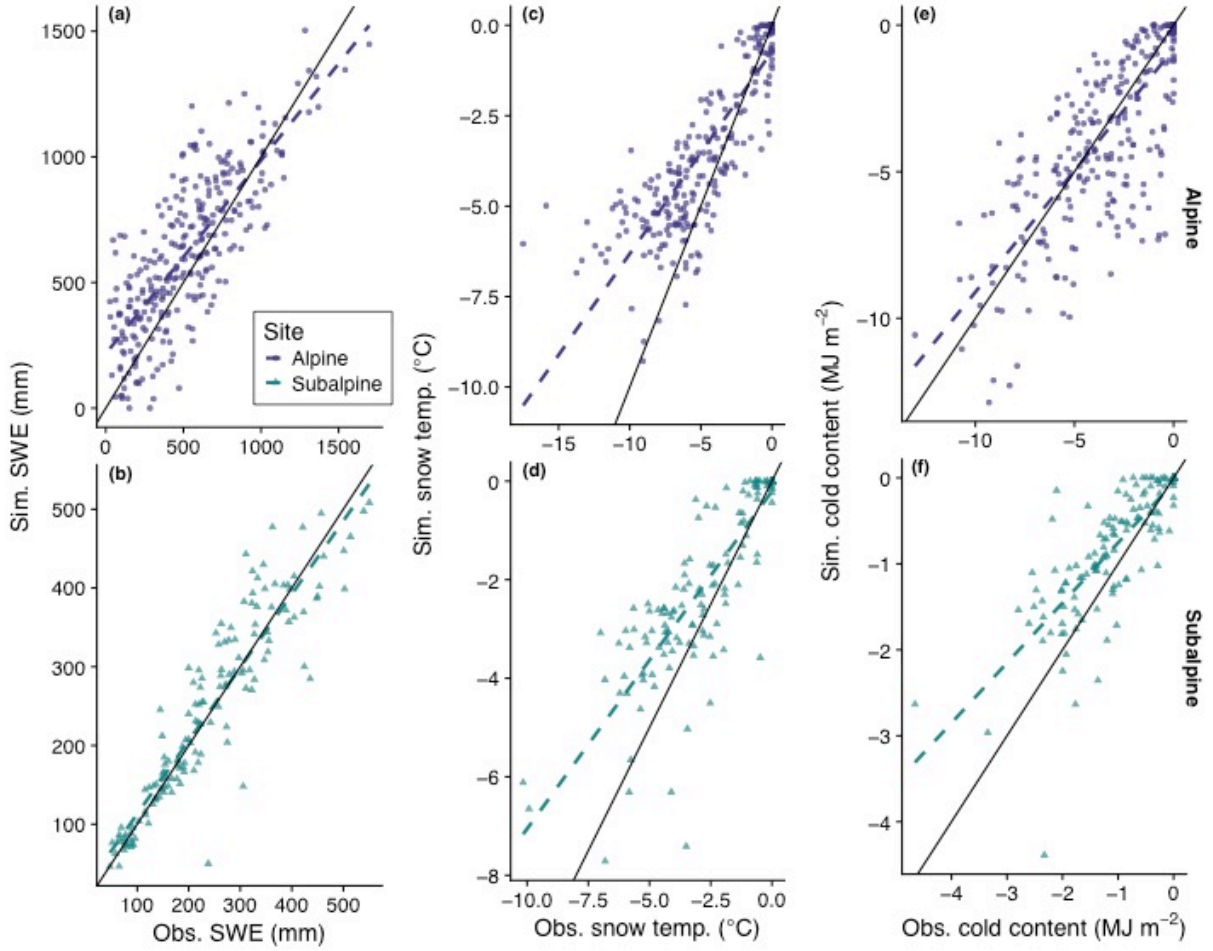

Figure 2.5. Plots of simulated versus snow-pit observed SWE (a,b), snowpack temperature (c,d), and cold content (e,f) in the alpine (top, WY1995–WY2013) and subalpine (bottom, WY2007–WY2013). The solid black line is the 1:1 line and the dashed lines are the lines of best fit as determined by ordinary least squares linear regression. Simulation error metrics are presented in Table 2.3.

Table 2.3. Statistics for SNOWPACK simulations relative to daily and annual observations from the snow pits in the alpine and subalpine, and Niwot SNOTEL in the subalpine. There is no SNOTEL station in the alpine and SNOTEL does not observe cold content and snowpack temperature. Comparisons are for the water years listed in the second column.

		Daily						Annual	
Site	**WY Range**	**SWE r^2**	**SWE Mean Bias (mm)**	**T_s r^2**	**T_s Mean Bias (°C)**	**CC r^2**	**CC Mean Bias (MJ m^{-2})**	**Max SWE Mean Bias (mm)**	**Max CC Mean Bias (MJ m^{-2})**
Alpine	1996-2013	0.63	95.8	0.74	1.1	0.63	-0.3	99 .0	-0.7
Subalpine (Snow Pit)	2007-2013	0.85	3.4	0.72	0.6	0.63	0.2	15.0	0.6
Subalpine (SNOTEL)	1991-2013	0.89	-5.4	NA	NA	NA	NA	44.1	NA

Modeled annual peak SWE and peak cold content were also similar to the previously reported pit values for WY2007 through WY2013 (Table 2.3). Additionally, simulated LTER subalpine peak cold content values were within the range of those reported in a simulation of a subalpine snowpack (-2.2 MJ m^{-2} to -1.7 MJ m^{-2}) at the nearby Fraser Experimental Forest during NASA's Cold Land Processes Experiment (Marks et al., 2008). Direct observations of snow surface sublimation were not available for comparison, but modeled sublimation rates were in line with other values reported in the literature for alpine and subalpine areas in the Colorado Rocky Mountains (Berg, 1986; Hood et al., 1999; Knowles et al., 2012; Molotch et al., 2007; Sexstone et al., 2016). On average, simulated snow-surface sublimation represented 28.8% (383 mm) and 11.4% (53 mm) of snow-season precipitation in the alpine and subalpine, respectively.

2.4.3 Meteorological and energy balance controls on cold content development: Simulation results

2.4.3.1 Primary control: Snowfall

Similar to the snow pit observations, simulated cold content was strongly related to cumulative precipitation in the alpine, indicating cold content developed primarily through the addition of new snowfall (Fig. 2.6a). The subalpine snowpack, however, frequently approached an isothermal state in the winter with cold content fluctuating between gains during snowfall and losses during dry periods (Fig. 2.6b). Due to this effect, cumulative precipitation in the subalpine explained less of the variance in cold content than in the alpine. Additionally, the cumulative mean of air temperature explained little of the variance in simulated cold content at both sites (Fig. 2.6c,d). In general, decreases in air temperature did not produce large increases in cold content, meaning periods of below-average air temperature did not significantly contribute to cold content development. These simulations support the results of the snow pit observations,

namely that of the two main meteorological quantities, precipitation exerts the primary control on cold content development.

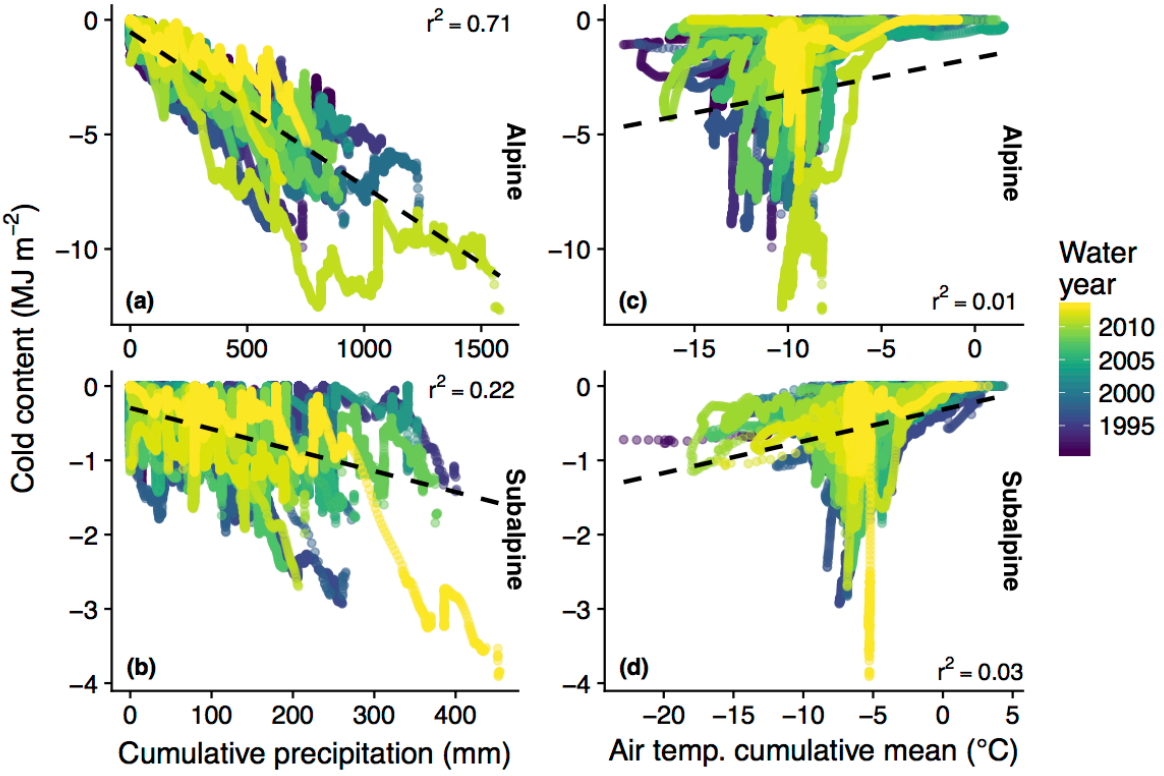

Figure 2.6. Simulated cold content plotted against cumulative precipitation in the alpine (a) and subalpine (b), and the cumulative mean of air temperature in the alpine (c) and subalpine (d). Shading denotes the corresponding water year.

Discretizing snow season days into those with and those without precipitation further clarifies the relationship between cold content development and snowfall. Figure 2.7 shows the monthly differences between days with and without precipitation in the alpine and subalpine in terms of cold content gains and losses. Precipitation days were commonly associated with cold content gains, particularly in December, January, and February when precipitation was coincident with low air temperatures. Days without precipitation, conversely, were associated with decreases in snowpack cold content, indicating a positive surface energy balance warmed the snowpack between snowfall events. Magnitudes were typically greater in the alpine where colder temperatures and increased precipitation led to greater cold content gains on snowfall

days, while higher wind speeds facilitated increased rates of energy transfer and cold content losses on days without precipitation.

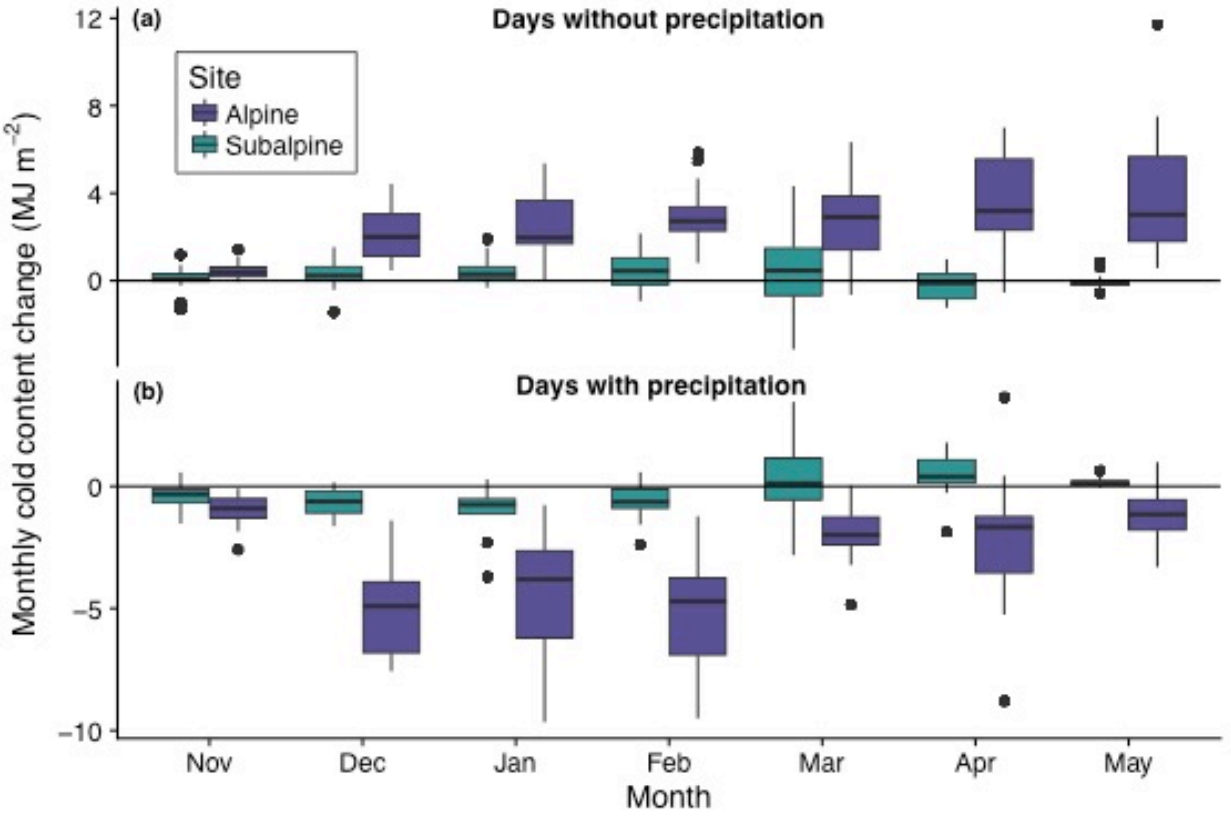

Figure 2.7. Simulated cold content gain and loss per month in the alpine and subalpine for days without precipitation (a) and days with precipitation (b). Values above the zero line correspond to a loss of cold content (i.e., cold content approaches zero), while values below correspond to a gain of cold content.

2.4.3.2 Secondary control: Negative surface energy balance

Although non-snowfall days were typically associated with cold content losses, flux-driven gains did sometimes occur on days without precipitation. On these days, Q_{net} was slightly negative, averaging -2.9 W m^{-2} in the alpine and -2.4 W m^{-2} in the subalpine, with Q_{LE} and Q_{LW} the primary negative energy balance terms at both sites (Fig. 2.8a,b). Q_H, Q_G, and Q_{SW} were typically positive, adding energy to the snowpack even during periods of increasing cold content. The majority of flux-driven cold content additions took place at night (1800 h through 0600 h), while daytime hours were commonly associated with cold content losses (Fig. 2.8c). Cold content gains between 0900 h and 1400 h accounted for less than 5% of total gains at both sites

(Appendix 2.4). In total, nighttime cold content additions outnumbered daytime additions by a 2.7:1 ratio in the alpine and 3.7:1 in the subalpine.

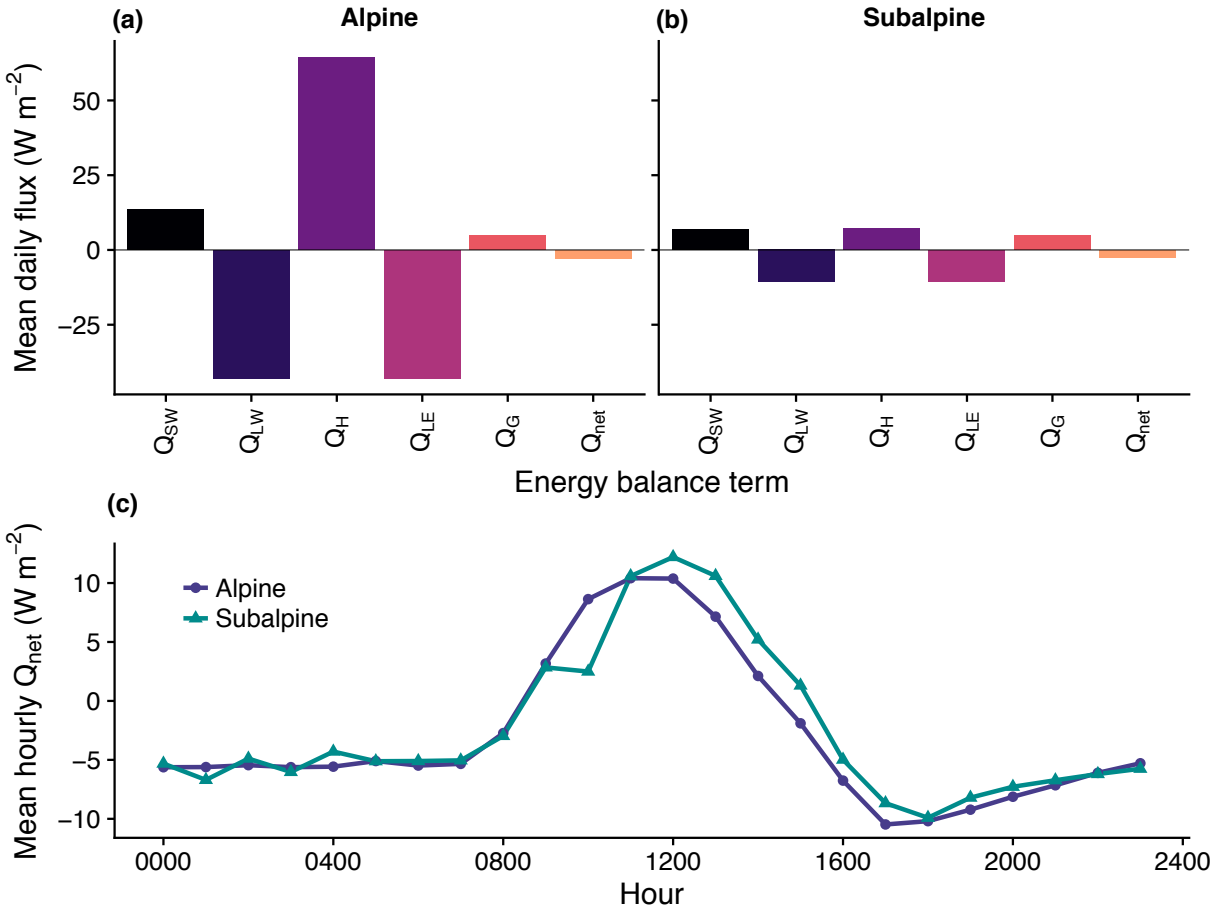

Figure 2.8. Simulated snowpack energy balance in the alpine (a) and subalpine (b), plus mean hourly $\boldsymbol{Q_{net}}$ (c) for days of cold content gain without precipitation.

2.4.3.3 Comparing the relative importance of cold content development processes

Overall, snowfall contributed more cold content to the snowpacks at each site than negative energy fluxes, while air temperature showed little relationship to cold content development. The number of snowfall days with cold content increases exceeded the number of non-snowfall days with increases in the alpine by a 4.2:1 ratio, with snowfall days responsible for 438% more cold content additions than non-snowfall days. On an average annual basis in the alpine, snowfall days contributed -12.5 MJ m^{-2} to cold content development and non-snowfall days -2.3 MJ m^{-2}. As previously noted, the effect of precipitation was smaller in the subalpine in terms of both the

variance explained by cumulative precipitation and the ratio of snowfall-to-non-snowfall cold content gains. Snowfall days in the subalpine were responsible for 166% more cold content gains than non-snowfall days, generating -4.1 MJ m^{-2} and -1.5 MJ m^{-2} of cold content development on an annual basis, respectively.

Although cumulative mean air temperature had little effect on seasonal cold content development, air temperature did influence the amount of cold content added to the snowpack per snowfall day. Figure 2.9 shows the daily change in cold content in the alpine and subalpine relative to daily total precipitation (a,b), and cold content from precipitation (c,d) on days with snowfall. Here the cold content from precipitation was calculated as in Eq. 2.2 but T_S was replaced with air temperature and d_S was replaced by the depth of precipitation. At both sites, the cold content from precipitation explained more of the variance in daily change in cold content than daily total precipitation alone, showing air temperature provides a secondary control on cold content development during snowfall events. Confirming previous results, the control exerted by precipitation on cold content development was stronger in the alpine than subalpine.

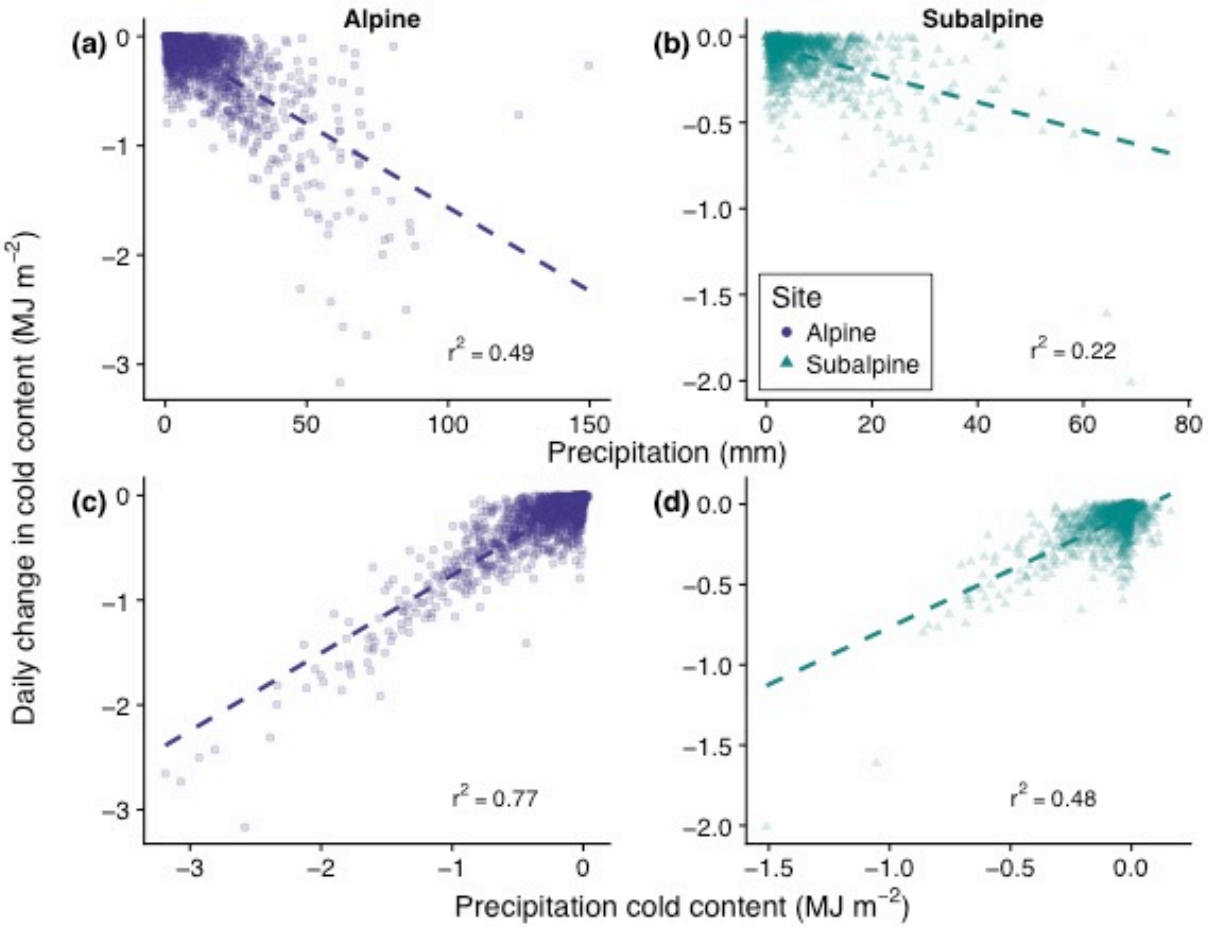

Figure 2.9. Simulated daily change in cold content plotted against daily precipitation in the alpine (a) and subalpine (b), and cold content from precipitation in the alpine (c) and subalpine (d).

2.4.3.4 The effect of cold content on snowmelt rate and timing

On seasonal time scales, increased annual peak cold content magnitude had a delaying, but statistically non-significant effect on snowmelt onset, according to both observations and simulations (not shown). However, using the 23 y of snowpack simulations, we found the date of peak cold content and spring precipitation—defined here as the total precipitation between the date of peak cold content and peak SWE—accurately predicted melt onset. A multiple linear regression (MLR) using the date of peak cold content and spring precipitation as the predictor variables explained 84.7% and 61.4% of the variance in snowmelt onset in the alpine and subalpine, respectively (Fig. 2.10). At both sites, later peak cold content and increased spring precipitation delayed melt onset. In the alpine, the MLR predicted a 1 d delay in snowmelt

timing per 1.6 d later in peak cold content timing or 8.8 mm extra spring precipitation. These values shifted to 2.3 d and 5.9 mm, respectively, in the subalpine. Furthermore, we found cold content exerted no statistically significant control on the seasonal snowmelt rate. Rather, statistically significant increases in the ablation slope were associated with later peak SWE timing and increased peak SWE magnitude.

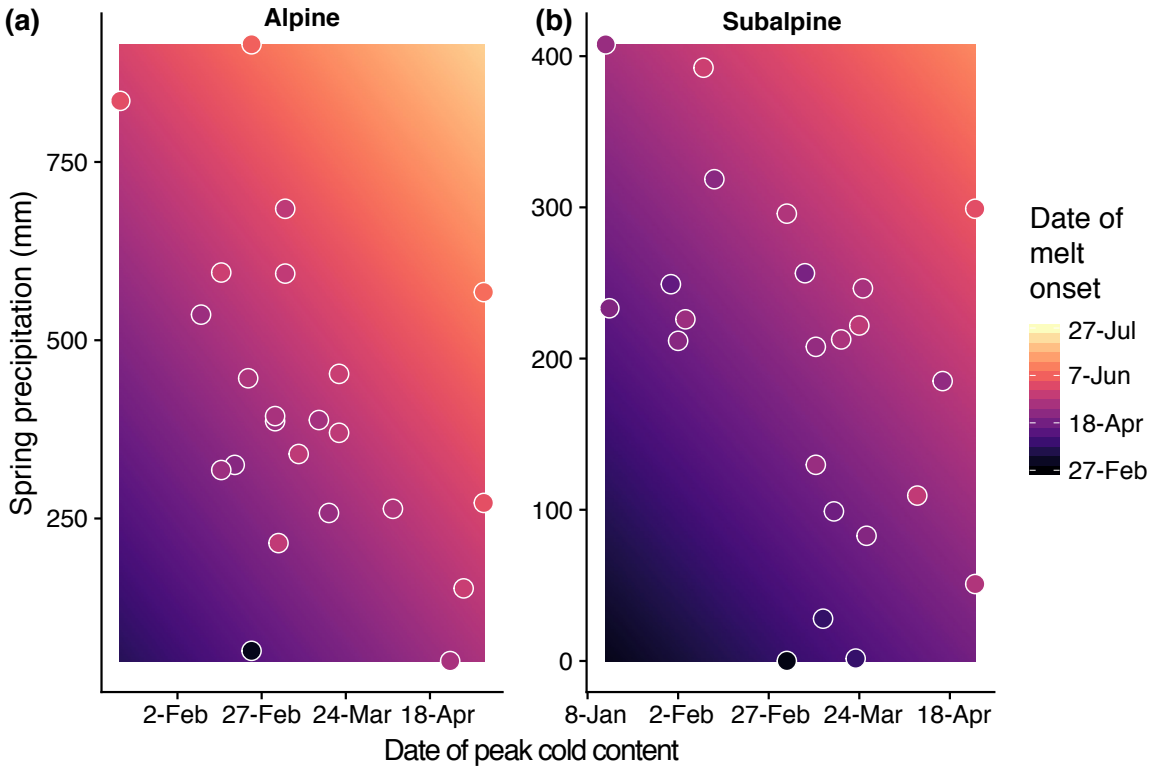

Figure 2.10. Annual melt onset as predicted by peak cold content timing and spring precipitation in the alpine (a) and subalpine (b). The background gradient in each plot displays the predicted melt onset date as calculated by a multiple linear regression, while the shading within each point represents the actual melt onset simulated in a given water year at its peak cold content date and spring precipitation value.

While peak cold content magnitude exerted little control on seasonal snowmelt timing and rate, the simulations indicated increased cold content had a damping effect on snowmelt timing and rate at sub-seasonal time scales from 1 d to 30 d. Greater initial cold content values were associated with decreased snowmelt rates (Fig. 2.11a,b) and longer delays between day zero and the day of first snowmelt (Fig. 2.11c,d). All relationships were significant at the 99% level, except for the effect of cold content on snowmelt timing for the 1 d time window in the

subalpine. Simulated melt rates in the alpine only exceeded 40 mm d^{-1} when initial cold content was between -0.1 MJ m^{-2} and 0 MJ m^{-2}. The same initial cold content range was responsible for all simulated melt rates greater than 15 mm d^{-1} in the subalpine. Examining only the 30 d window for snowmelt timing revealed further patterns at the two sites. Initial cold content explained 47.3% of the variance in time to first melt in the alpine and 37.6% in the subalpine using ordinary least squares regression. An initial cold content increase of 1.0 MJ m^{-2} led to a 3.7 d delay in snowmelt in the alpine and 12.1 d in the subalpine.

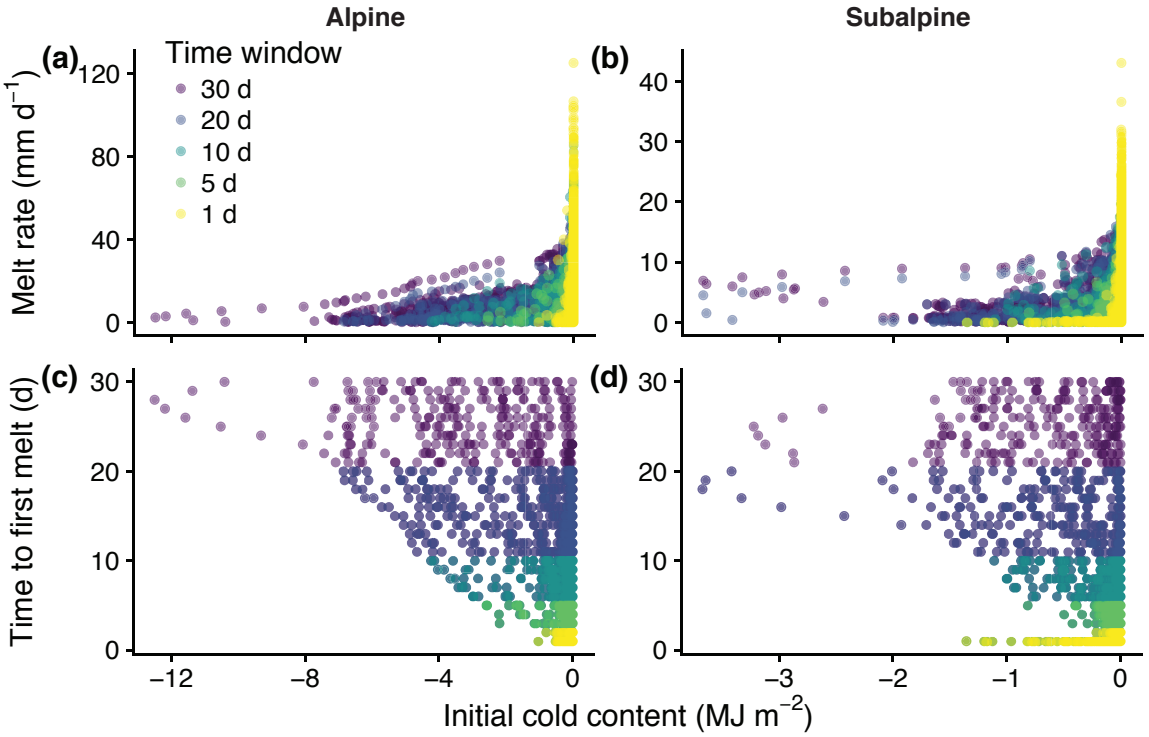

Figure 2.11. Simulated sub-seasonal snowmelt rate plotted against initial cold content in the alpine (a) and subalpine (b), and time to first melt plotted against initial cold content in the alpine (c) and subalpine (d) for time windows from 1 d to 30 d.

To examine the control of cold content on daily snowmelt rate and timing, we used CC_{6am} to represent the energy state of the snowpack at time t = 0 for each day. Figure 2.12a,b shows melt rates did not increase until CC_{6AM} neared 0 MJ m^{-2} in the alpine and subalpine. Both the number of melt days and the daily melt rate were greater when CC_{6AM} = 0 MJ m^{-2}. The

proportion of daily melt occurring on days when $CC_{6AM} = 0$ MJ m^{-2} ranged from 75.0% in the alpine to 79.5% in the subalpine. Mean melt rates were also greater when there was no energy deficit to satisfy in the alpine (21.1 vs. 14.3 mm d^{-1}) and subalpine (9.7 vs. 6.2 mm d^{-1}). Additionally, non-zero CC_{6AM} values were associated with delayed snowmelt onset (Fig. 2.12c,d). The mean time between 6AM and simulated snowmelt onset was 2.3 h in the alpine and 2.8 h in the subalpine when $CC_{6AM} = 0$ MJ m^{-2}. These values shifted to 5.7 h and 6.7 h, respectively, when $CC_{6AM} \neq 0$ MJ m^{-2}. Thus the presence of cold content produced a 3.4 h delay in alpine snowmelt onset and 3.9 h in the subalpine. These data indicate that even small energy deficits had a damping effect on daily snowmelt rate and timing.

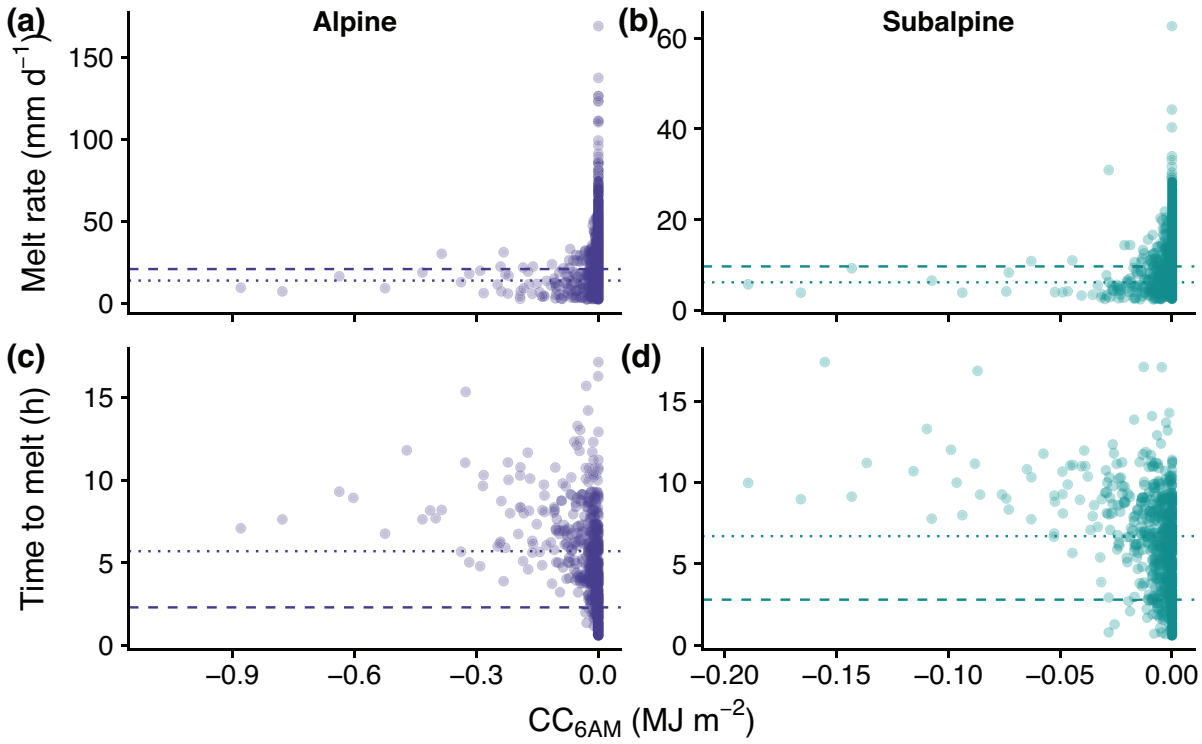

Figure 2.12. Simulated daily melt rates in the alpine (a) and subalpine (b) and time to snowmelt in the alpine (c) and subalpine (d) as a function of CC_{6AM}. The dashed line in each figure represents the mean melt rate (a,b) and time to melt (c,d) for days when $CC_{6AM} = 0$ MJ m^{-2} and the dotted line represents those quantities for days when $CC_{6AM} < 0$ MJ m^{-2}.

2.5 Discussion

2.5.1 Representation of cold content development processes in snow models

In Sect. 2.1 we noted the three main methods by which cold content is represented in snow models. Temperature index models typically compute cold content as an empirical function of air temperature (method 1), while physical models estimate cold content as a function of precipitation and the air temperature during precipitation (method 2) and/or as a residual of the snowpack energy balance (method 3). A model comparison is outside of the scope of this work, but the results presented above suggest method 2 was the primary pathway through which cold content developed at our continental, mid-latitude alpine and subalpine sites. We found air temperature had little influence on cold content development except when included as a variable in computing the cold content of new snowfall. Prior work from the subalpine site of the Niwot Ridge LTER showed a weak relationship between low air temperatures and snowpack cooling and that periods of snowpack cooling were generally coincident with clear skies and longwave emission from the snowpack (Burns et al., 2014). Thus, method 1 would likely misrepresent cold content development processes and incorrectly estimate cold content magnitude at our sites due to the irreplaceable role of snowfall in cold content development.

Based on first principles, method 3 is important in that cold content is an integration of both mass (i.e., snowfall) and energy balance processes. Due to high sublimation rates and a dry, cold climate, the alpine site should have a high potential to gain cold content through Q_{LE} and Q_{LW}. However, our results showed that daily energy balance cold content gains were small in comparison to those from snowfall. We also found no evidence in either the simulations or observations of consistent, large negative energy balances producing cold content. Rather, the energy balance was typically near zero before peak SWE and only became significantly positive

once melt commenced. Days with a negative surface energy balance were generally associated with nighttime cooling from Q_{LE} and Q_{LW}, with Q_{net} small in magnitude, averaging > -3.0 W m^{-2}. Marks and Winstral (2001) similarly noted the simulated energy balance in a semi-arid mountain basin was generally near 0 W m^{-2} until the melt season. Overall, these findings imply snowpack cold content development at our study locations is primarily a function of method 2 and that large flux-driven increases in cold content are unlikely, even in areas where the energy balance plays a larger relative role (e.g., the subalpine site studied here).

2.5.2 Sources of model uncertainty

Recent years have seen an increase in the number of papers leveraging physics-based models to quantify snowpack processes. To complement such work, researchers have also evaluated sources of snow model errors and biases (Clark et al., 2017; Essery et al., 2013; Lapo et al., 2015; Raleigh et al., 2016, 2015; Rutter et al., 2009). The preceding literature concludes physics-based snow models must: 1) Have accurate, quality controlled forcing data; 2) Be validated on at least one snowpack state variable, but preferably more; and 3) Have physics that accurately reflect snowpack processes. This study has followed these practices through: 1) A rigorous, hierarchical quality control and infilling forcing data protocol; 2) SWE, cold content, and snowpack temperature validation data from multiple years of snow pit observations; and 3) Use of the widely validated, physics-based SNOWPACK model. Despite our adherence to such protocols, there are still significant sources of uncertainty inherent to model-based snow studies.

Snow model intercomparison work has consistently shown there is no one best model and that model performance varies between and within sites and water years (e.g., Boone and Etchevers, 2001; Essery et al., 2013; Etchevers et al., 2004; Rutter et al., 2009; Slater et al., 2001). This body of research acknowledges that all models imperfectly represent snow cover

evolution and the snowpack energy balance. One example shortcoming of SNOWPACK relevant to the work presented herein is that the temperature of new snow is set to be equal to air temperature despite the fact that hydrometeor temperature is more accurately estimated as a function of the psychrometric energy balance (e.g., Harder and Pomeroy, 2013). Using the psychrometric approach gives snowfall a temperature near the wet bulb temperature, which is lower than air temperature when relative humidity is under 100% (Harder and Pomeroy, 2013). Thus, the temperature of new snow is likely to be overestimated by SNOWPACK, while cold content additions are underestimated. This means our computation of the total cold content contributed by precipitation is likely on the conservative side as using the wet bulb temperature would lead to increased cold content gains during snowfall.

Another source of uncertainty in our work is the use of an empirical method to estimate incoming longwave radiation as a function of air temperature, relative humidity, and incoming shortwave radiation (Appendices 2.1 and 2.2). Recent research has shown errors in incoming longwave radiation propagate into SWE, snow surface temperature, and energy balance biases (Lapo et al., 2015; Raleigh et al., 2016). We aimed to reduce the error in our incoming longwave radiation estimates by using the recommended clear sky and cloud correction protocols for Niwot Ridge (Flerchinger et al., 2009). At both the alpine and subalpine site, the mean biases were within the instrument range of error when compared to shorter-term observations, indicating the total estimated amount of incoming longwave radiation was acceptable. However, the low r^2 of the hourly estimates suggests the sub-daily fluctuations of incoming longwave radiation were not well simulated. Despite these issues, model performance was high in terms of simulated SWE, depth-weighted snowpack temperature, and cold content (Sect. 2.4.2). This may due to compensatory errors in the model (Etchevers et al., 2004; Kirchner, 2006) or because

SNOWPACK is relatively insensitive to the choice of incoming longwave radiation estimate (Schlögl et al., 2016).

Additionally, we had no long-term ground surface temperature data to force the model, so we used the SNOWPACK default value of 0°C. This produced mean Q_G values of 2.0 W m^{-2} and 0.8 W m^{-2} during periods of SWE > 1 cm in the alpine and subalpine, respectively. Previous work from the Niwot Ridge LTER using a heat flux plate indicated Q_G in the alpine to be negligible (Cline, 1997a), while other researchers showed the upper layer of alpine soil could approach temperatures significantly below freezing during periods of shallow snow cover (Brooks and Williams, 1999). Therefore, the SNOWPACK-simulated alpine Q_G is likely an overestimate. In the subalpine, the soil temperature at 5 cm below the surface is typically between -1°C and 0°C during the winter (Burns et al., 2014), meaning the use of the default 0°C ground surface temperature is reasonably in agreement with shorter term observations.

2.5.3 Differences between cold content development controls in the alpine and subalpine

Despite only a 506 m elevation difference between the two sites, the role of a negative energy balance in developing cold content in the subalpine was approximately double that of the alpine. Simulations of snowpack temperature indicated the increased sensitivity was likely due to the shallower subalpine snow depth. Diurnal snowpack temperature range generally decreases with depth (e.g., Burns et al., 2014; DeWalle and Rango, 2008; Sturm et al., 1995) and our simulations showed daily fluctuations to be largest in the snowpack's upper layers, converging towards 1.0°C as depth exceeded 500 mm (Fig. 2.13). This is the same depth at which the insulating effects of snow on soil temperature become marginal (Slater et al., 2017). Likely this is because the penetration of incoming shortwave radiation and sensible heat transfer through windpumping are limited to the top portion of the snowpack (Albert and McGilvary, 1992;

Colbeck, 1989a, 1989b; Lehning et al., 2002a), while the low thermal conductivity of snow modulates energy transfer below the active upper layers (Sturm et al., 1997). In this case, proportionally more of the shallower subalpine snowpack was interacting with surface energy exchange, making it more sensitive to positive and negative fluxes. Furthermore, subalpine cold content was consistently lower in magnitude, meaning it took less energy input to drive cold content to zero and relative fluctuations were larger. Therefore, shallower snowpacks with reduced cold content, like those in the subalpine, are more susceptible to relatively rapid changes in internal energy from surface energy fluxes.

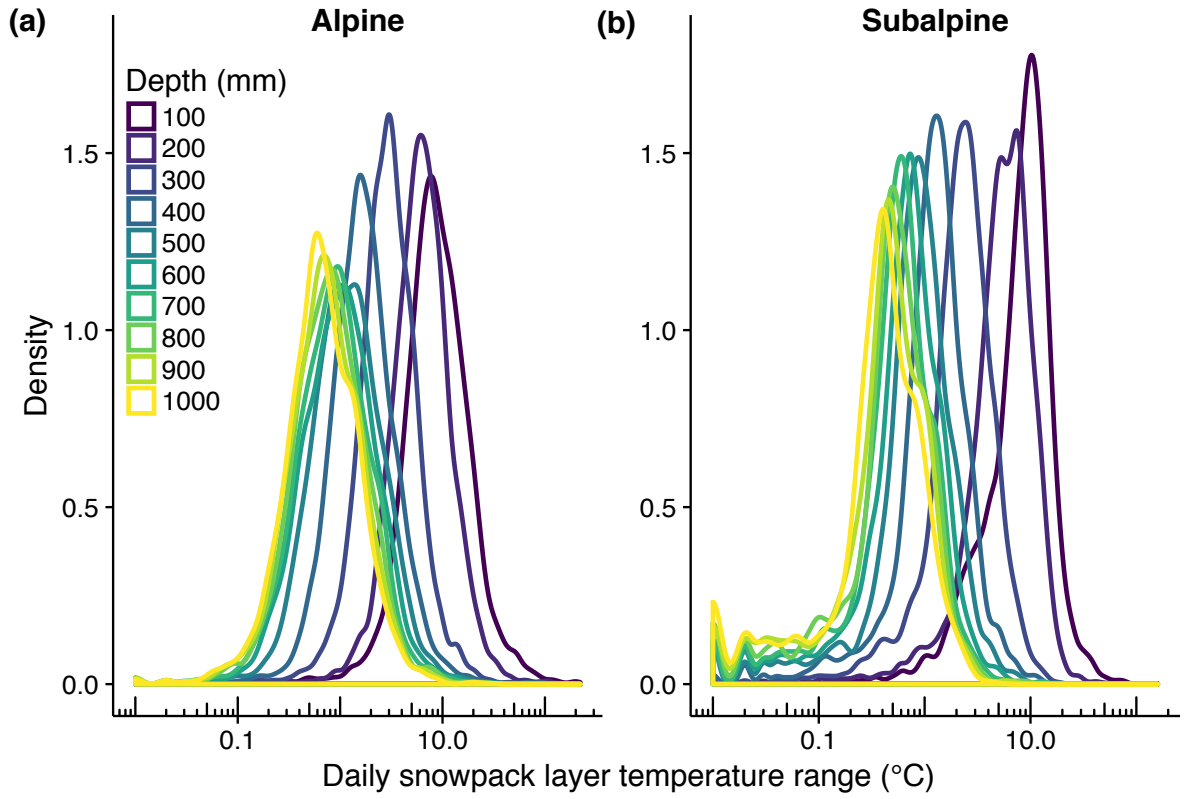

Figure 2.13. Kernel density estimates of simulated daily snowpack layer temperature ranges in the alpine (a) and subalpine (b). Line shading represents the bottom depth of the layer with layers near the top of the snowpack in purple and blue and lower layers in green and yellow.

2.5.4 Other controls on seasonal snowmelt timing and rate

Previous research has suggested uncertainty in the degree to which cold content controls snowmelt timing at daily to seasonal time scales. In our research, we found no statistically significant relationship between peak cold content magnitude and seasonal snowmelt onset using data from both observations and simulations. Rather, the majority of the variance in seasonal snowmelt onset was explained by the timing of annual peak cold content and total spring precipitation. Later peak cold content generally occurred due to cold spring storms depositing significant snowfall. If such events were then followed by continued snowfall, then snowmelt timing was delayed. Meanwhile, seasonal snowmelt rate, or the ablation slope, was primarily controlled by peak SWE magnitude and timing, with greater, later peak SWE corresponding to more rapid snowmelt.

These results all suggest later seasonal snowmelt onset and faster snowmelt rates are primarily a function of persistent snowfall. While snowfall events can add significant cold content to the snowpack, they also change other fundamental properties that can delay snowmelt timing, such as increasing surface albedo (Clow et al., 2016) and adding dry pore space that must be saturated (Seligman et al., 2014). Other research shows seasonal snowmelt onset is also related to air temperature (Kapnick and Hall, 2012) and snow surface impurities (Painter et al., 2010; Skiles et al., 2012). Although much work has been done evaluating the empirical controls exerted by snowpack and climatic properties on snowmelt rate and timing across large spatial extents (e.g., Trujillo and Molotch, 2014), relatively little research has been done at such scales on the physical processes (e.g., cold content and the snowpack energy balance). Given the importance of seasonal snowmelt timing to water resources management and various hydrologic processes, future synthesis work should evaluate the effect of physical processes on snowmelt

rate and timing across snow-dominated regions globally, leveraging both field observations and physics-based snow model simulations.

2.5.5 Cold content development processes in other seasonal snow classes and climates

Despite the research presented here, there are still unanswered questions regarding cold content development as well as its effect on snowmelt rate and timing. Firstly, we have only presented results from two sites within a single snow-dominated research catchment. Seasonal snow cover in the western United States spans a large elevation gradient and includes both maritime (e.g., the Cascades and Sierra Nevada) and continental (e.g., the Rocky Mountains) snowpack regimes (Armstrong and Armstrong, 1987; Serreze et al., 1999). Globally, seasonal snow cover includes an even greater number of classes, including the cold, thin snowpacks of the Arctic and the Canadian Prairies (Sturm et al., 1995). Therefore, an avenue for future research is to examine differences in cold content development across seasonally snow covered areas, with a particular focus on disentangling the effects of precipitation and air temperature during snowfall at sites with different snowpack characteristics. For example, snowpacks in California's Sierra Nevada are typically deep, but air temperature is generally near freezing, even during winter storm events. Considering the cold content of precipitation is a linear function of air temperature and precipitation depth (Eq. 2.2), a given unit of snowfall in the Sierra Nevada should contribute less snowpack cold content than that same unit in the colder Rocky Mountains. Therefore, the control that precipitation exerts on cold content development is likely different between the two locations. Additionally, it is uncertain how our results translate to cold, shallow tundra and taiga snowpacks. In this study, we observed marked differences in cold content development processes between the alpine and subalpine, with the energy balance exerting greater control in the

shallower subalpine snowpack. It may be that the energy balance is of even greater importance in tundra and taiga snowpacks, but further work is needed.

Secondly, a large amount of recent literature has shown unequivocally that, due to climate warming, patterns of snow accumulation and melt are changing across the globe with resultant effects on myriad hydrologic processes (Barnhart et al., 2016; Berghuijs et al., 2014; Knowles et al., 2006; Mote et al., 2005; Musselman et al., 2017a; Pederson et al., 2011b; Stewart, 2009). It is uncertain what role, if any, cold content plays in the climate-driven changes on snow processes. In our investigations we found pit-observed SWE was a strong predictor of cold content (alpine $r^2 = 0.84$; subalpine $r^2 = 0.50$), with subalpine cold content lower per unit SWE due to warmer depth-weighted snowpack temperatures. Both sites also exhibited a significant positive linear relationship between the cumulative mean of air temperature and snowpack temperature. Therefore, a unit of SWE in a warmer location or climate should correspond to reduced cold content due to increased snowpack temperature. Our work showed that decreased cold content magnitudes corresponded to faster snowmelt rates and earlier snowmelt timing at time scales less than 1 month. Therefore, reductions in snowpack cold content due to climate warming have implications for meltwater timing and availability, which could impact water resources management.

2.6 Conclusions

We have presented an analysis of snowpack cold content using data from a long-term snow pit record and 23 y of physics-based snow model simulations at an alpine and subalpine site within the Niwot Ridge LTER. The research questions were designed to fill important missing gaps in the snow hydrology literature, namely the meteorological and energy balance processes behind cold content development and how cold content controls snowmelt rate and timing. Observations

and simulations showed new snowfall was the primary pathway for cold content development at our sites, being responsible for 84.4% and 73.0% of modeled daily cold content gains in the alpine and subalpine, respectively. Snowfall days with cold content gains outnumbered non-snowfall days with gains by a 4.2:1 ratio in the alpine and 2.6:1 in the subalpine. A negative energy balance—averaging > -3.0 W m^{-2} in the alpine and subalpine—was responsible for the remainder of cold content gains, primarily due to the cooling effect of sublimation and net longwave emissions. At subdaily time scales, dry-period cold content increases occurred preferentially at night at both sites. We found no evidence in either the snow pit record or the simulation data for large negative energy fluxes generating significant snowpack cold content. Additionally, air temperature showed little to no relationship to cold content development at either of the sites we studied.

Seasonal snowmelt timing was not significantly correlated with peak cold content magnitude, but rather the timing of peak cold content and total spring precipitation controlled snowmelt onset. Later peak cold content and increased spring precipitation delayed snowmelt in both the alpine and subalpine, explaining 84.7% and 61.4% of the variance in peak SWE timing. Cold content magnitude did affect sub-seasonal snowmelt in that non-zero initial cold content values corresponded to delayed snowmelt timing and slower snowmelt rates. At daily time scales, the majority of melt events and the fastest melt rates occurred only when CC_{6AM} = 0.0 MJ m^{-2}. Any existing energy deficit at 6AM damped daily snowmelt rates.

The Niwot Ridge LTER provided the ideal study location for the research presented in this paper. The site's unique long-term snow pit and hourly meteorological records facilitated in-depth analyses into snowpack processes using both observations and physics-based snow model simulations. Lacking either data source would have limited the scope of this paper and added

further uncertainty. Therefore, we hope this work underlines the utility of long-term *in situ* snowpack and meteorological measurements as they allow for robust analyses on the observations themselves and also enable model validation on multiple snowpack properties (e.g., mass, depth-weighted temperature, and cold content), which improves the quality of simulated output.

2.7 Appendices

2.7.1 Appendix 2.1: Meteorological data quality control and infilling

The quality control routine for all observation types except precipitation followed the three-step procedure outlined in Meek and Hatfield (1994) where observations were flagged for removal if: 1) they fell outside of a prescribed minimum-maximum range for that day of year; 2) their hourly rate of change exceeded a given threshold; 3) the same value was recorded in four consecutive time steps, indicating a stuck sensor. A full description of the protocol for each variable falls outside the scope of this paper, but can be viewed in Meek and Hatfield (1994). The only changes made to their schema were applied to better represent climate processes on Niwot Ridge, particularly the high variability in hourly air temperature and wind speed common at dry, high-elevation, mountainous, continental locations. These modifications allowed more valid observations to pass the quality control checks than the original Meek and Hatfield (1994) protocol.

Following the quality control procedure, missing observations were imputed using a hierarchical routine based on the work of Liston and Elder (2006), Kittel (2009), and Henn et al. (2012), where gaps of 72 h and shorter were infilled using temporal techniques and longer gaps were infilled using a multi-station regression. Data gaps of 1 h were filled using a linear interpolation between the observations directly preceding and following the missing value. Gaps

between 2 h and 24 h were filled using an average of the value recorded 24 h prior and 24 h after the missing observation. Gaps between 25 h and 72 h were filled using a forecasted and back-casted autoregressive integrated moving average (ARIMA) model with imputed values linearly weighted by their temporal distance from the beginning/end of gap. Data gaps longer than 72 h, plus shorter gaps that could not be filled using the temporal protocol due to missing data, were infilled with a one- or two-station regression. We pursued this approach because each station collected the same required forcing data for SNOWPACK and the three stations were located within 7 km of one another (Fig. 2.1). If the two remaining stations were reporting valid observations, then the two-station regression was used. Otherwise, the one-station regression was employed. Regression equations were generated for each variable per month and 3 h time block where a day is divided into eight 3 h periods (e.g., 00:00–03:00, 03:00–06:00, etc.). Although such an approach neglects the spatial variability inherent to meteorological processes in complex terrain, the values generated by the regressions reproduce changes in conditions due to frontal passages and storm events. For periods when no stations were reporting, data were infilled using the mean value for the given station, variable, month, and 3 h time block.

Quality controlled, gap-filled relative humidity, air temperature, and incoming solar radiation measurements were used to generate two estimates of incoming longwave radiation at an hourly time step. The equations presented in Angström (1915) and Dilley and O'Brien (1998) were used to estimate clear sky atmospheric emissivity based on vapor pressure, which was calculated from relative humidity. Flerchinger et al. (2009) noted these two methods performed best at the subalpine site on Niwot Ridge relative to observations from the co-located AmeriFlux tower. Emissivity was then corrected for estimated cloud cover based on the ratio of observed solar radiation to maximum clear sky solar radiation using the approach of Crawford and Duchon

(1999). Finally, incoming longwave radiation was calculated using the Stefan-Boltzmann equation:

$$LW\downarrow = \epsilon\sigma T_a^4 \quad (2.5)$$

where $LW\downarrow$ is incoming longwave radiation (W m^{-2}), ϵ is the estimated atmospheric emissivity (dimensionless, 0 to 1), σ is the Stefan-Boltzmann constant (5.67×10^{-8} W m^{-2} K^{-4}), and T_a is air temperature (K).

Measuring solid precipitation is inherently difficult, particularly at higher wind speeds (Rasmussen et al., 2012; Yang et al., 1999) and snowpack simulations are reliant on accurate precipitation input to produce reliable output (Raleigh et al., 2015; Schmucki et al., 2014). Thus, any snow modeling project has the compounded problem of requiring accurate precipitation forcings and sensitivity to said forcings. For this study, two primary precipitation data sources were utilized along with site-specific gage corrections as described below.

Alpine precipitation data came from the quality controlled LTER dataset (http://niwot.colorado.edu/index.php/data/data/precipitation-data-for-saddle-chart-recorder-1981-ongoing). While snowfall undercatch is commonly documented in the literature, Williams et al. (1998) showed blowing snow events lead to significant overcatch at the LTER alpine precipitation gage from October through May. To correct the overcatch we created monthly precipitation reduction factors by comparing cumulative precipitation from the date of each snow pit observation to the following snow pit observation to the change in SWE between those observation dates when the change in pit SWE was positive. We found overcatch was greatest in months where Berg (1986) reported the highest frequency of blowing snow events (January, March—average reduction = 0.59) and lowest in months with fewer blowing snow events (December, February, April—average reduction = 0.86).

Subalpine precipitation data came from the quality controlled, gap-filled Kittel et al. (2015) dataset with further corrections applied for snow undercatch relative to the Niwot SNOTEL snow pillow during snowfall events, which averaged 2.1 mm per snowfall day. Air temperature during precipitation events showed the strongest control on undercatch with decreasing air temperature corresponding to increased negative precipitation biases. Notably, wind speed was not correlated with undercatch at the subalpine gage, likely due to the siting of the anemometer. This instrument is located 5 m above ground level in a roadside clearing and is generally unrepresentative of the wind speed magnitude in the dense subalpine forest where the snow pit, LTER precipitation gage, and Niwot SNOTEL station are located. Compared to the subalpine snow pit, accumulated precipitation in the gage was on average 88.3 mm or 32.3% lower than observed maximum SWE.

Daily precipitation observations from both datasets were temporally disaggregated to the hourly time step of SNOWPACK by dividing the daily total by 24 and equally distributing the values to each hour of the day. Hourly precipitation observations were not available, and therefore a more advanced disaggregation method was not pursued.

2.7.2 Appendix 2.2: Meteorological data infilling validation

Missing observations and measurements failing the quality control checks were more common in the alpine than subalpine (Table 2.4). The variable with the greatest number of missing values was solar radiation in the alpine due to a long instrument outage period in the 2000s. The multi-station regression was the most utilized infilling technique (temporal infilling accounted for, at most, 3.0% of the missing data) and cross-validation statistics are presented in Table 2.4. Generally, infilling performance was greater in the alpine due to the close proximity

of the high alpine meteorological station. Of the forcing variables, air temperature exhibited the highest infilling performance and wind speed the lowest.

Table 2.4. Cross-validation statistics for the multi-station regression infilling procedure for air temperature (T_a, °C), total incoming solar radiation (SW_{in}, MJ m^{-2}), wind speed (VW, m s^{-1}), and dew point temperature (T_d, °C). Note: Relative humidity values were converted to T_d for computing the multi-station regression.

Site	Variable	Missing Obs. (%)	Mean Bias	RMSE	r^2
Alpine	T_a	8.2	2.8×10^{-3}	1.6	0.97
	SW_{in}	25.3	-4.4×10^{-2}	0.4	0.83
	VW	6.0	-0.5	3.2	0.69
	T_d	6.9	-1.3	3.7	0.84
Subalpine	T_a	3.8	-6.4×10^{-2}	3.5	0.86
	SW_{in}	2.9	-4.8×10^{-2}	0.6	0.67
	VW	3.6	-0.3	2.1	0.30
	T_d	3.6	-2.9	4.7	0.81

Estimates of incoming longwave radiation exhibited low biases relative to shorter-term observations taken near the alpine and subalpine meteorological stations. In the alpine, measurements of incoming longwave radiation were taken at the Subnivean Laboratory from 1996 through 2008 and intermittently in more recent years. Here, the Dilley and O'Brien (1998) equation produced the best results relative to the observed data with a mean bias of 4.9 W m^{-2}. In the subalpine, the mean bias relative to Ameriflux observations (1999-07-12 through 2013-12-31) was 10.4 W m^{-2} with the Angström (1915) estimate providing the best match. The positive biases in the alpine and subalpine represented 2.0% and 4.1%, respectively, of the average hourly observed incoming longwave radiation, values which were within the manufacturer-reported precision range of ±10% for the Kipp and Zonen CG2 net pyrgeometer at the Subnivean Laboratory and the CNR1 net radiometer at the AmeriFlux tower. The coefficient of determination for hourly and daily incoming longwave values were 0.51 and 0.72, respectively, in the alpine and 0.44 and 0.60 in the subalpine.

2.7.3 Appendix 2.3: Snow pit observations

Table 2.5. Information on the time range and number of snow pit observations per water year at the alpine and subalpine sites in the Niwot Ridge LTER.

Site	Water year	Start	End	Total
Alpine	1995	1995-01-24	1995-07-05	21
	1996	1996-01-19	1996-06-21	20
	1997	1997-01-24	1997-06-30	20
	1998	1998-01-20	1998-06-22	18
	1999	1999-01-20	1999-06-22	15
	2000	2000-01-14	2000-06-06	17
	2001	2001-01-16	2001-06-05	15
	2002	2001-12-10	2002-03-25	10
	2003	2002-11-13	2003-06-18	15
	2004	2003-12-12	2004-06-07	18
	2005	2005-02-01	2005-06-21	12
	2006	2006-01-24	2006-06-06	11
	2007	2007-02-09	2007-05-10	4
	2008	2008-02-22	2008-06-17	7
	2009	2008-12-31	2009-06-25	18
	2010	2010-01-11	2010-06-09	21
	2011	2010-12-07	2011-07-06	21
	2012	2012-01-24	2012-05-23	16
	2013	2013-01-03	2013-06-10	13
Subalpine	2007	2007-02-07	2007-05-23	15
	2008	2007-12-20	2008-05-27	18
	2009	2008-12-22	2009-05-07	17
	2010	2009-10-28	2010-06-02	25
	2011	2010-12-15	2011-06-21	28
	2012	2011-11-15	2012-04-25	21
	2013	2012-12-13	2013-05-29	23

2.7.4 Appendix 2.4: Negative energy balance temporal distribution

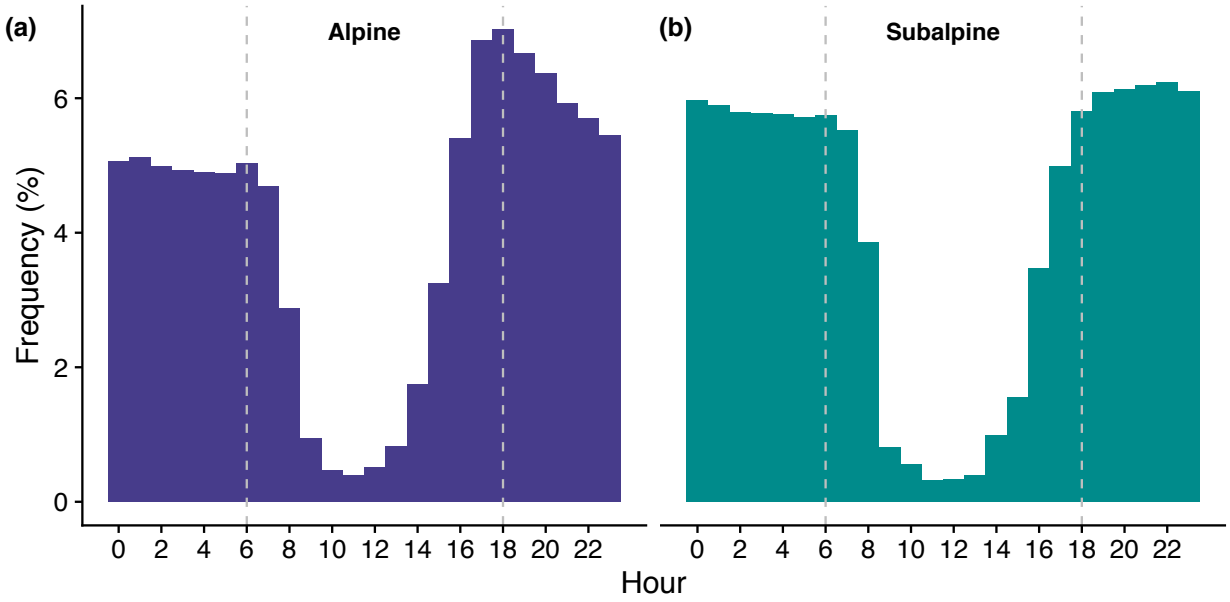

Figure 2.14. Histograms showing the timing of simulated cold content gains without snowfall in the alpine (a) and subalpine (b). The vertical dashed lines demarcate day (0600–1800 h) and night (1900–0500 h) at the two sites. Cold content gains occurred primarily at night, while daytime gains were concentrated in the early morning and evening hours. Less than 5.0% of simulated cold content gains occurred between 0900 and 1400 h at both sites.

Chapter 3

3 Evaluating the differential response of an alpine and subalpine snowpack to changes in climate

Abstract

Although future warming is expected to be widespread, climate change is predicted to have spatially variable effects on mountain snowpacks of the western United States. Past work has identified the areas likely to be most impacted by air temperature increases, but little is known about the physical controls on the differential response. For this study, we focused on two well-instrumented locations within the Niwot Ridge Long Term Ecological Research site to examine how changes to air temperature, total precipitation, and precipitation seasonality affect snow cover evolution. For our analysis, we created a 23 y baseline simulation using the SNOWPACK model forced by historical hourly meteorological data at an alpine and subalpine site from water year 1991 through 2013. We then perturbed air temperature, total precipitation, and precipitation seasonality independently to identify physical controls on the response to changes in climate. We found the alpine snowpack was less sensitive to increases in air temperature for three primary reasons: 1) Snowfall fraction decreased less rapidly with warming than in the subalpine; 2) Significant cold content was still added to the snowpack throughout the snow season, preventing mid-winter melt events; 3) Changes to snowmelt rate were non-significant because increases to the turbulent fluxes balanced decreases in the radiative fluxes with earlier melt onset. Additionally, at 3°C of warming and greater, the subalpine site experienced a fundamental shift where significant melt could occur throughout the entirety of the winter. Changes to total precipitation led to significant, but relatively consistent results at the two sites with later melt

onset and faster snowmelt rates being associated with increased precipitation. Changes to precipitation seasonality had a near-negligible impact on snow cover properties at both sites.

3.1 Introduction

Climate warming has altered patterns of snow accumulation and melt throughout the seasonal snow zone in the western United States. Increasing winter air temperatures have led to a reduced percentage of precipitation falling as snow (Knowles et al., 2006) and decreased snow water equivalent (SWE) accumulation (Clow, 2010; Harpold et al., 2012; Mote et al., 2018, 2005). Many areas have also seen a shift to earlier snowmelt onset (Clow, 2010; Regonda et al., 2005; Stewart et al., 2004b) and changes to seasonal melt patterns have impacted streamflow production (Regonda et al., 2005; Stewart, 2009; Stewart et al., 2005). In addition to the critical link between snowmelt and streamflow, there are other impacts of snow cover loss to consider in a warming world: the timing and magnitude of soil moisture fluctuations (Harpold and Molotch, 2015), soil temperature and microbial respiration (Blanken et al., 2009; Brooks and Williams, 1999; Groffman et al., 2006), forest greenness (Knowles et al., 2018; Trujillo et al., 2012), and water uptake and carbon sequestration by vegetation (Winchell et al., 2016), among many others. There is therefore considerable concern that future changes to snowpacks will have myriad impacts on mountain ecosystems worldwide.

Complicating the matter is the observation that the response of mountain snowpacks to rising air temperatures has been non-linear, although past warming has been prevalent across the entire western United States (Abatzoglou, 2011; Harpold et al., 2012; Harpold and Brooks, 2018; Kapnick and Hall, 2012; Mote et al., 2018, 2005). This has meant a unit increase in air temperature has not been associated with a spatially uniform change in various snowpack metrics (e.g., peak SWE, snowmelt onset, and snowmelt rate). Most previous work has ascribed the

variability of the snow accumulation and melt response to climate warming to empirical factors such as air temperature and/or elevation (Kapnick and Hall, 2012; Knowles et al., 2006; Mote et al., 2018). Generally, snowpacks in middle elevations with winter air temperatures between -5°C and 0°C have been more sensitive to warming than higher, colder sites. Although air temperature and elevation are useful empirical metrics for identifying snow-covered areas susceptible to climate warming (e.g., Nolin and Daly, 2006), relatively little work has examined the physical controls governing the non-linear response. For example, little is known about how the snowpack energy balance and cold content will respond to warming. Musselman et al. (2017a) showed that earlier snowmelt is generally associated with a shift to reduced positive energy fluxes, but it is uncertain how this finding is applicable to higher, colder sites that are less sensitive to warming. Quantifying the physical controls driving the non-linear response is therefore essential to better predicting the effect of increased air temperature on seasonal snow cover evolution.

According to the Intergovernmental Panel on Climate Change (IPCC), there is a high likelihood of warming continuing through the 21st century (IPCC, 2013). This is predicted to have large negative impacts on snow accumulation and melt in areas that rely on mountain snowpacks for water resources (Adam et al., 2009; Barnett et al., 2005; Barnett and Pierce, 2009; Mankin et al., 2015). In the western United States, where over 60 million people depend on meltwater for domestic, industrial, and agricultural purposes (Bales et al., 2006), significant temperature increases are likely to occur by century's end (e.g., Leung et al., 2004; USGCRP, 2017). This warming is expected to drive large-scale shifts from snow to rain across the region (A. A. Harpold et al., 2017a; Klos et al., 2014), which could reduce streamflow volume independent of changes to total precipitation (Berghuijs et al., 2014) and alter the spatial extent,

frequency, and intensity of rain-on-snow events (Musselman et al., 2018). Furthermore, streamflow efficiency is sensitive to snowmelt rate with slower rates producing less streamflow per unit of precipitation than faster rates (Barnhart et al., 2016). Therefore, it is possible that predicted decreases to snowmelt rate with climate warming (Musselman et al., 2017a) will also reduce streamflow in snow-dominated areas.

In addition to further warming, the western United States is likely to see changes in precipitation patterns with resultant impacts on mountain snowpacks (Easterling et al., 2017; Leung et al., 2004; Stewart et al., 2004a). Although future changes to precipitation total and seasonality are more uncertain than air temperature increases (IPCC, 2013), it is essential to evaluate the effect of total precipitation and precipitation seasonality on snow accumulation given inextricable link between SWE and precipitation. Past work has also shown that increases in precipitation may obscure the effect of warming air temperatures on snow accumulation and melt (Beniston et al., 2003; Hamlet et al., 2005; Pederson et al., 2011a; Stewart, 2009; Vincent et al., 2007). For example, positive trends in April 1 SWE at several snow course sites in the southern Sierra Nevada mountains were shown to caused by increases in precipitation over the study period (Mote et al., 2005). Thus, it is important that changes to precipitation be considered in simulations of future snowpack conditions.

Work over large spatial scales suggests that increases in precipitation would have to be substantial in order to make up for the effect of future warming air temperatures on snowpack accumulation (Adam et al., 2009; Marty et al., 2017) and streamflow (Barnett and Pierce, 2009; Udall and Overpeck, 2017). It has also been shown that the non-linear response of mountain snowpacks to increasing air temperatures will likely continue with further warming (Cooper et al., 2016; Klos et al., 2014; Luce et al., 2014; Musselman et al., 2017a, 2017c). Within this body

of previous research, there is still a need to investigate the physical processes controlling the differential responses of more/less sensitive snowpacks to changes in climate. In this context, the Niwot Ridge Long Term Ecological Research (LTER) site offers a unique opportunity to evaluate such processes. The LTER has long-term snow pit and meteorological measurements from a subalpine location likely to be more sensitive to warming as well as from a less sensitive colder, higher alpine location. This study leveraged the historical data from these sites along with a physics-based snow model and a range of likely changes to future climate to answer our two research questions:

1) Do the alpine and subalpine snowpacks exhibit differential responses to changes in air temperature, total precipitation, and precipitation seasonality?
2) How do changes to snowfall fraction, cold content, and the snowpack energy balance control the responses to the climate change scenarios?

3.2 Study site and data

This study utilized long-term meteorological and snow pit records from two sites within the Niwot Ridge LTER on the eastern slope of the Continental Divide in Colorado's Rocky Mountains (Fig. 3.1). The alpine and subalpine sites are respectively located at 3528 m and 3022 m, with treeline occurring at approximately 3400 m. For our study, the alpine site was representative of a snowpack likely to be less sensitive to climate perturbations, while the subalpine was potentially more sensitive. This was based on how December, January, and February (DJF) average air temperatures at the two sites compared to previous work, which has shown the largest sensitivity to warming to occur between approximately -5°C and 0°C (Kapnick and Hall, 2012; Knowles et al., 2006; Mote et al., 2018). Over the baseline historical period (1

October 1991 through 30 September 2013), average DJF air temperature was -10.3°C in the alpine and -6.2°C in the subalpine (Table 3.1).

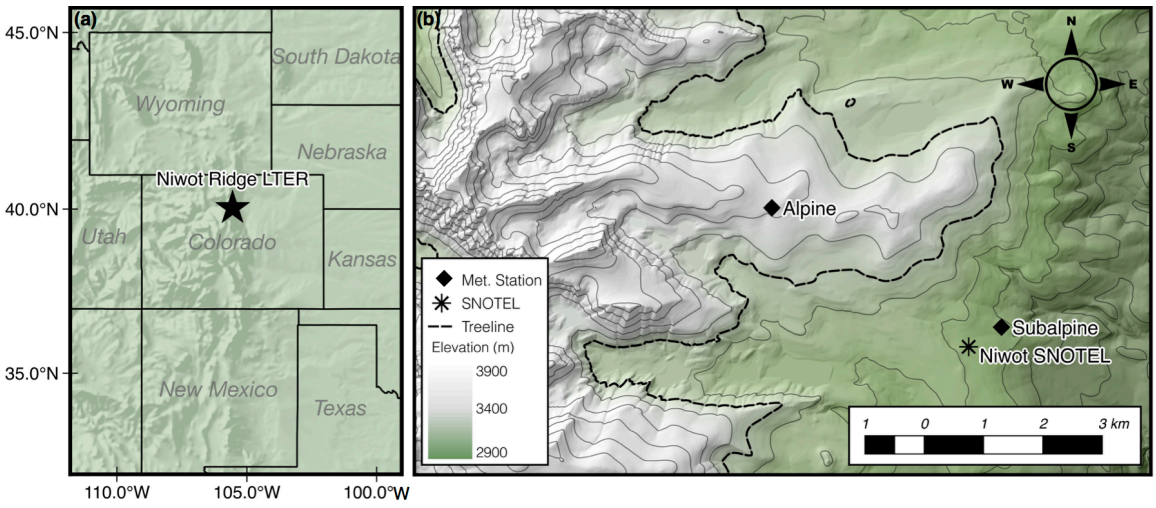

Figure 3.1. The location of the Niwot Ridge LTER within the western United States (a) and a topographical map showing the meteorological stations and snow pit sites. The dashed line in the LTER inset (b) represents approximate treeline (3400 m) and the thin, solid lines are 100 m contours.

Table 3.1. Mean meteorological quantities for December, January, and February (DJF) at the alpine and subalpine sites (WY1991–WY2013) along with mean peak SWE magnitude and timing for the two sites as observed in the snow pits (WY2007–WY2013).

Site	DJF air temperature (°C)	DJF wind speed ($m\ s^{-1}$)	DJF RH (%)	Peak SWE (mm)	Peak SWE date
Alpine	-10.3	11.4	67.1	843	06-May
Subalpine	-6.2	1.7*	55.8	395	26-April

*Subalpine wind speed uses corrected values from Jennings et al. (2018a)

Meteorological data were available from water year 1991 (WY, 1 October of the previous calendar year to 30 September) to WY2013. These data included hourly observations of air temperature, relative humidity, wind speed, incoming shortwave radiation, and precipitation. The raw observations were subjected to an intensive quality control and infilling procedure to ensure their suitability as model forcing data (Jennings et al., 2018a). The serially complete records of air temperature, relative humidity, and incoming shortwave radiation were used to calculate an empirical estimate of incoming longwave radiation based on the recommendations of Flerchinger

et al., (2009). The complete dataset is publicly available on the Niwot Ridge LTER webpage (Jennings et al., 2017).

The alpine and subalpine sites also have long-term snow pit records of SWE, depth-weighted snowpack temperature, and cold content (Williams, 2016; Williams et al., 1999). The record includes 292 snow pit measurements from WY1995–WY2013 in the alpine and 147 measurements from WY2007–WY2013 in the subalpine. According to these data, observed peak SWE in the alpine was approximately double peak SWE in the subalpine from WY2007 through WY2013, the period for which there were overlapping snow pit observations. Additionally, the snow pit data were used to validate simulated snow cover properties and to improve the forcing data, namely precipitation corrections for gage under-/over-catch, as well as to parameterize the canopy module for the subalpine model runs (Jennings et al., 2018a). We also used automated SWE data from the Niwot Snow Telemetry (SNOTEL) station, which is located within the LTER less than 1 km from the subalpine site at an elevation of 3021 m (Fig. 3.1).

3.3 Methods

3.3.1 SNOWPACK model description

SNOWPACK is a physics-based snow model forced by air temperature, relative humidity, wind speed, incoming shortwave and longwave radiation, and precipitation at an hourly or longer time step (Bartelt and Lehning, 2002; Lehning et al., 2002b, 2002a). The model simulates a one-dimensional snowpack with an arbitrary number of layers that have their own thickness, density, and temperature values, as well as snow grain size and type. New layers are added with snowfall, while melt and densification lead to a reduction in the number of layers. SNOWPACK also provides a full treatment of the snowpack energy balance:

$$\frac{dU}{dt} + Q_M = Q_{SW} + Q_{LW} + Q_H + Q_{LE} + Q_G + Q_R \quad (3.1)$$

where $\frac{dU}{dt}$ is the simulated rate of change in internal snowpack energy, Q_M is the energy available for melt (once cold content equals 0.0 MJ m^{-2}), Q_{SW} is net shortwave radiation, Q_{LW} is net longwave radiation, Q_H is sensible heat flux, Q_{LE} is latent heat flux, Q_G is ground heat flux, and Q_R is the heat advected by precipitation (all W m^{-2}).

Model configuration was the same as in Jennings et al. (2018a) except this study used SNOWPACK version 3.4.5 in place of version 3.3.0, which was used in the previous work. Additionally, we changed the way precipitation phase partitioning was handled by the model. Unless precipitation phase is assigned in the forcing data file, SNOWPACK calls the data preprocessor MeteoIO (Bavay and Egger, 2014) to designate whether the precipitation is rain, snow, or a mix of the two. In its stock configuration, the user indicates whether MeteoIO should use either a single air temperature threshold to partition rain and snow or a range between two air temperature values with a linear mix of precipitation phase in between. Jennings et al. (2018a) used an air temperature threshold of 2.5°C to better represent the high rain-snow air temperature thresholds commonly found at upland, continental sites (Jennings et al., 2018b; Ye et al., 2013). For this work, we updated MeteoIO to include a binary logistic regression model (e.g., Froidurot et al., 2014; Jennings et al., 2018b) that partitions precipitation between rain and snow as a function of air temperature and relative humidity:

$$p(snow) = \frac{1}{1 + e^{(\alpha + \beta \mathrm{T}_a + \gamma \mathrm{RH})}} \quad (3.2)$$

where $p(snow)$ is the probability of snow (0 to 1, dimensionless), α, β, and γ are the optimized model coefficients (-10.04, 1.41, and 0.09, dimensionless), T_a is air temperature (°C), and RH is relative humidity (%). Precipitation is set to be snow when $p(snow)$ >= 0.5 and rain when

$p(snow) < 0.5$ (Fig. 3.2). The binary logistic regression model was shown to be the most effective method in a Northern Hemisphere comparison (Jennings et al., 2018b), so we used this method in this study to provide consistently high performance across the climate change perturbations.

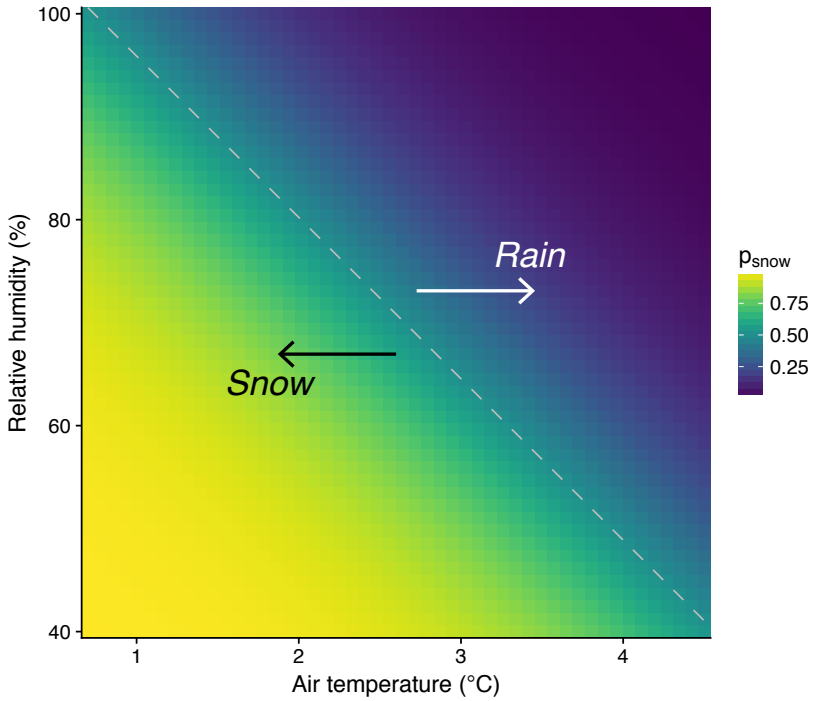

Figure 3.2. Snow probability as a function of air temperature and relative humidity (Eq. 3.2) where yellow shading indicates an increased likelihood of snow and blue shading an increased chance of rain. The gray dashed line separates snow probability values greater than or equal to 0.5 (left) and less than 0.5 (right).

Furthermore, SNOWPACK was chosen for this work because the model has been extensively validated in the literature in terms of its ability to represent SWE, snow depth, snowpack temperature, cold content, snow microstructure, and energy balance partitioning (Etchevers et al., 2004; Jennings et al., 2018a; Lehning et al., 2001; Lundy et al., 2001; Meromy et al., 2015; Rutter et al., 2009). In addition, SNOWPACK and its spatially distributed version, Alpine3D (Lehning et al., 2006), have been effectively used to explore the effect of climate change on snow cover properties in various areas with differing physiographic and climatic

properties (Bavay et al., 2013; Marty et al., 2017; Meromy et al., 2015; Musselman et al., 2017c; Rasmus et al., 2004).

3.3.2 Baseline model runs

We used the model setup described in the section above and the quality controlled forcing data from Jennings et al. (2018a) to simulate the alpine and subalpine snowpacks for the period WY1991–WY2013. Simulated SWE, depth-weighted snowpack temperature, and cold content for the baseline (i.e. historical) runs were validated on the equivalent snow pit and SNOTEL observations (Table 3.2). The switch to SNOWPACK 3.4.5 yielded a negligible change in performance relative to version 3.3.0 used in Jennings et al. (2018a).

Table 3.2. Validation metrics for the baseline simulations compared to snow pit SWE, depth-weighted temperature (T_s), and cold content (CC) data in the alpine and snow pit plus SNOTEL data in the subalpine.

Site	WY range	SWE r^2	SWE mean bias (cm)	T_s r^2	T_s mean bias (°C)	CC r^2	CC mean bias (MJ m^{-2})
Alpine	1995–2013	0.6	10.9	0.6	1.3	0.6	1.3
Subalpine (snow pit)	2007–2013	0.7	-3.4	0.7	0.9	0.6	0.6
Subalpine (SNOTEL)	1993–2013	0.9	-1.2	NA	NA	NA	NA

3.3.3 Climate perturbations

The baseline simulations were then perturbed based on the predicted likely changes to climate in the southwestern United States and Colorado as presented in the US Global Change Research Program's (USGCRP) Fourth National Climate Assessment (USGCRP, 2017) and 5th Assessment Report of the IPCC (IPCC, 2013). Both reports utilize output from a suite of climate models that are included in the 5th phase of the Coupled Model Intercomparison Project (CMIP5). Although there is a range of representative concentration pathways (RCP—the CO_2 emission scenario that limits increases in surface energy to a given W m^{-2} value) and associated model output, we focused on RCP4.5 and RCP8.5. In RCP4.5, emissions peak in 2040 before

declining, while emissions continue to rise unabated in RCP8.5. Thus, RCP8.5 represents a greater increase in atmospheric carbon dioxide and air temperature. Details on the reports' methods can be found within the source documents.

For the climate perturbations in this work, we focused on three key meteorological quantities:

1) Air temperature increases (ΔT) with associated increases in incoming longwave radiation
2) Changes to total precipitation (ΔP_{tot})
3) Changes in precipitation seasonality (ΔP_{seas})

We applied the above perturbations individually to the forcing data in order to isolate the impact of individual components of climatic change on snow accumulation and melt processes. The ranges and increments for these perturbations are detailed in the subsections below.

3.3.3.1 Air temperature and incoming longwave radiation increases

We used the delta-change approach by applying air temperature increases in 0.5°C increments from +0.5°C to +4.0°C. Each increase was applied uniformly to the baseline hourly data and we did not consider seasonal changes to air temperature or impacts to the diurnal temperature range. The values for the ΔT perturbation scenario were chosen based on the USGCRP report, which showed air temperatures in the western United States may increase by between 2.7°C and 4.8°C in RCP4.5 and RCP8.5 by the end of the 21st century (Vose et al., 2017). According to both the USGCRP and IPCC, increases in air temperature are highly probable between 2030 and 2100. There are no areas in the region where air temperature is expected to decrease in either report.

In addition to increasing air temperature, we also increased incoming longwave radiation through the Stefan-Boltzmann law:

$$LW_{in} = \sigma \varepsilon_a T_a^4 \tag{3.3}$$

where LW_{in} is incoming longwave radiation (W m^{-2}), σ is the Steffan-Boltzmann constant (5.67 × 10^{-8} W m^{-2} K^{-4}), ε_a is atmospheric emissivity (0 to 1, dimensionless), and T_a is air temperature (K). In the empirical equations we used to compute LW_{in}, ε_a was estimated as a function of humidity and cloud cover (Jennings et al., 2018a). In our perturbations, we kept hourly ε_a values from the baseline scenario constant due to the high uncertainty in future humidity and cloud cover (IPCC, 2013).

3.3.3.2 Changes to total precipitation

To reflect potential changes to total precipitation, we perturbed the hourly precipitation data from the baseline in 5% increments from -20% to +20%. As with the ΔT scenario, we used the delta-change approach and applied the perturbations uniformly across the forcing dataset. Although predicted changes to precipitation in the western United States are typically < 10% in the RCP 4.5 and 8.5 scenarios, the IPCC and USGCP both show greater uncertainty in these predictions as compared to air temperature increases. Additionally, the two reports present a large spread in in interannual variability, approaching ±50% relative to mean observed total precipitation.

3.3.3.3 Changes to precipitation seasonality

In order to isolate the effects of changing precipitation seasonality from changing total precipitation, we kept annual precipitation constant while varying the proportions of winter and spring precipitation in 10% increments. In this case, we increased winter precipitation by 10% (DJF+10), 20% (DJF+20), and 30% (DJF+30) while reducing springtime precipitation by the same amounts. Although changes to spring precipitation are less likely than the winter increases according to the USGCRP report, we still wanted to evaluate the effect of a shift from winter to spring precipitation as snowmelt rate and timing are highly sensitive to spring snowfall (Clow et al., 2016; Jennings et al., 2018a; Seligman et al., 2014). We followed the same protocol as with

the winter increases, but increased March, April, and May precipitation (MAM+10, MAM+20, and MAM+30), while decreasing the winter precipitation amounts.

3.3.4 Assessing changes to snow accumulation and melt, snowfall fraction, cold content, and the snowpack energy balance

In regard to the first research question, we analyzed the SNOWPACK output data from the climate change simulations to look for evidence of a differential response between the snowpacks at the two sites. We used a set of four snowpack metrics designed to capture seasonal snow cover evolution:

1) Peak SWE: The total water stored in the snowpack at its maximum.
2) Melt timing (i.e., the date of peak SWE): Although melt may occur before the date of peak SWE, this metric is often used as the timing of melt onset as it signifies the start of the main snowmelt period in seasonal snowpacks.
3) Snowmelt rate: The average snowmelt rate between melt onset and the first date of SWE = 0.
4) Snow-covered days: The total number of days with snow cover.

The first three metrics above are of interest to water managers as they represent how much, when, and at what rate meltwater will be produced. The last metric is important to the earth's climate as snow has a higher albedo than bare ground, meaning a greater proportion of incoming solar radiation is reflected when snow is on the ground.

After analyzing the output data for evidence of a differential response of the two snowpacks, we then focused on research question two by assessing three components of physical control: 1) snowfall fraction—the proportion of annual precipitation falling as snow, 2) cold content, and 3) the snowpack energy balance. In this work snowfall fraction was considered a primary response driver as it represents the amount of rain or snow entering the snowpack or

bare ground if no snow cover was present. This is critical given the differing effects rain and snow have on snowpack properties and land surface hydrology. The next component we considered was cold content, which is a measure of the snowpack's energy deficit:

$$CC = c_i \rho_s d_s (T_s - T_m) \quad (3.4)$$

where CC is snowpack cold content (MJ m^{-2}), c_i is the specific heat of ice (2.1× 10^{-3} MJ kg^{-1} $°C^{-1}$), ρ_s is the density of snow (kg m^{-3}), d_s is snow depth (m), T_s is the depth-weighted snowpack temperature (°C), and T_m is the melting temperature of ice (0°C). We expected cold content to be impacted by the perturbations because the cold content of new snowfall is simulated as a linear function of air temperature and precipitation (Cherkauer et al., 2003; Lehning et al., 2002a; Wigmosta et al., 1994). Finally, we analyzed changes to the snowpack energy balance (Eq. 3.1) that occurred with the climate perturbations. Q_{SW} is generally the prime source of melt energy in mountain snowpacks (e.g., Bales et al., 2006; Cline, 1997a; Jepsen et al., 2012; Marks and Dozier, 1992), but we were also interested in how changes to the rest of the energy balance were associated with the snowpack responses at the two sites. For this part of the analysis we focused only on Q_{SW}, Q_{LW}, Q_H, and Q_{LE} as Q_G and Q_R contributed near-negligible amounts of energy to Q_M in the baseline and climate change scenarios.

3.4 Results

3.4.1 Changes to snow accumulation and melt

SWE accumulation decreased at the two sites with air temperature increases, but the snowpacks exhibited a differential response to warming (Fig. 3.3a,b; Table 3.3). The subalpine site was more sensitive to the ΔT perturbations, with mean peak SWE declining 15.4% $°C^{-1}$ as compared to 4.9% $°C^{-1}$ in the alpine. The loss of snow covered days and the progression of melt onset per degree of warming were also more pronounced in the subalpine. For example, an increase of 2°C

was associated with a loss of 32.8 d in annual snow cover duration relative to the baseline in the subalpine and 21.4 d in the alpine, a relative difference of 53.3%. Similarly, subalpine melt onset advanced by 2.6 more days per 1°C of warming than alpine melt onset. Daily snowmelt rate also declined significantly in the subalpine, while the alpine increase was not significant at the 95% level. Changes to snowmelt rate in the ΔT perturbations will be discussed further in the energy balance results section below (Sect. 3.4.4).

Simulated snow cover evolution at both sites was strongly impacted by the ΔP_{tot} perturbations (Fig. 3.3c,d; Table 3.3). The small differences between the alpine and subalpine suggest the response was relatively consistent between the two sites, in contrast to the differential response to the ΔT scenarios. Each 10% increase in total precipitation was associated with a 12.1% increase in peak SWE in the alpine and a 15.4% increase in the subalpine. A gain in total precipitation also had a slight delaying effect on snowmelt onset and a lengthening effect on the snow covered season with similar values at the two sites. Melt rate was also responsive to total precipitation with each 10% increase being associated with a 1.5 mm d^{-1} increase in alpine melt rates and a 0.9 mm d^{-1} increase in the subalpine. Because our ΔP_{tot} perturbations reflected both gains and losses, our simulations also showed that decreases in total precipitation induced significant changes to the alpine and subalpine snowpacks, namely reduced peak SWE, earlier melt onset, fewer snow covered days, and damped snowmelt rates. These changes were all equal in magnitude, but opposite in sign to the precipitation increases—e.g., a 10% decline in total precipitation produced 12.1% and 15.4% decreases in peak SWE in the alpine and subalpine, respectively.

The ΔP_{seas} perturbations had little effect on most of the metrics we evaluated (Fig. 3.3e,f; Table 3.3), suggesting precipitation seasonality plays less of a role in snow cover evolution at

our sites than either air temperature or total precipitation. Although the values were small, the subalpine site experienced a larger relative increase in peak SWE compared to the alpine. The other notable change was a shift towards earlier melt onset when winter precipitation increased at the expense of spring precipitation in the alpine. In this case, each 10% increase in DJF precipitation was associated with a 1.3 d progression in melt onset.

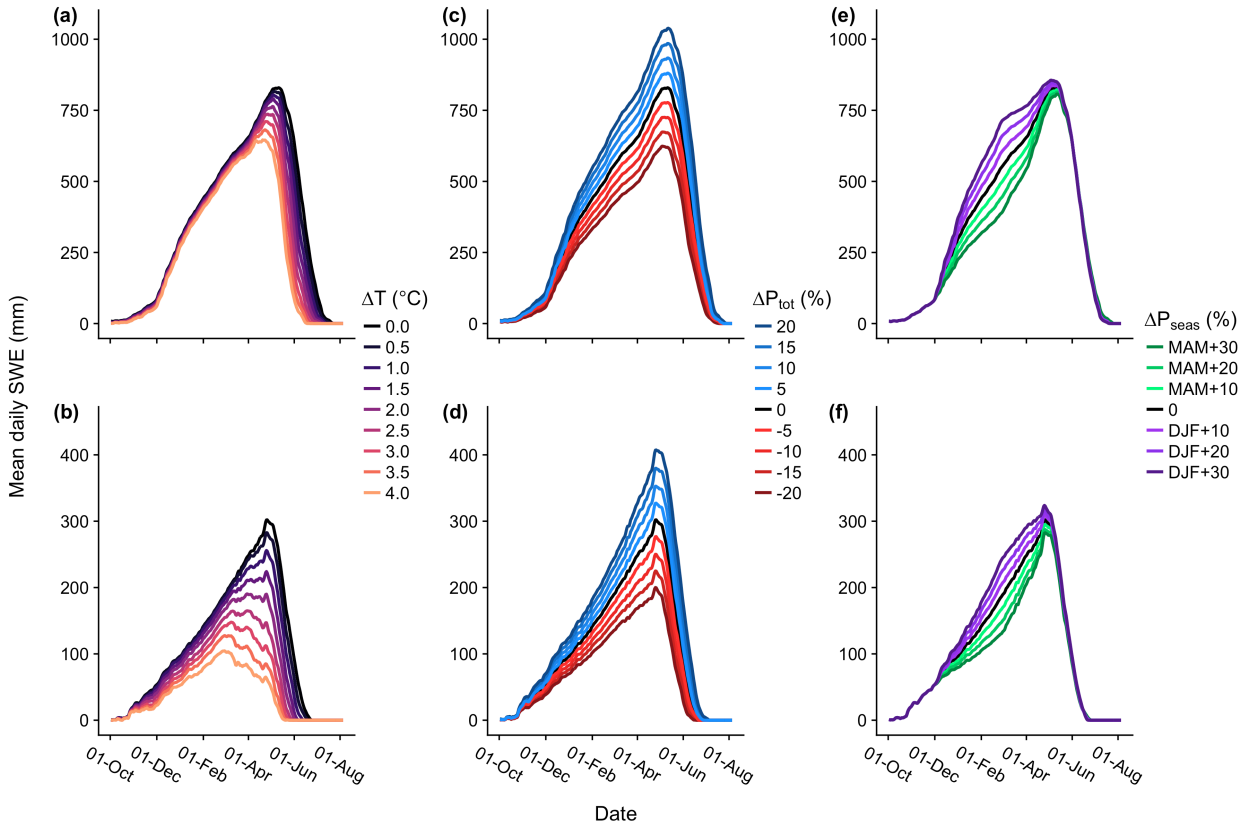

Figure 3.3. Mean daily SWE for the ΔT (a,b), ΔP_{tot} (c,d), and ΔP_{tot} (e,f) perturbations for the 23 simulation years in the alpine (top row) and subalpine (bottom row).

Table 3.3. Changes to mean snow accumulation and melt metrics associated with the baseline and different climate perturbation scenarios. The change values are given in their units and then as a percentage of the mean baseline value (except for the change in melt onset date). For the ΔT perturbations, the change is given per °C, while change is given per 10% for the precipitation perturbations. For precipitation seasonality, we set the percent change to be positive when the value increased with greater DJF precipitation (i.e., the 0.4% relative increase in alpine peak SWE is per 10% increase in DJF precipitation). The * indicates the change was not significant at the 95% level.

Site	Scenario	Change in peak SWE (mm $°C^{-1}$) or (mm per 10%)	Change in peak SWE (% $°C^{-1}$) or (% per 10%)	Change in melt onset date (d $°C^{-1}$) or (d per 10%)	Change in SCD (d $°C^{-1}$) or (d per 10%)	Change in SCD (%$°C^{-1}$) or (% per 10%)	Change in melt rate (mm d^{-1} $°C^{-1}$) or (mm d^{-1} per 10%)	Change in melt rate (% $°C^{-1}$) or (% per 10%)
	ΔT	-43.9	-4.9	-6.2	-10.7	-4.1	0.2*	1.0*
Alpine	ΔP_{tot}	108.8	12.1	1.3	4.6	1.8	1.5	7.3
	ΔP_{seas}	3.2	0.4	-1.3	0.0*	0.0*	-0.3	-1.6
	ΔT	-54.3	-15.4	-8.8	-16.4	-7.5	-0.4	-4.2
Subalpine	ΔP_{tot}	54.6	15.4	1.7	7.0	3.2	0.9	8.5
	ΔP_{seas}	6.7	1.9	0.2	0.5	0.2	0.0*	-0.2*

3.4.2 Changes to snowfall fraction

The ΔT perturbations had a significant effect on snowfall fraction at the two sites (Fig. 3.4). In the alpine, mean snowfall fraction declined from 83.9% in the baseline to 74.8% with the +4.0°C warming scenario, while subalpine snowfall fraction decreased from 71.0% in the baseline to 54.7% in the greatest warming scenario. This meant, on average, the alpine saw total annual snowfall decline from 1167 ± 239 mm in the baseline to 1042 ± 211 mm in the +4.0°C perturbation. Similarly, the subalpine declined from 527 ± 115 mm of annual snowfall in the baseline to 407 ± 92 mm with 4.0°C of warming. In terms of sensitivity to warming, the subalpine site was more affected, seeing a 5.7% $°C^{-1}$ reduction in snowfall fraction, compared to 2.7% $°C^{-1}$ in the alpine.

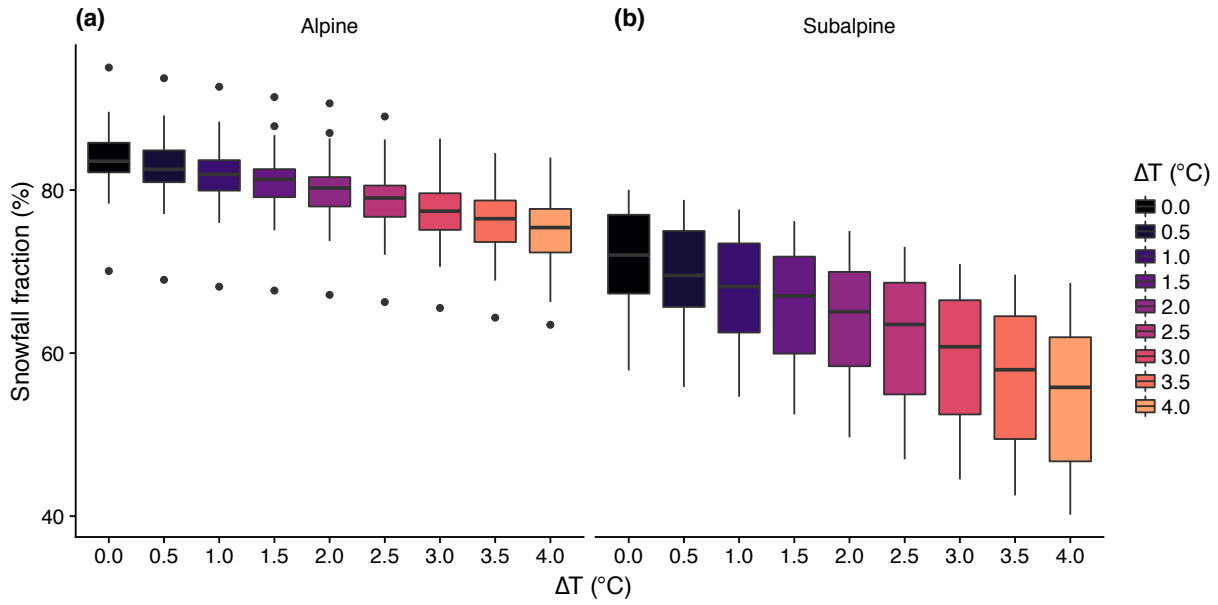

Figure 3.4. Annual snowfall fraction for the baseline and ΔT perturbations in the alpine (a) and subalpine (b) for the 23 year simulation years. Boxplots show the median, interquartile range, and outliers for the annual snowfall fraction. Snowfall fraction for ΔP_{tot} and ΔP_{seas} not shown due to negligible changes produced by the precipitation perturbations.

There was a negligible change in snowfall fraction with the ΔP_{tot} perturbations (not shown). Because the increases and decreases were applied uniformly across the forcing dataset, changes to snowfall were accompanied by nearly equal changes to rainfall. Therefore, all of these scenarios were within 0.1% of the baseline snowfall fractions of 83.9% in the alpine and 71.0% in the subalpine. As would be expected, the changes to annual snowfall were pronounced for the ΔP_{tot} perturbations. Each 10% increase in total precipitation was associated with a 116.8 mm increase in annual snowfall in the alpine and 58.4 mm in the subalpine. Conversely, a decrease in total precipitation led to losses equivalent in magnitude to the gains at the two sites.

The ΔP_{seas} perturbations produced slight increases in snowfall fraction when precipitation was shifted from MAM to DJF (not shown). The effect was greater at the warmer subalpine site where the DJF+ scenarios shifted precipitation to a time of the year when snow was more likely. In this case, the DJF+30 perturbation produced a 72.2% annual snowfall fraction, compared to 69.9% for MAM+30. Again, the effect was small, with an increase in snowfall fraction of just

0.4% per 10% increase in subalpine DJF precipitation. In the alpine, the change in snowfall fraction was even lower, with only a 0.8% range between the DJF+30 and MAM+30 scenarios.

3.4.3 Cold content

Seasonal patterns of cold content development and removal were significantly impacted by the ΔT perturbations (Fig. 3.5a,b, Table 3.4). In the subalpine, average annual peak cold content was reduced by more than half for the +4.0°C scenario relative to the baseline, declining to -0.6 MJ m^{-2} from -1.5 MJ m^{-2}. Average annual alpine peak cold content was less affected in relative terms by the ΔT perturbations, declining from -6.1 MJ m^{-2} in the baseline to -4.1 MJ m^{-2} in the +4.0°C warming scenario, a loss of 32.7%. In absolute terms, the alpine saw a greater MJ m^{-2} decline per 1°C of warming. This was likely due to the fact that the subalpine snowpack goes isothermal several times throughout the winter (i.e. cold content equals zero) even in the baseline. This meant the alpine had a greater absolute range in which its cold content could be reduced by warming.

Cold content development is strongly related to total precipitation at the two study sites (Jennings et al., 2018a), meaning the ΔP_{tot} perturbations had a large effect on seasonal cold content patterns (Fig. 3.5c,d, Table 3.4). As with snow accumulation and melt, the response of alpine and subalpine cold content was similar with small differences between the two in terms of the relative change in peak cold content magnitude. Changes to the timing of peak cold content were non-significant at the 95% level at the two sites.

Although the ΔP_{seas} perturbations had a minimal impact on snow accumulation and melt, they did induce significant changes in seasonal cold content patterns (Fig. 3.5e,f, Table 3.4). A shift to more winter precipitation (DJF+) led to more rapid cold content development and higher

peak cold content than the MAM+ perturbations. However, the DJF+ perturbations exhibited a rapid decline in cold content relative to MAM+, likely because less cold content was being added to the snowpack during spring storm events due to reduced snowfall. At both sites, cold content magnitudes tended to converge in April and May during the main period of snowpack ripening before peak SWE.

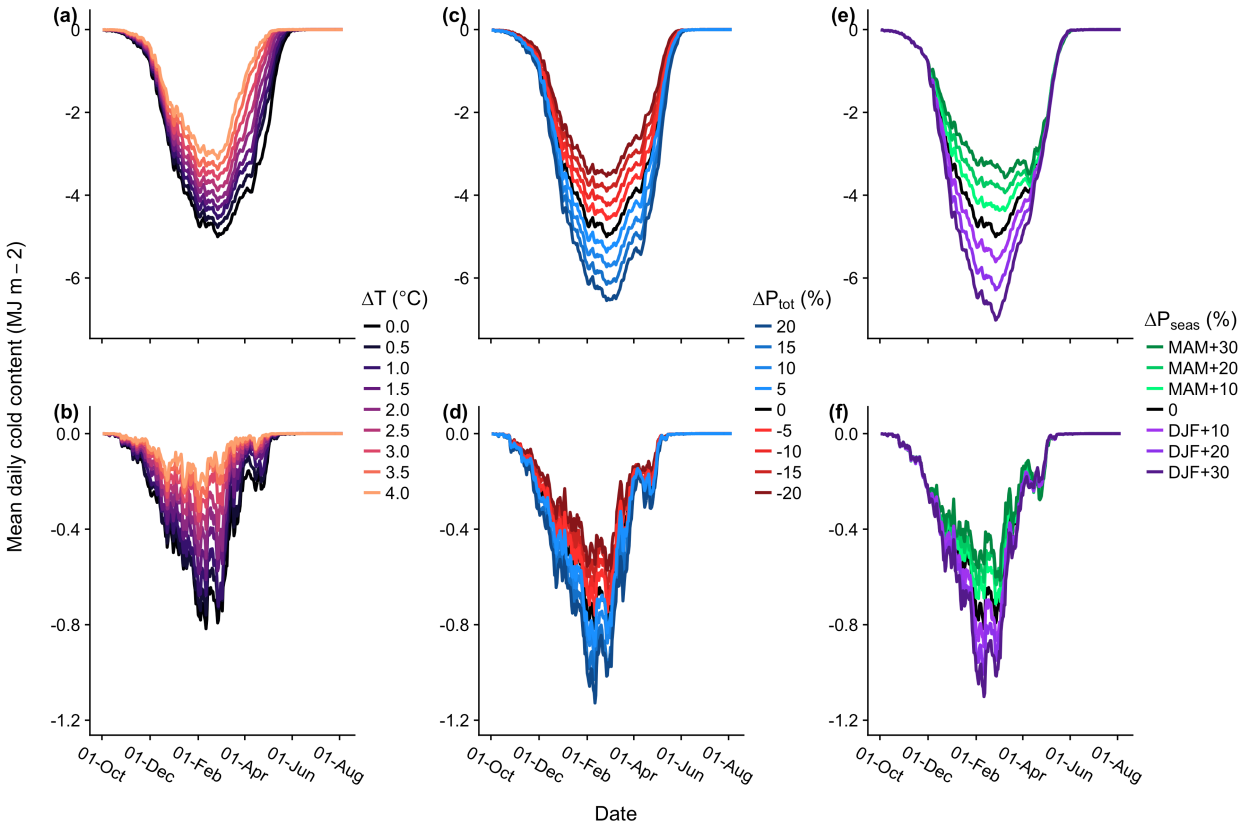

Figure 3.5. Same as Figure 3.3 but for mean daily cold content.

Table 3.4. Same as for Table 3.3, but values correspond to changes in cold content. Note: A positive value for a change in cold content indicates a loss, while a negative value represents a gain. Cold content is an energy deficit and a negative value.

Site	Scenario	Change in peak CC (MJ m^{-2} $°C^{-1}$) or (MJ m^{-2} per 10%)	Change in peak CC (% $°C^{-1}$) or (% per 10%)	Change in peak CC date (d $°C^{-1}$) or (d per 10%)
Alpine	ΔT	0.5	8.2	-2.0
	ΔP_{tot}	-0.8	-13.7	0.5*
	ΔP_{seas}	-0.5	-7.8	-6.2
Subalpine	ΔT	0.2	15.5	-7.5
	ΔP_{tot}	-0.2	-14.9	-0.1*
	ΔP_{seas}	-0.1	-5.0	2.4

Changes to seasonal patterns of cold content development and removal in the ΔT perturbations were a direct result of changes in the cold content added to the snowpack per day during snowfall (Fig. 3.6). Because air temperature remained constant for the ΔP_{tot} and ΔP_{seas} perturbations, all changes to cold content were due to increases or decreases in snowfall. For the baseline scenario, each 50 mm of daily snowfall was responsible for, on average, -1.0 MJ m^{-2} of cold content additions to the alpine snowpack and -0.6 MJ m^{-2} to the subalpine snowpack. Each 1°C of warming was associated with a loss of 0.05 MJ m^{-2} of cold content for every 50 mm of daily snowfall. This meant the cold content added to the snowpack by each 50 mm of snowfall fell to -0.9 MJ m^{-2} in the alpine and -0.5 MJ m^{-2} in the subalpine with 2°C of warming.

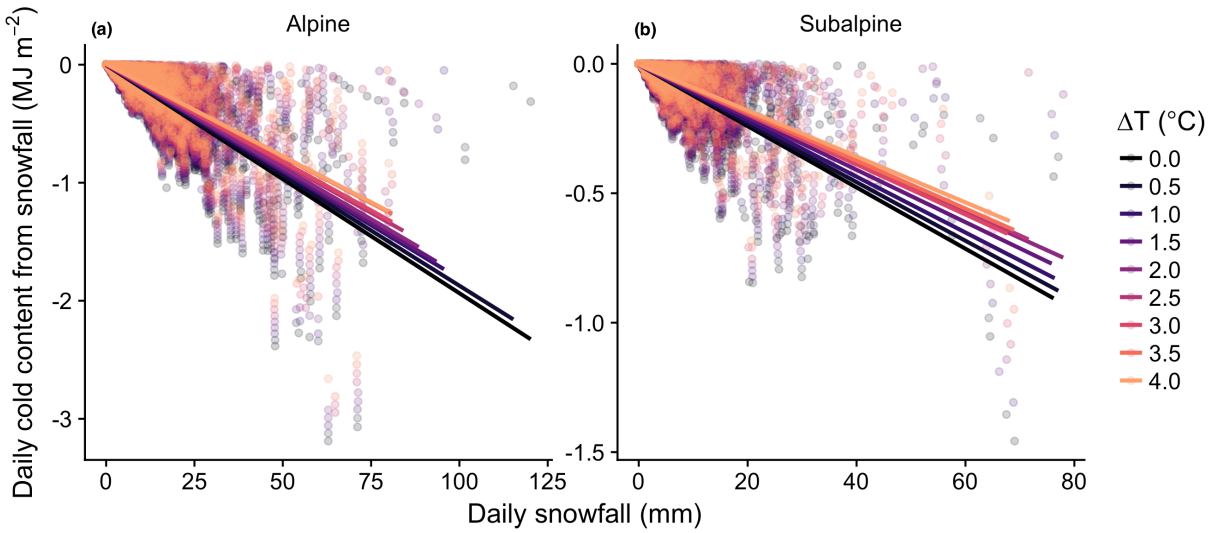

Figure 3.6. Daily cold content additions from snowfall plotted against daily snowfall for the ΔT perturbations in the alpine (a) and subalpine (b). The solid lines of best fit were computed using ordinary least squares regression and show a decrease in cold content from snowfall with increasing air temperatures. ΔP_{tot} and ΔP_{seas} figures not shown because the cold content from snowfall at a given daily snowfall value remained unchanged (air temperature during snowfall remained constant).

Warming and reductions in total and winter precipitation were all associated with reduced amounts of total cold content added by precipitation per water year (Fig. 3.7). In both the alpine and subalpine, the greatest amounts of total cold content from precipitation occurred in the +20%

ΔP_{tot} perturbations, which is unsurprising given the linear relationship between air temperature and precipitation and cold content (Eq. 3.4). A shift from MAM to DJF precipitation also produced significant cold content gains relative to the baseline scenario at both sites due to increasing precipitation in colder months.

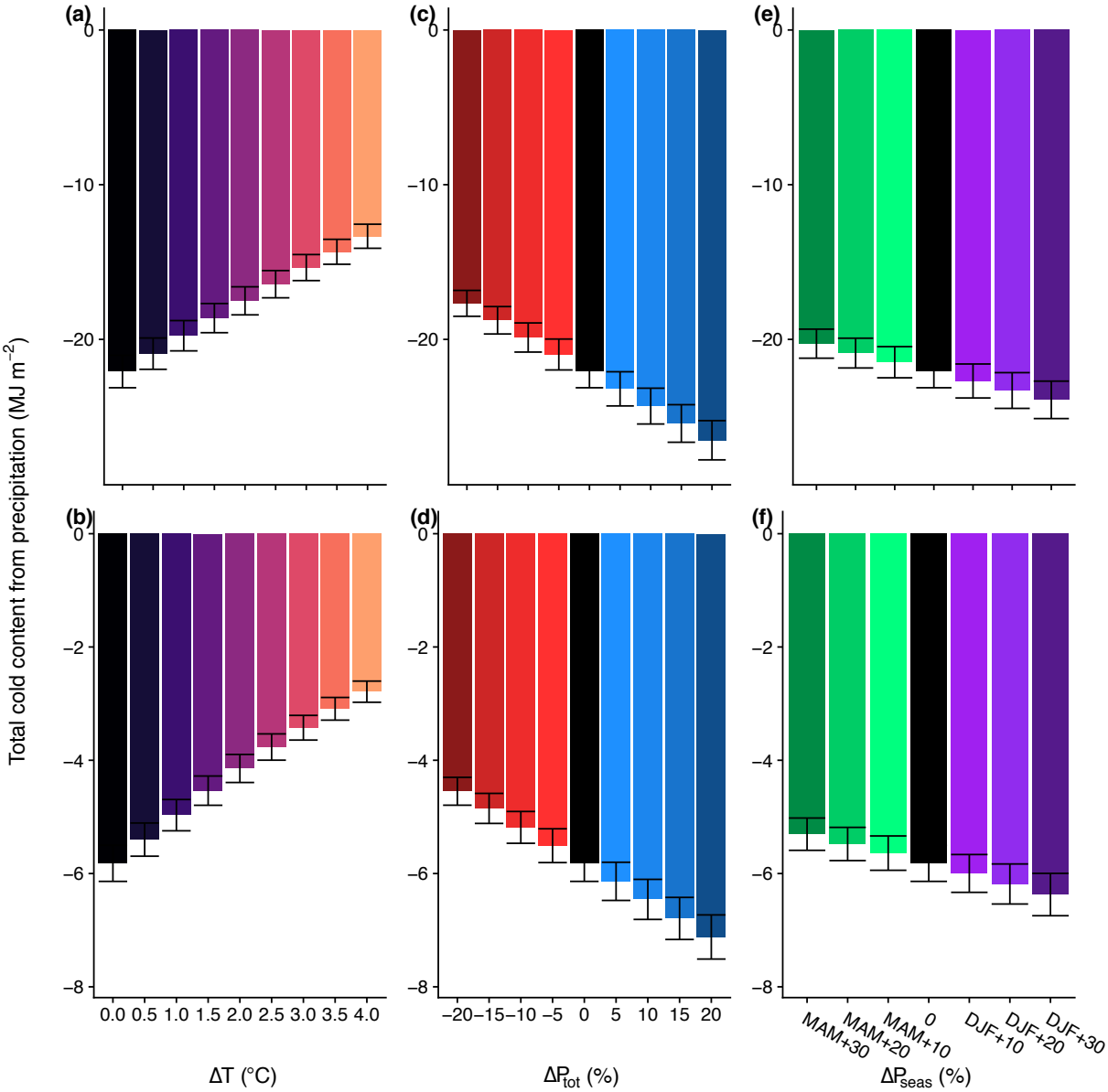

Figure 3.7. Average total content per water year added by precipitation for the ΔT (a,b), ΔP_{tot} (c,d), and ΔP_{tot} (e,f) perturbations in the alpine (top row) and subalpine (bottom row). The black whiskers represent ±1 standard error.

3.4.4 The role of the snowpack energy balance during snowmelt

As noted above, the warming scenarios significantly reduced melt rates in the subalpine, while the increases to alpine melt rate were not statistically significant at the 95% level. This was caused by a significant decrease in melt-period Q_M in the subalpine with warming and a non-significant increase in the alpine (Fig. 3.8a,b). At both sites, the ΔT perturbations produced earlier snowmelt timing (Fig. 3.3a,b, Table 3.3), which led to a decrease in the net radiative fluxes (Fig. 3.8c,d). This decline was primarily a result of reduced incoming solar radiation as the melt period shifted earlier in the year away from the summer solstice (i.e., away from when solar zenith angles are greatest). The advance of snowmelt timing with warming also decreased Q_{LW} as melt-period air temperatures decreased with the larger ΔT perturbations. This may appear counter-intuitive, but the forward shift in melt timing had a greater effect on melt-period air temperatures and the resultant incoming longwave radiation than the applied warming. Furthermore, an increase in the turbulent fluxes balanced the decrease in the radiative fluxes in the alpine, an effect not simulated in the subalpine where the turbulent fluxes increased only 1.8 W m^{-2} from the baseline to the +4.0°C scenario (Fig. 3.8e,f). On average, Q_H and Q_{LE} were approximately 10X greater in the alpine than subalpine because forest cover significantly damped the turbulent fluxes at the snow surface at the latter site.

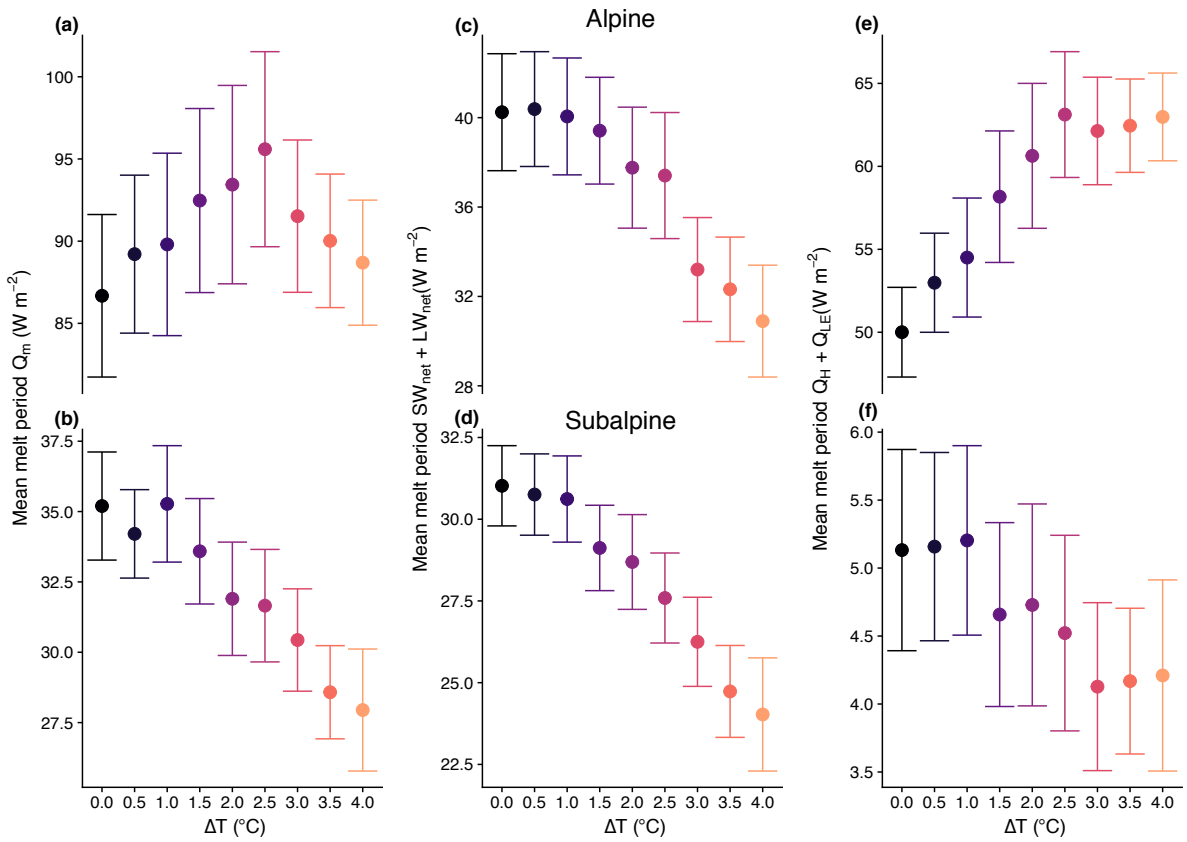

Figure 3.8. Mean melt period Q_M (a,b), radiative fluxes (c,d), and turbulent fluxes (e,f) in the alpine (top) and subalpine (bottom). Here the melt period is defined as the time between peak SWE and the snow-off date. The points are the average hourly flux value across the melt periods from the 23 simulation years with whiskers representing ±1 standard error for each ΔT scenario.

Changes to total precipitation also had an effect on the snowpack energy balance, with the positive ΔP_{tot} perturbations leading to greater melt rates and vice versa for the negative perturbations (Fig. 3.3c,d, Table 3.3). These changes were interlinked with the effect of precipitation on the duration of snow cover and the associated differences in available energy at the earth's surface. Shifts in the date of melt onset were small for both sites relative to the change in snow covered days, meaning the majority of changes to the energy balance were caused by a lengthening of the melt season for the positive perturbations and a contraction for the negative perturbations. This can be seen by relatively uniform changes to Q_M, the radiative fluxes, and the turbulent fluxes in Figure 3.9. Both Q_{SW} and Q_{LW} increased at the two sites in the positive ΔP_{tot} scenarios as the melt period extended into a time of greater insolation and increased air

temperatures. Similarly, Q_H and Q_{LE} both increased in the alpine and subalpine with the positive ΔP_{tot} perturbations.

The timing of snowmelt onset and melt rate were both relatively insensitive to the ΔP_{seas} perturbations (Fig. 3.3e,f, Table 3.3). Similarly, the snowpack energy balance showed little variation across the changing percentages of precipitation seasonality. Changes to Q_M, the radiative fluxes, and the turbulent fluxes (not shown) were all negligible.

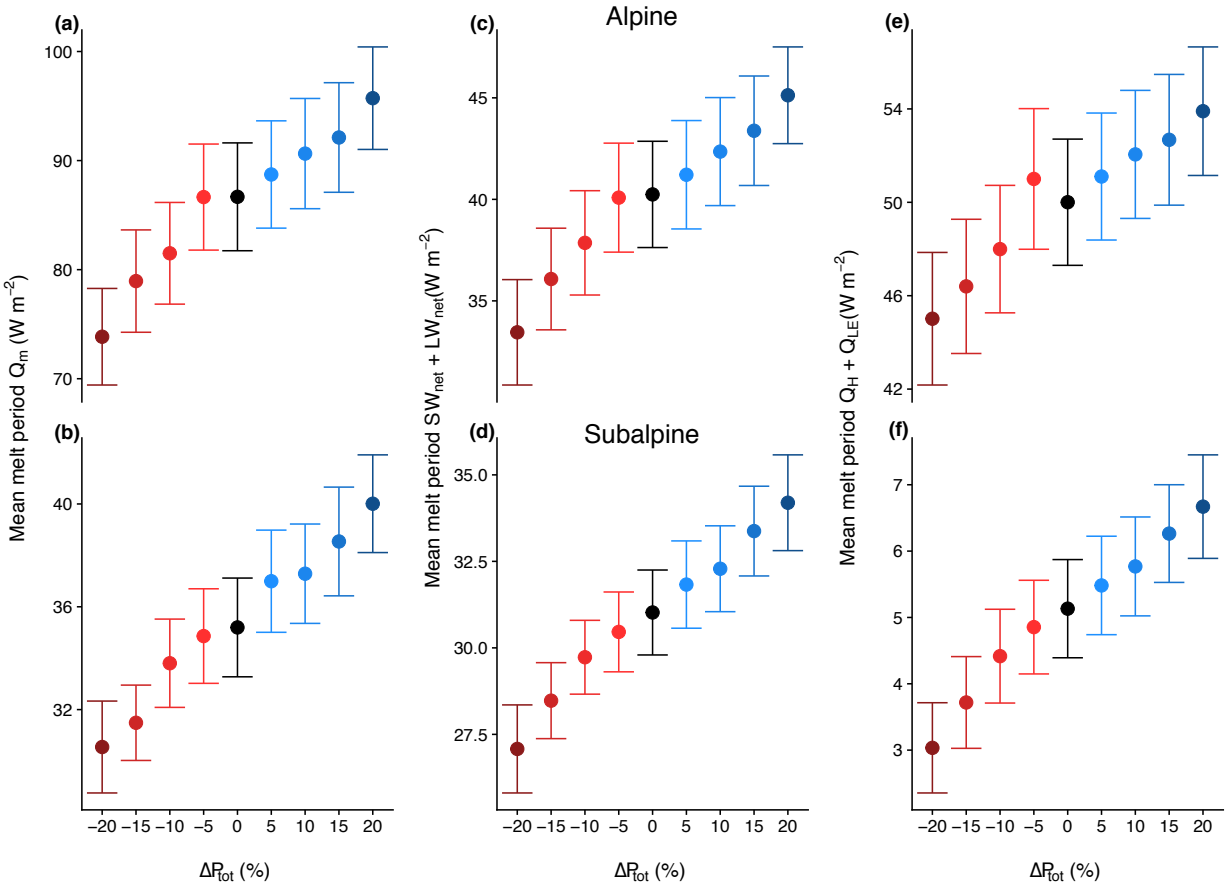

Figure 3.9. Same as with Figure 3.8 but for the ΔP_{tot} perturbations.

3.4.5 Interaction between cold content and the snowpack energy balance

The three perturbation scenarios display marked differences in the way cold content and the snowpack energy balance interact to control changes to snow accumulation and melt. Figure 3.10 displays the average daily cold content plus the average net flux into the snowpack for the

different perturbations. In this figure, a colored line plotted beneath the horizontal gray zero line indicates the net flux was not great enough, on average, to satisfy the cold content for that day. Conversely, colored lines above the zero line indicates that, on average, the net flux was greater than cold content and melt could occur.

As noted above, changes in melt onset were most pronounced for the ΔT perturbations relative to the precipitation scenarios. This is indicated in the ΔT plot, which shows marked divergence in where the colored lines cross the zero line (Fig. 3.10 a,b). Although there is significant spread in the colored lines for the ΔP_{tot} (Fig. 3.10 c,d) and P_{seas} (Fig. 3.10 e,f) perturbations, these lines tended to converge as they approached positive values later in the snow season, whereas the ΔT lines continued to diverge. This is reflective of the physical processes controlling the differential response of the two sites to warming air temperatures and the more consistent response to precipitation changes. Both snowfall fraction and the cold content of new snowfall were reduced in the ΔT perturbations, meaning it took less energy to satisfy the snowpack's internal energy deficit. This was compounded by the fact that the net radiative and turbulent fluxes were greater throughout the snow cover season for the warmer ΔT perturbations. For example, DJF and MAM net fluxes were respectively 2.0 W m^{-2} and 27.8 W m^{-2} greater in the alpine and 1.8 W m^{-2} and 8.1 W m^{-2} greater in the subalpine for the +4.0°C scenario relative to the baseline.

For the +3.0°C and greater warming scenarios, daily average cold content was no longer greater than daily average net flux in the subalpine (Fig. 3.10b), meaning melt was probable throughout the entirety of the snow cover season. This shift led to a marked increase in the number of winter melt events, with total annual average pre-peak SWE melt approximately doubling from 71.7 mm in the baseline to 146.6 mm in the +4.0°C scenario. This meant pre-peak

SWE melt increased proportionally from 20.3% of peak SWE in the baseline to 97.6% in the warmest ΔT perturbation. Thus, the amount of water lost to melt during the winter nearly equaled the total water stored in the snowpack at peak SWE with 4.0°C of warming. In some simulation years for the three warmest ΔT perturbations, subalpine snow cover shifted from seasonal to transient, representing a substantial shift in the hydrology of the subalpine snowpack. Conversely, winter melt stayed minimal in the alpine relative to the subalpine, reaching a maximum annual average of 48.0 mm (6.5% of peak SWE) in the in the +4.0°C scenario. Changes to winter melt were small for the precipitation scenarios despite the changes to cold content, suggesting the increase for the ΔT perturbations was an effect of interactions between enhanced positive fluxes and reduced cold content.

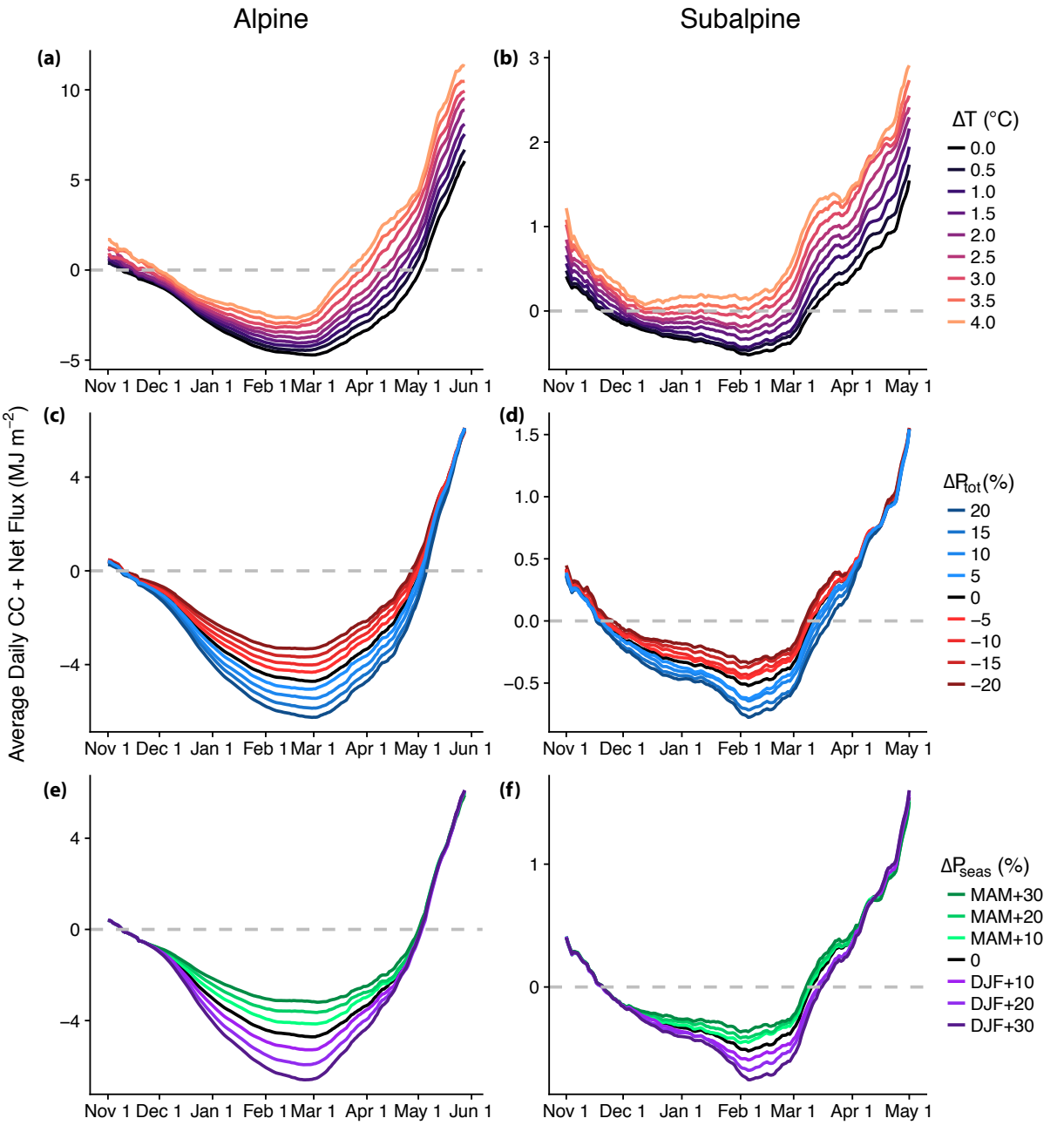

Figure 3.10. Average daily cold content plus net flux for the ΔT (a,b), ΔP_{tot} (c,d), and ΔP_{tot} (e,f) perturbations in the alpine (left column) and subalpine (right column). The gray dashed line at 0 MJ m^{-2} represents cold content being equal to the net fluxes in magnitude. Colored lines above the zero line indicate that the net fluxes were, on average, greater in magnitude than snowpack cold content, meaning melt could occur.

3.5 Discussion

3.5.1 Physical controls on the perturbation responses

We found the higher, colder alpine site to be less sensitive to the effects of warming air temperatures on snow accumulation, snowmelt onset, and snowmelt rate. This can be explained

through the physical controls we evaluated in the results section presented above. First of all, snowfall fraction at the alpine site was reduced by a lesser percentage with each degree of warming relative to the subalpine. This meant that frequent snowfall persisted in the alpine despite air temperature increasing by the same amount as in the subalpine. Warmer air temperatures also reduced the amount of cold content added to the snowpack per snowfall event. Loss of snowfall combined with warming led to average annual peak cold content approaching -0.4 MJ m^{-2} in the subalpine and -3.0 MJ m^{-2} in the alpine in the +4.0°C scenario. The significantly diminished subalpine cold content made the site more prone to midwinter melt events, which reduced peak SWE accumulation as mass was lost to melt before the main snowmelt season. Importantly, at 3°C of warming and above, the subalpine snowpack was substantially altered by a shift in the melt season from spring to the entirety of the winter. No longer was cold content large enough to buffer against midwinter melt. Instead, melt was probable and likely throughout the entirety of the snow cover season. Furthermore, warming-induced changes to snowmelt rate were non-significant in the alpine because a loss in the radiative fluxes caused by a shift in the melt period to reduced insolation was approximately balanced by an increase in the turbulent fluxes as a result of high wind speeds and warming temperatures. Although the turbulent fluxes increased slightly in the subalpine, this change was not enough to balance the effect of significantly diminished radiative fluxes.

Changes in total precipitation had significant impacts on snow accumulation at both sites, which is unsurprising given their cold winter and spring air temperatures (i.e., mass increases during the snow season almost uniformly lead to increased snowfall). The ΔP_{tot} perturbations were done percentage-wise, meaning the alpine saw a greater absolute increase in peak SWE for each 10% increase in total precipitation, but relative changes were similar at the two sites. In

other words, the response to total precipitation was fairly consistent compared to the differential response to warming air temperatures. Increased snowfall was associated with slightly delayed snowmelt onset and faster snowmelt as the melt period lengthened and shifted into a time of increased insolation. Although cold content was significantly altered by precipitation perturbations, these changes did not translate into large effects in seasonal melt onset. This is likely because the changes in cold content did not occur with increases in the snowpack energy balance as in the warming scenarios.

The final perturbation scenario we considered, ΔP_{seas}, had a near-negligible impact on our study sites. As noted above, cold winter and spring temperatures meant that precipitation fell mainly as snow, even when seasonality was shifted preferentially towards MAM. We kept total precipitation constant for these perturbations, so annual snowfall went relatively unchanged at the two sites, with the subalpine seeing a slight reduction in the MAM+ scenarios. Although we discuss the broader applicability of our results below, we note here that the effect of seasonality will likely be higher at warmer sites where a shift from DJF to MAM would result in significantly more rain and reduced snowfall fractions. Furthermore, we applied the climate change scenarios independently in order to individually examine the effect of the ΔT, ΔP_{tot}, and ΔP_{seas} perturbations. As with the application of the ΔP_{seas} scenarios to warmer sites, our results suggest that simultaneously increasing air temperature and shifting precipitation towards MAM would lead to a greater response at the warmer subalpine site.

3.5.2 Implications for water resources management in a warming climate

Climate change poses a serious challenge to water resources management through its effects on the timing and volume of water deliveries to reservoirs and other infrastructure (Barnett et al., 2005; Milly et al., 2008). This study supports the results of previous research, namely that

climate warming has and will continue to reduce snow accumulation (Harpold et al., 2012; Mote et al., 2018), produce earlier snowmelt onset (Clow, 2010; Regonda et al., 2005; Stewart, 2009), and reduce snowmelt rates (Musselman et al., 2017a). In addition to those key changes, the fact that the alpine and subalpine snowpacks responded differently to simulated warming brings up two further considerations. One, snow accumulation decreased at a greater relative rate in the subalpine compared to the alpine. Thus, streamflow forecasts that rely on statistical relationships between snow accumulation at a point and streamflow volume will likely degrade as the amount of snow monitored at a single station becomes progressively less and less representative of the snow accumulation in the elevations above it. Two, the temporal gap in snowmelt onset between the two sites increased with warming. In the baseline, subalpine peak SWE occurred an average of 21 d before alpine peak SWE. In the +4.0°C perturbation, this temporal gap expanded to 35 d, representing a relative increase of 66.7%. Compounding the problem is that a significantly larger proportion of subalpine meltwater was produced before peak SWE in the warming scenarios. Thus, reservoir operations will likely have to updated as more meltwater is delivered earlier in the season and as elevational patterns of snowmelt onset change with continued warming.

3.5.3 Assumptions and shortcomings

By using the delta-change approach, we assumed that future increases to air temperature would be uniform and the diurnal temperature range would be unaffected. However, past work has shown that snowpacks across an elevational gradient are sensitive to the diurnal temperature range (Nayak et al., 2010) and that warming is associated with a decrease in the diurnal temperature range (Karl et al., 1991). Therefore, we are likely missing changes to snow cover evolution induced by variations in the diurnal temperature range. Such changes may include a decrease in nighttime cooling of the snowpack and reduced refreezing of liquid water, meaning

daytime positive energy fluxes could go towards melting the snowpack instead of warming it. We also assumed temperature and precipitation changes would be equivalent at the two sites despite previous research in the Rocky Mountains showing climate trends to be spatially heterogeneous, even over small spatial scales. For example, Kittel et al. (2015) presented significant increases in high-alpine precipitation, while changes to subalpine precipitation were not significant over their study period. In addition to precipitation, other research has shown changes to air temperature are dependent on elevation (McGuire et al., 2012; Pepin and Losleben, 2002; Williams et al., 1996). However, it should be noted that past studies using SNOTEL measurements may be affected by inhomogeneities in the temperature data (Oyler et al., 2015).

For this paper we only examined two point locations and did not consider the broader spatial extent of the Niwot Ridge LTER and the associated variability in snowpack accumulation and melt (Jepsen et al., 2012). Previous research has shown that point observations of SWE are limited in their representativeness of the surrounding landscape (Molotch and Bales, 2006, 2005) and that meltwater outflow and timing can vary over short distances (Webb et al., 2018a, 2018b). This is due to both variability in snowpack internal properties and the spatial variation of the snowpack energy budget (Dadic et al., 2013; Marks and Winstral, 2001; Pomeroy et al., 2003). Thus, there is evidence to suggest that proximate snowpacks experiencing the same changes in climate would respond differently due to variations in physiography (e.g., Tennant et al., 2017). Additionally, our work focused on only two cold continental sites, despite the large diversity of seasonal snow cover classes in the western United States (Armstrong and Armstrong, 1987; Serreze et al., 1999; Trujillo and Molotch, 2014). We chose these locations because of their long-term meteorological and snow pit records and because they could represent sites that past work

has shown to be more (the subalpine) and less (the alpine) sensitive to the impacts of climate change on snow accumulation and melt. Although this research cannot be transferred directly to other areas, we believe our findings can be used to inform future research. Continuing to explore the differential response of alpine and subalpine snowpacks to warming will be critical considering that elevations above 3000 m in the Colorado River Basin provide approximately 50% of streamflow to the river (Hammond et al., 2018).

3.5.4 Other factors

Recent research has shown how landscape properties and disturbances govern snow accumulation and melt processes. For example, the seasonal evolution of subalpine snowpacks is strongly controlled by the interactions between forest characteristics and climate (Dickerson-Lange et al., 2017; Lundquist et al., 2013; Molotch et al., 2009; Roth and Nolin, 2017), suggesting that forest cover can affect the response of subalpine snowpacks to changes in air temperature and precipitation (Tennant et al., 2017). Furthermore, landscape-scale disturbances to forested areas, such as wildfire and bark beetle infestation have already had marked impacts on mountain snowpacks (Gleason et al., 2013; Livneh et al., 2015). Light absorbing impurities, such as dust, also have a pronounced effect on snowmelt timing and streamflow generation (Painter et al., 2017; Skiles et al., 2012). Both dust and post-wildfire char decrease surface albedo, which increases Q_{SW} and contributes to greater Q_M values (Deems et al., 2013; Gleason and Nolin, 2016; Painter et al., 2012, 2010). Therefore, research on the future of snow in the western United States should consider the effects of landscape disturbances and light absorbing impurities on snow accumulation and melt as they may exacerbate the warming response, particularly if feedbacks between snow and forest regeneration are considered (Knowles et al., 2017). For this study, we focused only on changes in climate given the high certainty in future

air temperature increases (IPCC, 2013) as well as the strong correlation between winter precipitation and snow accumulation and melt in cold continental areas (Serreze et al., 1999; Trujillo and Molotch, 2014).

Furthermore, Harpold and Brooks (2018) reported that relative humidity can help explain the differential inter-regional response to climate warming. Their analysis of 462 SNOTEL stations indicated that sites with lower relative humidity saw a reduced impact of increased air temperatures on snowpack ablation relative to sites with higher relative humidity. They note that drier sites, like the ones studied here, are buffered against the effects of climate warming through energy losses from Q_{LW} and Q_{LE}. While this work explains the large-scale controls on the non-linear response of snowpacks to climate warming, our work shows there can still be significant differences over short distances at sites with similar seasonal relative humidity values.

3.6 Conclusion

The snowpacks at the two sites evaluated in this study displayed a differential response to simulated climate warming, while the response to changes in total precipitation and precipitation seasonality were relatively consistent. Increases to air temperature led to decreased snow accumulation, shortened snow cover duration, and advanced melt timing to a greater degree in the subalpine snowpack than the alpine. This was primarily a result of subalpine snowfall fraction decreasing at more than twice the rate per 1°C of warming in addition to pronounced changes in the seasonal evolution of cold content and the snowpack energy balance. At 3°C of warming and greater, cold content was no longer of a high enough magnitude to buffer against positive energy fluxes during the winter, leading to a substantial proportion of melt occurring before peak SWE in the subalpine. Due to lower air temperatures and higher snowfall, this same effect was not simulated in the alpine. Additionally, subalpine melt rates declined by 8.5% per

1°C of warming as the melt period shifted earlier in the year towards a time of reduced insolation. In the alpine, the loss in melt-period radiative energy was balanced by an increase in simulated turbulent fluxes, leading to a non-significant change in melt rates. Increases in total precipitation had a marked effect on seasonal snow cover evolution at both sites, producing greater peak SWE, higher snowmelt rates, and longer snow cover duration. Conversely, decreases in total precipitation reduced peak SWE, slowed snowmelt rates, and contracted the snow cover season. The relative changes were similar at the two sites, suggesting a consistent response to variations in total precipitation as opposed to the differential response to increasing air temperatures. The snowpacks showed little sensitivity to precipitation seasonality, indicating the timing of precipitation was less important than air temperature and total precipitation at our two study sites.

Chapter 4

4 The sensitivity of modeled snow accumulation and melt to precipitation phase methods across a climatic gradient in the western United States

Abstract

Climate warming is driving a shift from snow to rain in cold and temperate regions globally, the hydroclimatic impacts of which are simulated using snow, hydrologic, and land surface models. Although air temperature thresholds and ranges are most commonly used to partition rain and snow within these models, there are a wide variety of precipitation phase methods that can be employed. However, little is known about how the selection of a precipitation phase method affects uncertainty in modeled snow accumulation and melt. This work aims to close this knowledge gap through physics-based snow model simulations at 11 sites in the western United States that span a climatic gradient from warm maritime to cold continental. We kept model setup consistent across the sites and forced the SNOWPACK model with serially complete, infilled, hourly meteorological data. A total of 12 simulations were run at the study sites with each model run corresponding to a different precipitation phase method. The methods used for precipitation phase determination were air, dew point, and wet bulb temperature thresholds, air temperature ranges, and binary logistic regression models. At the warm maritime sites, relative differences between the maximum and minimum annual snowfall fractions predicted by the different methods were sometimes greater than 100%, while the two coldest sites typically experienced relative differences less than 15%. Ranges in annual peak SWE were consistently greater than 200 mm at the warm maritime sites, exceeding 400 mm at some sites and years. Again, the coldest sites expressed reduced sensitivity with peak SWE ranges typically less than

20 mm. Method choice also affected other snow cover evolution properties, including the date of peak SWE, snowmelt rate, and snow cover duration with the warmer sites being more sensitive. In some cases the range in peak SWE date and snow cover duration exceeded one month. Overall, this work shows that wetter sites with winter temperatures near freezing (i.e. maritime) are most sensitive to the choice of precipitation phase method. This has serious implications for estimates of water storage, melt timing, and land surface albedo in simulations of past and future hydroclimatic conditions.

4.1 Introduction

One of the most prominent impacts of climate warming has been a shift from snow to rain in temperate and cold regions across the globe (e.g., Knowles et al., 2006; Trenberth, 2011), a trend that is expected to continue with further increases in air temperature (Bintanja and Andry, 2017; Klos et al., 2014; O'Gorman, 2014; Safeeq et al., 2015). In order to assess how this change affects global hydroclimate, researchers have employed snow models, hydrologic models, and land surface models of varying degrees of complexity (e.g., Barnett et al., 2005). One trait many of these models share is the partitioning of rainfall and snowfall based on a spatially uniform air temperature threshold or a range between two thresholds with a linear mix of liquid and solid precipitation in between. Recent work has called into question this simplistic treatment of precipitation phase (Feiccabrino et al., 2015; A. A. Harpold et al., 2017c) because of the pronounced spatial variability of the temperature at which rain and snow fall in roughly equal frequency (Jennings et al., 2018b; Ye et al., 2013). This suggests the use of a spatially uniform air temperature threshold is likely to produce errors in modeled precipitation phase with resultant effects on hydroclimatic simulations.

The use of a spatially uniform air temperature threshold appears logical given the strong temperature-dependence of precipitation phase. Observational work has shown that precipitation is primarily solid at temperatures at and below the freezing point (Auer Jr, 1974; Avanzi et al., 2014; Kienzle, 2008; United States Army Corps of Engineers, 1956). In general, as air temperature increases above 0°C, the probability of snowfall decreases following a sigmoidal curve (Dai, 2008; Fassnacht et al., 2013). As such, many models employ temperature thresholds greater than 0°C, but some still rely on the freezing point to separate rain and snow. More recent work has shown humidity exerts a secondary control on precipitation phase with snowfall more probable at a given temperature in more arid conditions (Froidurot et al., 2014; Gjertsen and Ødegaard, 2005; Jennings et al., 2018b). Surface air pressure also affects phase partitioning, but to a lesser degree than air temperature and humidity, with snowfall more common at higher temperatures when surface pressure is lower (i.e. at higher elevations) (Ding et al., 2014; Jennings et al., 2018b; Rajagopal and Harpold, 2016).

Given the secondary controls exerted by humidity and surface pressure on the probability of rain versus snow, precipitation phase methods have been developed to leverage this information into more accurate rain and snow predictions. These methods include dew point temperature thresholds (Marks et al., 2013; Ye et al., 2013), wet/ice bulb temperature thresholds (Anderson, 1968; Harder and Pomeroy, 2013), and binary logistic regression equations that predict the probability of snow as a function of various meteorological quantities (Froidurot et al., 2014; Jennings et al., 2018b). Recent work has shown that the spatial variability of phase partitioning is reduced when using humidity information in addition to air temperature (Ye et al., 2013). Furthermore, methods incorporating humidity better predict precipitation phase than air temperature-only methods relative to observations across the Northern Hemisphere (Jennings et

al., 2018b), likely due to their better representation of the hydrometeor energy balance (Harder and Pomeroy, 2013; A. A. Harpold et al., 2017c).

The wide variety of precipitation phase methods and marked spatial variability in rain-snow partitioning suggests method selection can introduce significant uncertainty to model output in areas where snow contributes to the annual hydrologic cycle. Previous work has shown precipitation phase method selection leads to variations in snowfall fraction—the percentage of precipitation that falls in a given year as snow— approaching 30% or greater (A. A. Harpold et al., 2017a; Jennings et al., 2018b; Raleigh et al., 2016). However, how this variability in snowfall fraction translates into divergences in simulated snow accumulation and melt is more uncertain. Harder and Pomeroy (2014) used the Cold Regions Hydrologic Model to evaluate how various snow cover properties were affected by precipitation phase method selection in three cold research basins in Canada. They found simulated SWE and snow cover duration were both sensitive to method choice with the methods producing the greatest snowfall fractions leading to increased SWE and longer snow covered periods. Method selection also leads to divergence in the SWE produced by individual storm events and in annual peak SWE, with higher air temperature thresholds producing greater SWE (Mizukami et al., 2013; Raleigh and Lundquist, 2012; Wayand et al., 2017). Other research has shown that simulated snow depth is typically greater when using higher air temperature thresholds or ranges, particularly in periods immediately following precipitation (Fassnacht and Soulis, 2002; Wen et al., 2013).

Most of the work above focused on single sites or a selection of sites with broadly similar hydroclimatic characteristics. However, this overlooks the significant spatial variability of phase partitioning and the uncertainty associated with such variability. For example, a comparison of three models with different precipitation phase methods showed that snowfall fraction at colder

sites was less sensitive to the choice of a method than warmer sites (Raleigh et al., 2016). Jennings et al. (2018b) also showed that uncertainty in annual snowfall fraction peaked at average annual air temperatures between 0°C and 5°C with less uncertainty at temperatures above and below that range. To date, no work has explored how a diverse selection of precipitation phase methods would affect simulated snow cover evolution across a climatic gradient. I.e., is the importance of phase method selection dependent on climate? This question is further compounded when future warming-driven changes to snow accumulation and melt are taken into consideration. Sites with average winter air temperatures near freezing are generally considered most sensitive to the effects of warming (e.g., Nolin and Daly, 2006) and these sites have also expressed the greatest sensitivity to precipitation phase method. Thus, it may be the case where the sensitivity of snow accumulation and melt to precipitation phase method selection is greater than the climate warming signal.

Given the importance of snow to the hydrologic cycle in the western United States—and cold and temperate regions globally—we aim to show how precipitation phase methods induce different degrees of variability in simulated snow cover evolution across a climatic gradient. We will do this through quantification of different snow accumulation and melt metrics and how they are affected by method selection at sites that span a climatic gradient from warm maritime to cold continental. We will then evaluate how the sensitivity is controlled by air temperature, relative humidity, and precipitation at the different sites.

4.2 Study sites and data

We selected sites across the western United States (Fig. 4.1) with long-term forcing and validation data that represented a range of snow conditions from transient snow with rain-on-snow and midwinter melt events to cold, deep seasonal snowpacks with little melt once the snow

season began. For this work, three stations at the HJ Andrews Experimental Forest were used to represent warm, maritime snowpacks. The two stations at the Southern Sierra Critical Zone Observatory (CZO) also have a warm, maritime climate, but seasonal snowpacks develop more consistently. The final maritime site is Dana Meadows in Yosemite National Park, which has a deep seasonal snowpack due to considerable winter snowfall and low temperatures. The semi-arid Johnston Draw basin within the Reynolds Creek Experimental Watershed is in the intermountain transition zone between maritime and continental. Finally, the two stations on Niwot Ridge are representative of cold continental locations. More information on the sites is presented in the text below and in Table 4.1.

Figure 4.1. The western United States with the 5 study sites. Details on the stations at each site along with their meteorological characteristics are detailed in the following paragraphs and in Table 4.1.

The HJ Andrews Experimental Forest is part of the Long Term Ecological Research (LTER) network. Although there are multiple study sites within the forest, we focused on the three meteorological stations with long-term forcing and validation data: Cenmet (HJA-CEN), Vanmet (HJA-VAN), and Uplmet (HJA-UPL). Due to its lower elevation, the HJA-CEN site only develops seasonal snowpacks during some winters, but is otherwise transient. HJA-VAN and HJA-UPL typically develop seasonal snowpacks, but snow is transient in some years. Winter melt and rain-on-snow events are common throughout the HJ Andrews (Harr, 1986; Jennings

and Jones, 2015; Mazurkiewicz et al., 2008; Perkins and Jones, 2008). This site represents a typical maritime climate within the rain-snow transition zone.

The Upper (SSC-UPR) and Lower (SSC-LWR) Providence Creek stations in the Southern Sierra CZO are within the maritime zone and generally develop seasonal snowpacks. Reported annual snowfall fractions range between 20% and 60%, and rain-on-snow events can occur at both stations (Hunsaker et al., 2012). SSC-UPR and SSC-LWR can be either rain- or snow-dominated depending on the climate of a particular year (Hunsaker et al., 2012). This site represents maritime climates in the seasonal snow zone where winter melt events are frequent but snow cover persists throughout the winter.

The Dana Meadows station (YOS-DAN) is located within Yosemite National Park and is part of the Yosemite Hydroclimate Network (Lundquist et al., 2016). YOS-DAN receives significant winter precipitation, which produces snow depths several meters deep due to low winter temperatures (Lundquist et al., 2016; Rice et al., 2011). Although it has a maritime climate, annual snowfall fraction can exceed 90% (Lundquist et al., 2016) thanks to the station's high elevation and strongly seasonal precipitation. Winter melt makes up a relatively low proportion of annual snowmelt at this elevation (Rice et al., 2011).

Johnston Draw is a sub-watershed within the larger Reynolds Creek Experimental Watershed, which is part of the CZO network. Reynolds is within the rain-snow transition zone (Nayak et al., 2010) and has a semi-arid intermountain climate, bridging the divide between maritime and continental. We focused our simulations on three stations with co-located meteorological and snow depth measurements: 125 (JD-125), 124b (JD-124b), and 124 (JD-124). Previous work has shown average annual snowfall fraction ranges from 39% at the lower station to 53% at the highest (Godsey et al., 2018). Similar to the HJ Andrews study sites,

seasonal snowpacks develop at the Johnston Draw stations in some years, but not in others. Due to high wind speeds and complex terrain, snow patterns vary across sites from year to year (Godsey et al., 2018). Additionally, winter melt and rain-on-snow events occur throughout the Reynolds Creek Experimental Watershed (Marks et al., 2001; Marks and Winstral, 2001).

The Niwot Ridge LTER has a cold continental climate (Greenland, 1989) with previously reported annual snowfall fractions ranging between 63% and 80% (Caine, 1996; Knowles et al., 2015). The C1 station (NWT-C1) is in the subalpine area of Niwot Ridge and Saddle (NWT-SDL) is situated above treeline in the alpine. Winter melt and rain-on-snow events are rare at both stations, particularly at NWT-SDL. High winter wind speeds are responsible for significant spatial variation in snow depth at NWT-SDL (Erickson et al., 2005; Litaor et al., 2008), while a dense stand of lodgepole pine reduces the effect of wind on snow cover evolution at NWT-C1.

Table 4.1. Station information plus average annual and December/January/February (DJF) climatic conditions for the 8 years of the study period (WY2004–WY2011).

				Annual				DJF				
Site	**Station**	**Code**	**Elevation (m)**	**T_a (°C)**	**RH (%)**	**VW (m s^{-1})**	**PPT (mm)**	**T_a (°C)**	**RH (%)**	**VW (m s^{-1})**	**PPT (mm)**	**PPT* (%)**
HJ Andrews	Cenmet	HJA-CEN	1020	7.5	81.2	1.0	2308	1.7	86.3	1.0	957	41.5
	Vanmet	HJA-VAN	1275	7.0	76.8	1.2	2259	1.3	80.4	1.3	956	42.3
	Uplmet	HJA-UPL	1295	6.5	77.3	0.8	2841	0.7	81.6	0.8	1133	39.9
Southern Sierra CZO	Lower Providence	SSC-LWR	1753	8.4‡	68.3	0.9	1538	1.3	79.5	0.6	821	53.4
	Upper Providence	SSC-UPR	1981	9.1	57.4	1.2	1613	2.3	63.7	0.9	878	54.4
Yosemite Nat. Park	Dana Meadows	YOS-DAN	2987	1.4	55.6	1.3	811	-5.5	62.7	1.4	468	57.7
Johnston Draw	125	JD-125	1508	7.9	57.6	1.7	586	-1.5	74.3	1.7	217	37.0
	124b	JD-124b	1778	6.8	59.2	1.8	718	-2.1	74.5	1.9	301	41.9
	124	JD-124	1804	6.9	56.8	4.4	580	-2.2	72.5	5.3	198	34.1
Niwot Ridge	C1	NWT-C1	3022	2.6	60.8	2.7	917	-6.3	62.3	4.1	216	23.6
	Saddle	NWT-SDL	3528	-0.7	64.3	8.5	1483	-9.9	71.4	11.7	592	39.9†

*Column corresponds to percentage of annual precipitation that falls during DJF.
‡Average T_a values are cooler at SSC-LWR than SSC-UPR due to differences in vegetation and physiography at the two stations (M. Safeeq, personal communication, 20 June 2018).
†High DJF precipitation percentage likely due to gage overcatch reduction factors. The alpine precipitation gage sees significant overcatch due to blowing snow (Williams et al., 1998a) and reduction factors were developed relative to observed changes in the NWT-SDL snow pit SWE (Jennings et al., 2018a).

4.3 Methods

4.3.1 Model setup and forcing data preparation

We used the one-dimensional, physics-based SNOWPACK model (Bartelt and Lehning, 2002; Lehning et al., 2002b, 2002a) to evaluate the sensitivity of snow cover evolution to various precipitation phase methods. SNOWPACK is forced with air temperature (T_a), relative humidity (RH), wind speed (VW), incoming shortwave radiation (SW_{in}), incoming longwave radiation (LW_{in}), and precipitation (PPT) at an hourly or longer time step. Part of our motivation for using SNOWPACK, in addition to the model's consistent performance in snow model studies (Etchevers et al., 2004; Rutter et al., 2009) and extensive validation (Jennings et al., 2018a; Lehning et al., 2001; Lundy et al., 2001; Meromy et al., 2015), was that it offers the user the option to include precipitation phase as part of the forcing data. In this scheme, the user can identify a time step as all-snow (0) or all-rain (1), or a mix of precipitation (decimal values between 0 and 1). Further details on the precipitation phase methods implemented in this study are provided in Sect. 4.3.2 below and model validation is given in Appendix 4.1.

We ran SNOWPACK at an hourly time step and kept model setup nearly identical across the sites in order to make the precipitation phase sensitivity results as comparable as possible. In some cases, this approach overlooked important changes to the snow accumulation and melt processes (e.g., snowfall interception, enhancement of incoming longwave radiation) caused by forest cover, notably at the HJ Andrews site and, to a lesser extent, NWT-C1. However, we wanted the simulations to represent snow cover evolution without introducing the confounding hydrologic effects of interception and model representation thereof, meaning the canopy module for SNOWPACK was not activated at any of the sites. The only changes made to model setup were the meteorological measurement heights (Appendix 4.2), which were provided as part of the various forcing datasets.

Where possible, we relied on quality control and infilling methods from the dataset creators given their familiarity with meteorological processes at their respective sites. At HJ Andrews, the provided data were quality controlled, but not serially complete. We first infilled data with instruments at different heights located at the same station when those measurements were available. We used linear regressions from the other stations to fill all other missing data. For the Southern Sierra CZO sites, we performed an additional quality control routine based on Meek and Hatfield (1994) in order to clean up spurious data points. We then infilled missing data by regressing the two sites. All other datasets were serially complete and we performed no further quality control or infilling procedures. Additionally, none of the sites had LW_{in} measurements available for the entirety of the study period. We used the empirical estimates of LW_{in} provided with the Niwot Ridge and Yosemite datasets to force SNOWPACK. For the other sites, we used the empirical Unsworth and Monteith (1975) formulation that is included with the forcing data preprocessor MeteoIO. At the HJA stations, we bias-corrected the LW_{in} estimate based on one year of LW_{in} observations from HJA-VAN that showed a -56.9 W m^{-2} wintertime bias. This was significantly larger in magnitude than the bias previously found in the Unsworth and Monteith (1975) estimate (Flerchinger et al., 2009), suggesting its performance is more spatially variable than previously noted.

4.3.2 Precipitation phase methods

We evaluated a selection of precipitation phase methods found in the literature, including the more typical T_a thresholds and ranges as well as methods incorporating humidity (Table 4.2). For the T_a, dew point (T_d), and wet bulb (T_w) thresholds, precipitation was designated as all-rain when the temperature was warmer than the threshold and all-snow when cooler than or equal to the threshold. When using the T_a ranges, a linear mix of precipitation phase was given when T_a

fell within the range during precipitation with all-rain above the warmer threshold and all-snow below the cooler threshold. The binary regression methods (Froidurot et al., 2014; Jennings et al., 2018b) computed the probability of snow (p_{snow}) as a function of T_a and RH (Reg_{Bi}, Eq. 4.1) and as a function of T_a, RH, and surface pressure (P_s, Reg_{Tri}, Eq. 4.2). Precipitation was set to be all snow when p_{snow} >= 0.5 and rain when p_{snow} < 0.5:

$$p_{snow} = \frac{1}{1 + e^{(-10.04 + 1.41T_a + 0.09RH)}} \quad (4.1)$$

$$p_{snow} = \frac{1}{1 + e^{(-12.8 + 1.41T_a + 0.09RH + 0.03P_s)}} \quad (4.2)$$

Each of the study sites included RH as part of their meteorological observations, but only the HJ Andrews and Reynolds Creek sites had observations of T_d, while no sites had long-term T_w measurements. To keep precipitation phase methods constant across the sites, we calculated T_d (Alduchov and Eskridge, 1996) and T_w (Stull, 2011) as empirical functions of T_a and RH. The empirical formulation tracked observed T_d at Reynolds with an r^2 of 1.0 and a slight cool bias of -0.3°C. There were no observations on which to validate the T_w estimates, but Stull (2011) shows biases typically < 1.0°C.

It should be noted that although this work pursues a wide variety of precipitation phase methods, it is not completely comprehensive. For example, some models fit a sigmoidal curve between two thresholds when assigning precipitation phase in a T_a range (e.g., Fassnacht et al., 2013; Kienzle, 2008; Leavesley et al., 1995). However, we did not include this method because it should produce little variability in annual snowfall fraction relative to the linear T_a ranges if a uniform distribution of air temperature and precipitation is assumed within the temperature range. Additionally, atmospheric and climate models are being increasingly used to simulate precipitation rate and phase. The wide variety of microphysics schemes available suggests that a

critical examination of these methods should be made, as well. However, such an analysis is beyond the scope of the current work.

Table 4.2. Details on the precipitation phase methods used in this work. The temperature value for each threshold method is given in the "Rain-snow threshold" column. The "All-snow threshold" and "All-rain threshold" columns respectively give the T_a values below which all precipitation is snow and above which all precipitation is rain for the T_a range methods. The regression models compute phase as a function of meteorological conditions during precipitation and are not associated with a threshold value. Due to a large variety of precipitation thresholds and ranges (Feiccabrino et al., 2015; A. A. Harpold et al., 2017c; Jennings et al., 2018b), the citations are listed if the values are approximate.

Category	Method	Rain-snow threshold (°C)	All-snow threshold (°C)	All-rain threshold (°C)	Citation(s)
T_a threshold	T_{a0}	0.0	NA	NA	(Jennings et al., 2018a; Lehning et al., 2002a*; Lynch-Stieglitz, 1994; Rajagopal and Harpold, 2016; Wen et al., 2013)
	T_{a1}	1.0	NA	NA	
	T_{a2}	2.0	NA	NA	
	T_{a3}	3.0	NA	NA	
T_a range	T_{ar0}	NA	-0.5	0.5	(Cherkauer et al., 2003; Tarboton and Luce, 1996; United States Army Corps of Engineers, 1956; Wayand et al., 2016; Wigmosta et al., 1994)
	T_{ar1}	NA	-1.0	3.0	
T_d threshold	T_{d0}	0.0	NA	NA	(Marks et al., 2013; Zhang et al., 2017)
	T_{d1}	1.0	NA	NA	
T_w threshold	T_{w0}	0.0	NA	NA	(Anderson, 1968; Harder and Pomeroy, 2013; Marks et al., 2013)
	T_{w1}	1.0	NA	NA	
Binary logistic regression	Reg_{Bi}	NA	NA	NA	(Froidurot et al., 2014; Jennings et al., 2018b)
	Reg_{Tri}	NA	NA	NA	

*The SNOWPACK default is a 1.2°C T_a threshold.

4.3.3 Evaluating the effect of method selection on snowfall fraction and simulated snow cover evolution

For water years (WY, 1 October of the previous calendar year to 30 September) 2004–2011, we simulated snow cover evolution at the 11 stations using the SNOWPACK model. Each station had a total of 12 unique runs corresponding to the different precipitation phase methods. All forcing data and model setup remained the same across the runs at each site except for the precipitation phase method (model validation metrics for the different methods at each site can be found in Appendix 4.1). We evaluated the effect of precipitation phase method selection by quantifying changes to snowfall fraction and various metrics of seasonal snow cover evolution (Fig. 4.2). These metrics include: peak SWE magnitude and timing, snow-off date, snowmelt

rate, and snow cover duration. Peak SWE magnitude is the maximum amount of water held within the snowpack, while peak SWE timing is the date when peak SWE occurs, also known as melt onset. The melt season lasts from the date of peak SWE to the snow-off-date, which is the first date on which SWE equals zero. For this work, we set snowmelt rate to be the daily average snowmelt rate between peak SWE timing and snow-off date. Snow cover duration is the total number of days when simulated SWE is greater than zero. We present both mean simulated quantities at the various sites and metrics of variability, including standard deviation, coefficient of variation, and range. Stations with greater variability in their snow cover evolution metrics were considered to be more sensitive to the choice of precipitation phase method.

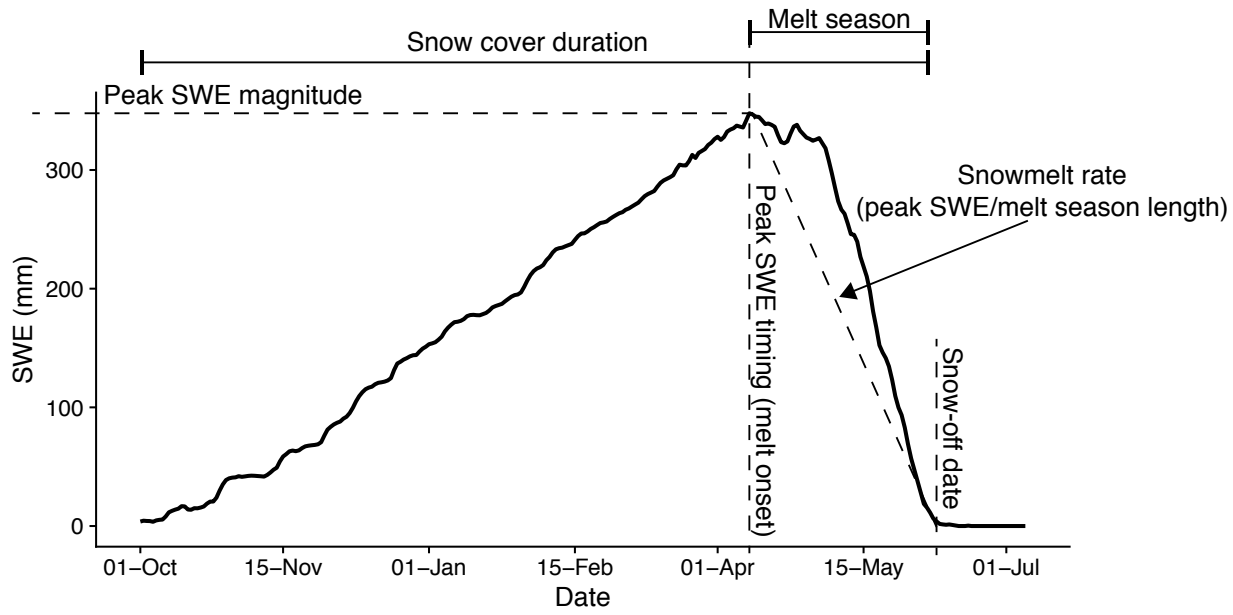

Figure 4.2. Example niveograph showing seasonal snow cover evolution, adapted from Trujillo and Molotch (2014).

4.3.4 Evaluating the relationships between climate and snow cover sensitivity

In addition to quantifying the variability introduced by the different precipitation phase methods, we evaluated the control exerted by daily meteorology and seasonal climate on snow cover evolution sensitivity at our study sites. We first examined how daily T_a and RH introduced

variability into simulated snowfall fraction. We did this by grouping all average daily meteorological conditions in 1°C T_a bins from -8°C to +8°C and 10% RH bins from 60% to 100% on days with precipitation. We then calculated the standard deviation in daily snowfall fraction within each bin across all sites and methods. Those results were used to determine the T_a range that produced the greatest standard deviation in daily snowfall fraction. Next, we computed the proportion of DJF+MAM precipitation that fell within that T_a range at each site for each simulation year and used that percentage to predict annual snowfall fraction standard deviation with ordinary least squares regression. Finally, we quantified how DJF+MAM T_a and PPT controlled variability in peak SWE at our study sites by computing a multiple linear regression with the two meteorological quantities acting as the predictor variables.

4.4 Results

4.4.1 Mean simulated snow cover properties

The study locations showed significant differences in simulated snow cover evolution. Values presented in Table 4.3 were computed by taking the mean of all 12 simulations at each station, where each simulation corresponded to a different precipitation phase method. Mean peak SWE ranged from 73.1 mm at JD-124 to 1146.1 mm at HJA-UPL. The date of peak SWE, or melt onset, also displayed large variability with values ranging from 24 January at JD-125 to 13 May at NWT-SDL. Melt rates were all greater than 10 mm d^{-1} during the ablation season except for at the JD stations. The greatest melt rates were simulated at HJA-UPL and NWT-SDL. The latest snow off date was 20 June at NWT-SDL, while the earliest occurred on 22 February at JD-124. Snow cover duration was greatest at NWT-SDL at 241.1 d. Conversely, snow cover was simulated for less than 3 months, on average, at JD-125 and JD-124.

Table 4.3. Mean snow cover evolution metrics for the 11 stations. Each value was calculated as the mean across all water years and all precipitation phase methods.

	Peak SWE (mm)		Peak SWE date		Melt rate (mm d^{-1})		Snow-off date		SCD (d)	
Station	**Mean**	**SD**	**Mean**	**SD (d)**	**Mean**	**SD**	**Mean**	**SD**	**Mean**	**SD**
HJA-CEN	522.7	252.9	16-Feb	22.0	15	3.9	16-Apr	29.8	158.4	28.2
HJA-VAN	643.1	305.9	14-Feb	22.2	14.5	3.2	22-Apr	31.8	173.1	27.9
HJA-UPL	1146.1	469.9	14-Mar	23.0	24.9	7.3	14-May	32.1	201.1	22.4
SSC-LWR	531.9	160.1	8-Mar	19.0	17.6	3.6	16-Apr	19.3	145.6	27.8
SSC-UPR	617.9	298.8	5-Mar	26.6	17.6	6.0	19-Apr	25.6	149.2	35.6
YOS-DAN	674.4	236.7	18-Mar	17.5	10.9	4.1	25-May	25.5	208.2	40.3
JD-125	83.4	46.5	24-Jan	28.5	4	1.5	25-Feb	31.8	78.1	31.5
JD-124b	177.5	87.6	1-Feb	25.8	5.7	2.5	23-Mar	23.7	122.4	23.9
JD-124	73.1	35.0	2-Feb	31.4	3.5	2.8	22-Feb	36.0	77.6	30.7
NWT-C1	407.2	78.5	22-Apr	10.8	11.9	2.8	5-Jun	8.6	225.3	19.2
NWT-SDL	915	234.2	13-May	10.0	24.4	10.1	20-Jun	9.2	241.1	14.9

4.4.2 Effect of precipitation phase method on snowfall fraction

The sites displayed marked differences in the annual snowfall fraction simulated by the different precipitation phase methods (Fig. 4.3, Table 4.2). Average annual snowfall fraction (all methods, all years) ranged from 32.3% at the HJA-CEN station to 92.4% at the YOS-DAN station (Table 4.2). In this case, more strongly seasonal precipitation at YOS-DAN (Table 4.1) produced a higher annual snowfall fraction than NWT-SDL, despite the former station's warmer average T_a. These two stations also had the lowest standard deviation in annual snowfall fraction, suggesting precipitation phase method selection was less important at these sites. Conversely, the standard deviation of annual snowfall fraction was greater than 6.0% at the remaining stations, reaching a maximum of 9.6% at JD-124b. For all sites except YOS and NWT, all coefficients of variation were greater than 10%, with a maximum of 25.0% at HJA-CEN. The warmer sites also had a wider range in their annual snowfall fraction. In some years at HJA, SSC, and JD, the relative difference between the minimum simulated annual snowfall fraction and the maximum exceeded 100%, meaning the snowiest simulations produced more than double the snowfall of the rainiest.

At NWT-SDL and YOS-DAN the relative difference in annual snowfall fraction was typically less than 15%.

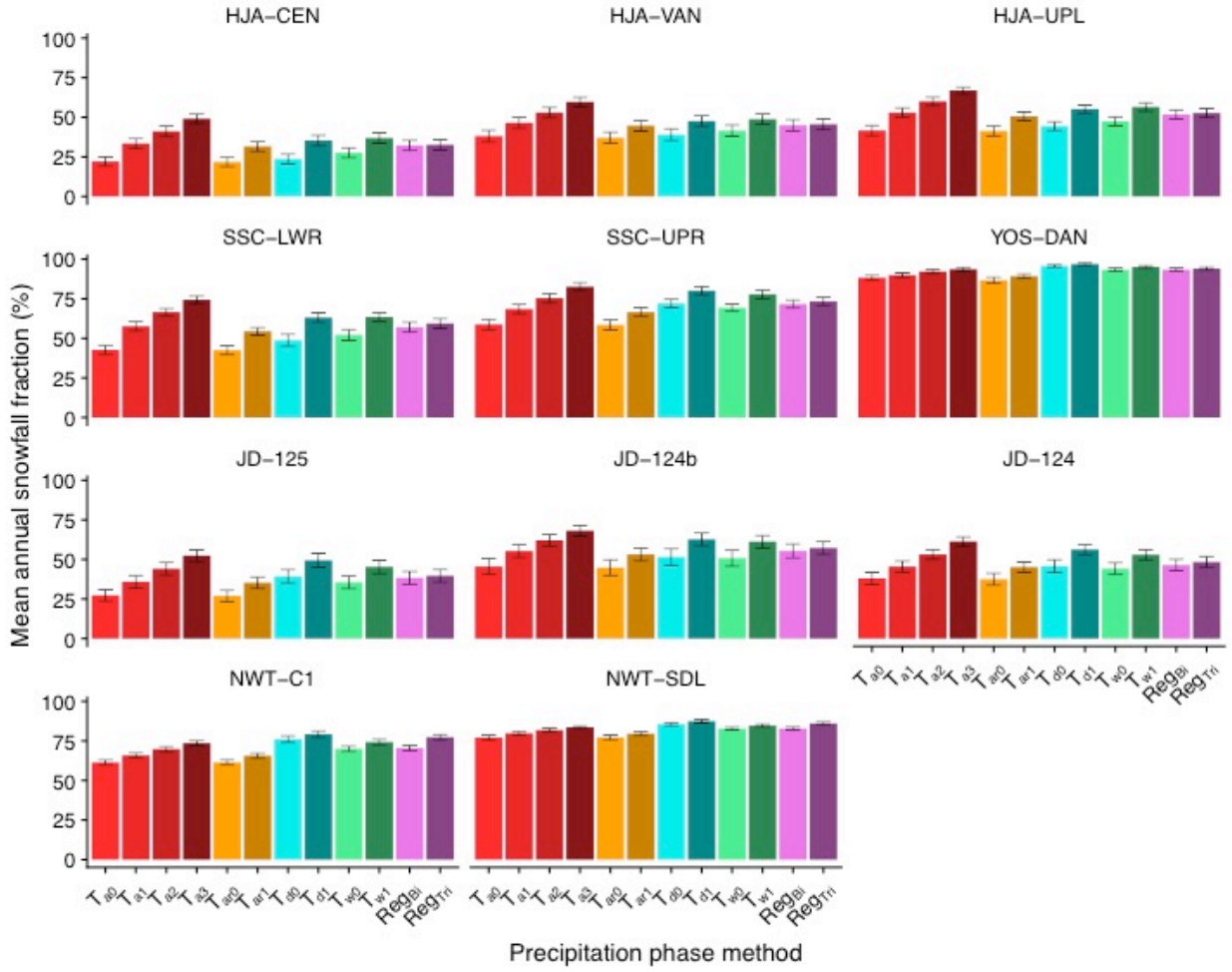

Figure 4.3. Mean annual snowfall fraction at the 11 study sites for the 12 different precipitation phase methods. The whiskers represent the standard error of annual snowfall fraction for the 8 simulation years. For this plot and all subsequent figures showing the station data, the maritime sites are shown in the top two rows, the intermountain site is in the third row, and the continental site is in the bottom row.

Table 4.4. Summary statistics for average annual snowfall fraction computed using the 12 different precipitation phase methods at the 11 study sites.

	Average annual snowfall fraction (%)			
Station	**Average**	**SD**	**CV**	**Range**
HJA-CEN	32.3	8.1	25.0	27.4
HJA-VAN	45.5	6.5	14.2	22.6
HJA-UPL	51.8	7.5	14.6	25.7
SSC-LWR	56.8	9.6	16.9	32.3
SSC-UPR	71.2	7.8	10.9	25.0
YOS-DAN	92.4	3.3	3.5	10.1
JD-125	39.1	8.0	20.4	26.0
JD-124b	55.7	7.2	12.9	23.2
JD-124	47.9	7.2	14.9	23.9
NWT-C1	70.4	6.0	8.6	18.2
NWT-SDL	82.4	3.4	4.1	10.3

There was a large range in the aggregate mean annual snowfall fraction (all stations, all years) for the different methods (Fig. 4.4). The highest T_a and T_d thresholds produced the greatest annual snowfall fractions, while T_{a0} and T_{r0} produced the lowest. The absolute difference in mean annual snowfall fraction between T_{a3} and T_{ar0} was 20.9%, meaning using T_{a3} over T_{ar0} gave a relative increase of 42.9% in annual snowfall fraction. The T_w and T_d thresholds produced greater snowfall fractions than the equivalent T_a thresholds because the former two are cooler than T_a when relative humidity is less than 100%. Additionally, there was a negligible difference between T_{a0} and T_{ar0} as well as between T_{a1} and T_{ar1}, suggesting the use of a range over a threshold introduces minimal variability in snowfall fraction. The regression methods, Reg_{Bi} and Reg_{Tri}, produced the 5th and 6th greatest annual snowfall fractions.

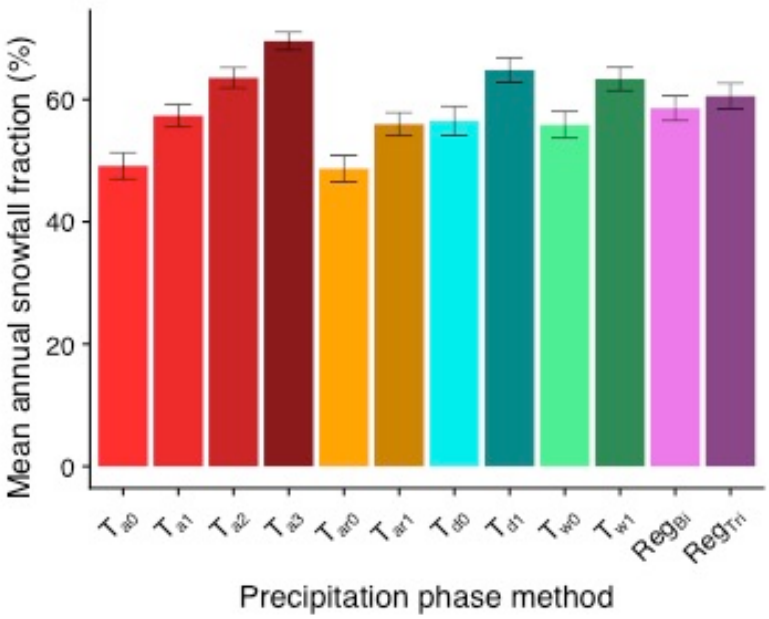

Figure 4.4. Mean annual snowfall fraction for the different precipitation phase methods at the 11 stations. The whiskers represent the standard error of annual snowfall fraction for the 11 stations. Ranked from highest to lowest annual snowfall fraction, the methods are: T_{a3} (69.6%), T_{d1} (64.8%), T_{a2} (63.6%), T_{w1} (63.4%), Reg_{Tri} (60.6%), Reg_{Bi} (58.6%), T_{a1} (57.4%), T_{d0} (56.5%), T_{ar1} (56.0%), T_{w0} (55.9%), T_{a0} (49.2%), and T_{ar0} (48.7%).

4.4.3 Effect of precipitation phase method on simulated snow cover evolution

There were marked differences between the stations in terms of the effect of precipitation phase method choice on seasonal snow cover evolution (Fig. 4.5). NWT-SDL and YOS-DAN showed little sensitivity in annual snowfall fraction across the methods and this was reflected in the negligible differences in mean daily SWE at the two stations. Conversely, there was wide divergence in simulated SWE at the remaining maritime sites and at the Johnston Draw stations.

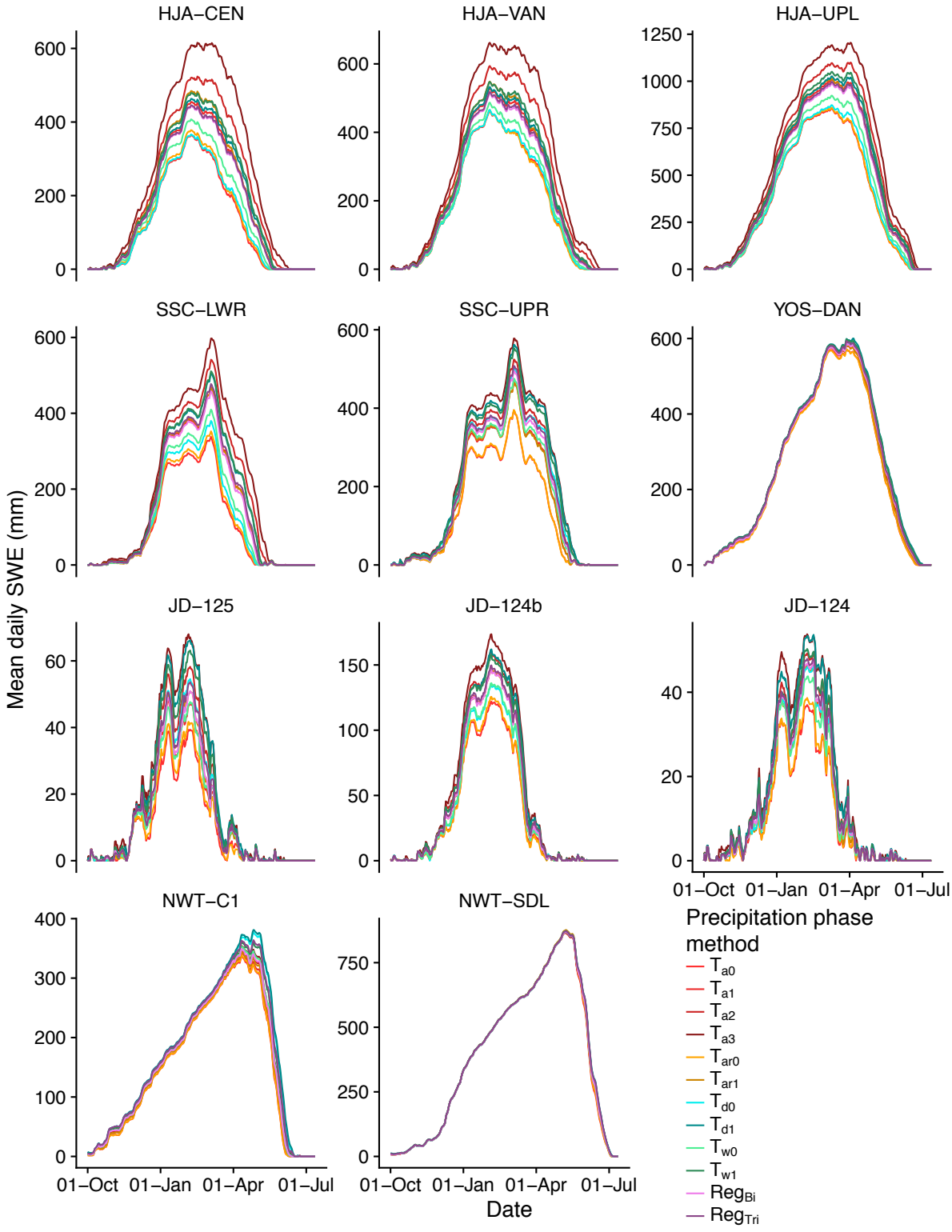

Figure 4.5. Mean daily SWE for each precipitation phase method (colored lines) at the different stations. The mean daily SWE was computed by averaging the SWE on each day for the given precipitation phase method across the simulation years.

Breaking down the analysis to the individual snow cover evolution metrics reveals more differences in the sensitivity of the sites to precipitation phase method selection (Fig. 4.6). In terms of peak SWE standard deviation and range, the HJA and SSC stations were most sensitive, with the range in peak SWE across the phase methods exceeding 200 mm in most years. Conversely, YOS and NWT were relatively insensitive as their ranges were nearly always less than 100 mm. Although the JD stations showed little sensitivity in terms of range, they expressed significant sensitivity when looking at the coefficient of variation due to their low mean annual peak SWE (Table 4.3). Thus, percentage-wise, JD was as sensitive as the two warm maritime sites to the selection of a precipitation phase method. JD was also sensitive to precipitation phase method selection in terms of peak SWE date. At HJA and JD, the range in peak SWE date approached one month and greater in certain years, while it was generally less than 10 days at the other sites. We found the greatest differences in peak SWE dates were generally simulated on years with low/transient snow cover. In these cases, late-season precipitation was simulated as rain by the low thresholds and snow by the high thresholds, meaning an early SWE maximum was recorded as the peak in the former case and a late SWE maximum in the latter case.

Similar sensitivities were simulated for snow-off date and snow cover duration with the warm maritime sites and JD being the most sensitive. In some years, the snow-off date occurred more than a month later with the high thresholds than with the low thresholds at JD and HJA. Conversely, the range was always 10 days or fewer at YOS and NWT. In terms of snow cover duration, ranges among the thresholds typically exceeded 3 weeks at HJA, SSC, and JD. NWT-C1 approached the sensitivity of the warmer stations, while NWT-SDL and YOS-DAN were the least sensitive. For both snow-off date and snow cover duration, JD had the greatest coefficient

of variation values, showing the semi-arid intermountain site was quite sensitive to precipitation phase method selection in relative terms.

Finally, differences among the sites were relatively low for melt rate sensitivity. JD stations had the greatest sensitivity in terms of the coefficient of variation due to their low mean annual melt rates, which were an order of magnitude lower than those simulated at the other sites (Table 4.3). Ranges for the different stations were relatively similar to one another with the interquartile ranges generally showing some degree of overlap. Overall, melt rate at YOS-DAN was the least sensitive to precipitation phase method in terms of standard deviation, coefficient of variation, and range.

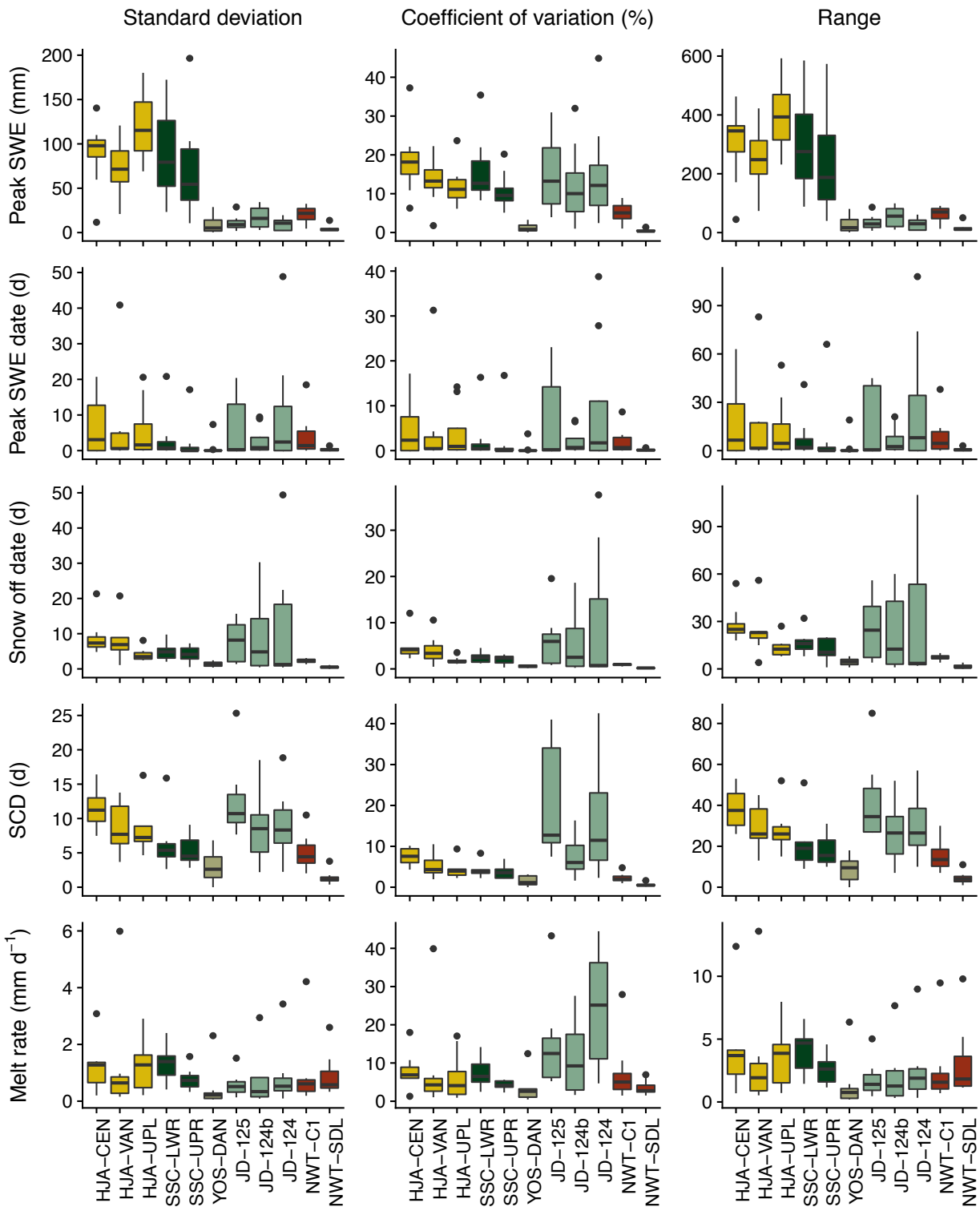

Figure 4.6. The sensitivity of various snow cover evolution metrics to precipitation phase method at the study stations. The standard deviation, coefficient of variation, and range were computed across the precipitation phase methods within each simulation year at each station, and the boxplots show the distribution of those values across all the simulation years. The boxplots for standard deviation and range use the units shown in the y-axis title, while all coefficient values are percentages.

In addition to looking at intra-station differences, we also examined how the methods compared in aggregate across all the stations. Figure 4.7 shows that T_{a3} produced the greatest values for each of the snow cover evolution metrics, while T_{a0} and T_{ar0} were generally responsible for the lowest values. T_{a2}, T_{d1}, and T_{w1} showed strong overlap in their ranks for the different methods, suggesting that, in aggregate, there was less divergence in snow cover evolution for these methods than for others. Additionally, Reg_{Tri} produced consistently higher snow cover evolution ranks (e.g., greater SWE, longer snow cover duration) than Reg_{Bi}, indicating that including surface pressure as a predictor variable led to increased snowfall at the stations studied here. It is also notable that the T_{ar} methods produced similar ranks to their equivalent T_a thresholds (i.e., the T_{ar0} range is centered on T_{a0}). Finally, the T_w and T_d thresholds were associated with greater snow cover evolution ranks than the T_a thresholds at the same degree value.

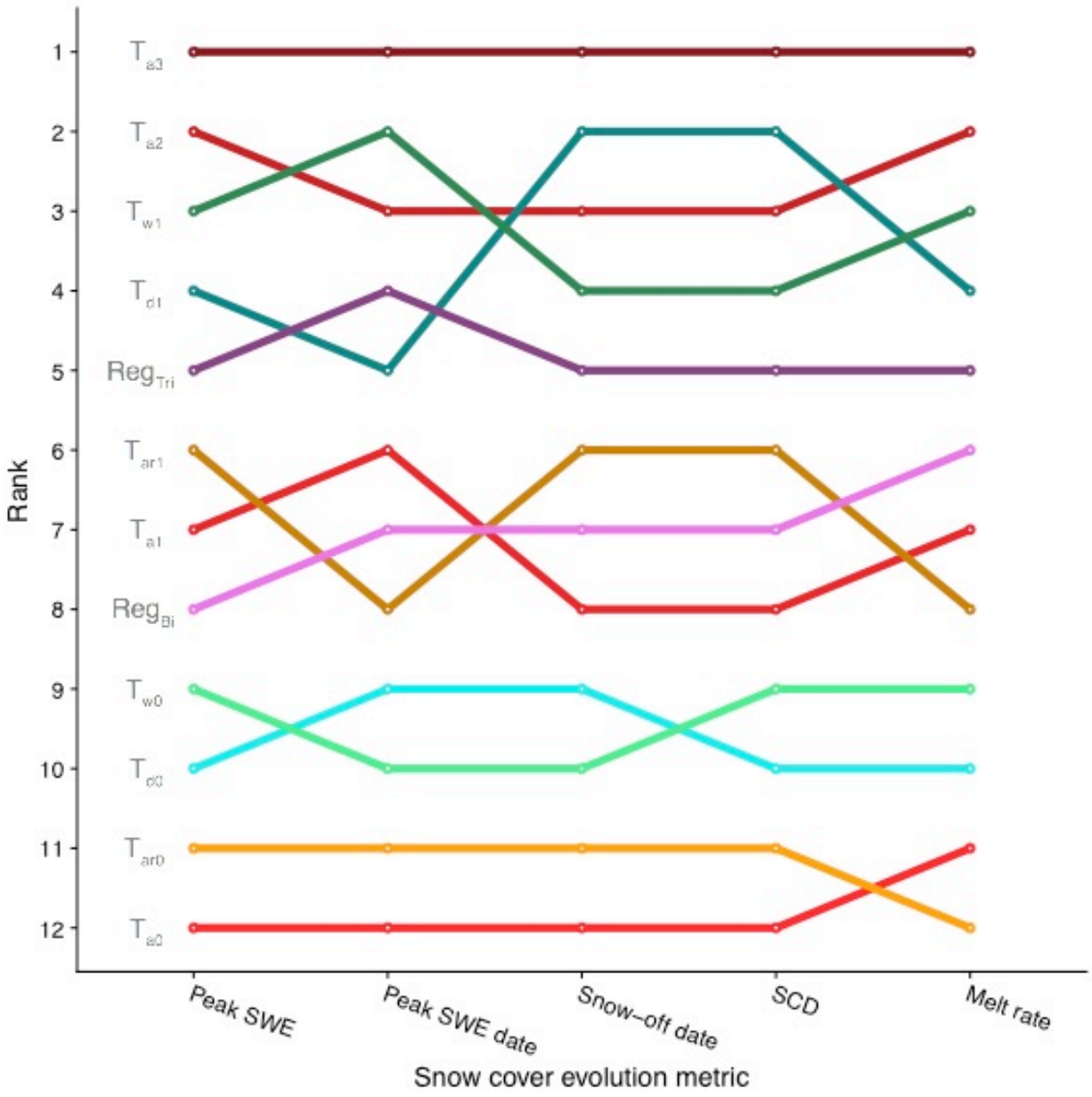

Figure 4.7. Rank plot of the precipitation phase methods in terms of peak SWE, peak SWE date, snow-off date, snow cover duration (abbreviated SCD in plot), and melt rate. Ranks were calculated for each snow cover evolution metric by averaging the values for that metric across the individual stations. Ranks closest to 1 (top of plot) correspond to increased peak SWE magnitude, later peak SWE date, later snow off date, longer snow cover duration, and faster melt rate.

4.4.4 Climatic controls on model sensitivity

All of the precipitation phase methods in this paper partitioned precipitation into rain or snow, or a mix of the two, using T_a or T_a and RH (only Reg_{Tri} uses P_s). This combined with the large differences in seasonal T_a and RH, as well as in annual snowfall fraction across the sites, led to

the question of how variability in snowfall fraction is produced. We therefore evaluated the control daily T_a and RH exerted on the standard deviation of daily snowfall fraction across all sites and all methods. In general, snowfall fraction standard deviation was greatest at daily T_a values between 0°C and 4°C (Fig. 4.8). RH provided a secondary control, with greater variability at lower RH values. Overall, the largest standard deviations in snowfall fraction were simulated at daily RH less than 80% and T_a between 1°C and 3°C. However, it should be noted that 75.2% of all precipitation recorded at these sites occurred in the 90%–100% RH bin. Therefore, although daily snowfall fraction standard deviations were highest at lower RH values the majority of the variability in annual snowfall fraction was an effect of T_a. In this context, the percentage of DJF+MAM precipitation that fell within the 0°C–4°C T_a range explained 74.0% of the variance in annual snowfall fraction standard deviation across the study sites (Fig. 4.9).

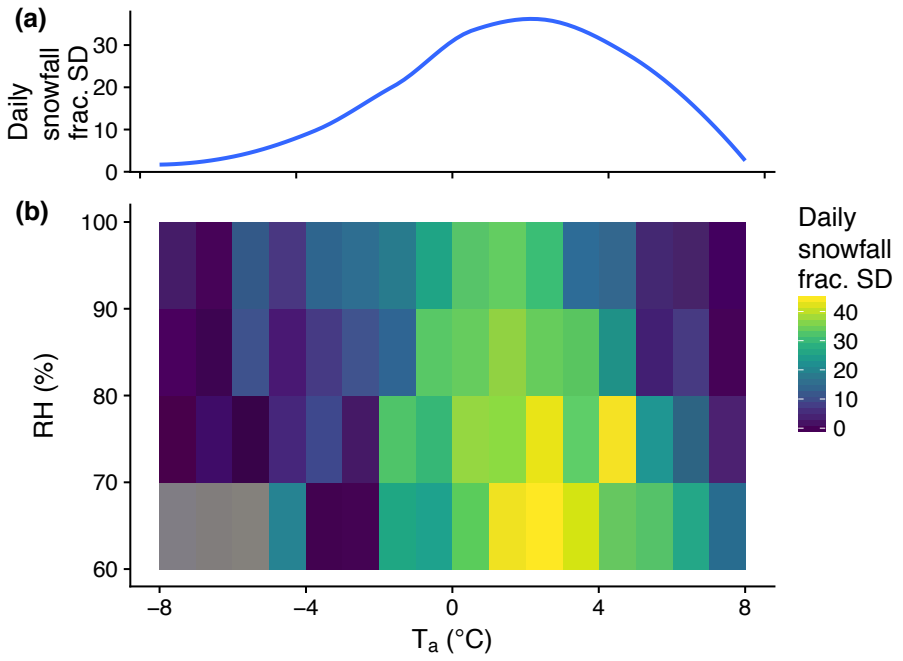

Figure 4.8. The standard deviation of daily snowfall fraction as a function of T_a (a) and as a function of T_a and RH (b). We binned the meteorological quantities within the ranges shown and calculated the standard deviation of snowfall fraction per T_a bin (a) and T_a/RH bin (b) using simulated precipitation phase from all stations and all methods.

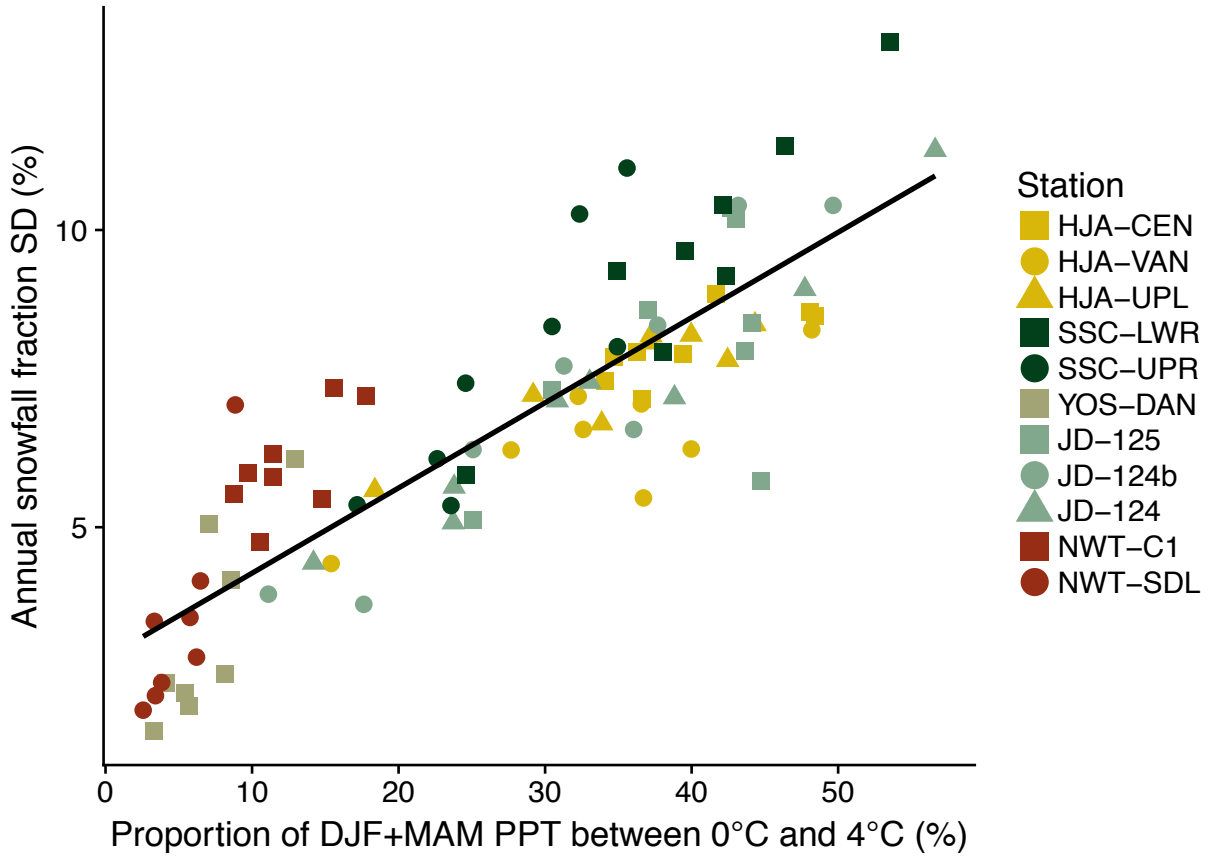

Figure 4.9. Standard deviation in annual snowfall fraction as predicted by the proportion of DJF+MAM PPT falling between 0°C and 4°C. Each point represents one simulation year at a station identified by the color and shape. The black line of best fit was calculated using ordinary least squares regression ($r^2 = 0.74$, *p-value* < 0.0001).

Moving past variability in daily and annual snowfall fraction, we next evaluated how sensitivity in peak SWE was related to seasonal climate. A multiple linear regression with DJF+MAM T_a and DJF+MAM PPT as the predictor variables explained 78.6% of the variance in the range of annual peak SWE at the stations (Fig. 4.10). In this case, warmer T_a and increased PPT were both associated with greater ranges in the peak SWE simulated by the different precipitation phase methods. This meant the maritime sites HJA and SSC had the greatest sensitivity to precipitation phase method due to their relatively warm T_a and high PPT values. Conversely, moderate PPT values and lower T_a led to minimal sensitivity at the cold continental NWT stations and the cold maritime YOS-DAN station. Again, the effect of T_a on sensitivity is

manifest in the data. In high snowfall years at NWT-SDL, DJF+MAM PPT approached that of the low DJF+MAM PPT years at HJA and SSC. However, despite the increased PPT at NWT-SDL, the range in peak SWE predicted by the different precipitation phase methods remained low. Additionally, the multiple linear regression performed here is likely only valid for the range of climatic conditions at our study sites. For example, extrapolating the regression to T_a values above 5°C would indicate greater peak SWE sensitivity for a given PPT value. However, moving towards increasingly warmer T_a would likely lead to lower peak SWE ranges due to the increasing probability of rainfall versus snowfall.

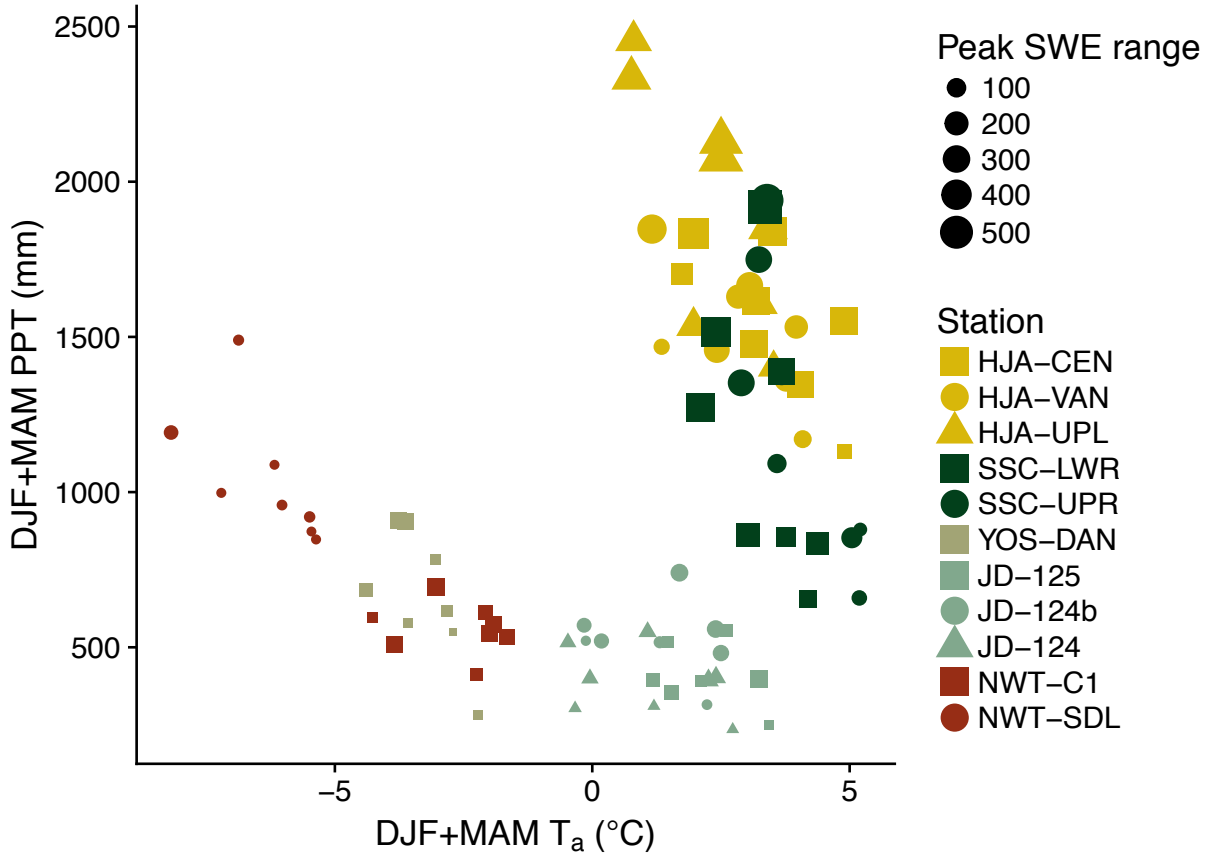

Figure 4.10. Range in annual peak SWE as simulated by the different precipitation phase methods at the 11 study stations. Each point represents one simulation year at a given station and larger points correspond to increased uncertainty in peak SWE. Predicting the peak SWE range as a function of DJF+MAM T_a and PPT using multiple linear regression yielded an r^2 of 0.79.

4.5 Discussion

4.5.1 A best precipitation phase method?

In this work we showed that the selection of a precipitation phase method introduces variability in modeled snow accumulation and melt, with our study sites expressing varying degrees of sensitivity. Although the different methods corresponded to relatively higher and lower objective function values (Appendix 4.1), uncertainties in the forcing data, model structure, and parameters, as well as a lack of precipitation phase observations prevent this work from being a referendum on the "best" precipitation phase method for snow modeling. Our aim was to highlight how snow simulations were affected across a climatic gradient by the choice of precipitation phase method. Additionally, our goal was not to create the best model setup at each site, but rather to keep model setup consistent in order to compare the sensitivity of phase partitioning without introducing other uncertainties. Thus, the low r^2 and higher bias values at certain stations could likely be improved with model tuning, but we did not pursue such an approach.

Although we cannot declare a "best" method, previous work has shown that, in general, methods incorporating humidity information outperform T_a-only methods (Harder and Pomeroy, 2013; Jennings et al., 2018b; Marks et al., 2013; Ye et al., 2013). In that context, one can consider the Reg_{Bi} model as a baseline given its top rank in a Northern Hemisphere precipitation phase method comparison (Jennings et al., 2018b). Our study showed that Reg_{Bi} typically produced low biases relative observed snow depth and SWE (Appendix 4.1) and led to snow cover evolution metrics that were neither extremely high nor low (Fig. 4.7). The higher T_a, T_d and T_w thresholds produced greater peak SWE and longer snow cover duration, while the lower thresholds led to less accumulation and shorter snow cover duration. Additionally, our model-based study showed that uncertainty in precipitation phase peaked between 0°C and 4°C (Fig.

4.8), which is the same air temperature range reported by Ding et al. (2014) in which precipitation phase methods exhibit degraded performance relative to observations. Moving forward, work needs to be done validating precipitation phase methods, but using spatially uniform high and low thresholds will likely lead to overprediction and underprediction, respectively, of peak SWE and snow cover duration.

In their work highlighting the different types of precipitation phase methods, Harpold et al. (2017c) called for improved automatic monitoring of precipitation phase through the installation of disdrometer networks. Given the spatially variable sensitivity of simulated snow cover evolution to precipitation phase method that we have shown in this work, we echo their recommendation. Due to their relatively high cost, precipitation phase research using disdrometers has generally been performed at a limited number of sites over short study periods (e.g., Wayand et al., 2016; Yuter et al., 2006). Visual observer reports (Dai, 2008, 2001), snow boards (Wayand et al., 2017) and snow depth sensors (Rajagopal and Harpold, 2016; Zhang et al., 2017) are alternative methods, but each have their drawbacks. Therefore, permanent disdrometer installations in transient and seasonal snow zones should be considered, especially if coordinated with the already established CZO and LTER networks.

4.5.2 Physical mechanisms controlling sensitivity to phase method

The warm maritime sites HJA and SSC expressed the largest peak SWE ranges from precipitation phase method selection (Fig. 4.6). These ranges were typically larger than 200 mm and sometimes exceeded 500 mm, indicating large uncertainty in snowpack water storage. Additionally, snow-off date ranges typically exceeded two weeks at these stations, meaning the timing of complete melt was also affected by precipitation phase method. These large variations in snow cover evolution were likely due to the combined effect of reduced frozen mass entering

the snowpack and subsequent changes to the snowpack energy balance. For the former, both HJA and SSC had high proportions of precipitation falling between 0°C and 4°C (Fig. 4.9), which led to wide ranges in annual snowfall fraction (Table 4.4). The methods producing lower annual snowfall fractions (e.g., T_{a0} and T_{ar0}) generally corresponded to earlier snow-off dates (Fig. 4.7) simply because there was less frozen mass to melt. In other words, the energy required to melt the entire snowpack was reduced relative to the methods producing higher snowfall fractions, and the snowpack could be melted over a shorter time period.

Compounding the response of the warm maritime sites was the fact that snow and rain have different fates when they enter a snowpack with resultant effects on the snowpack energy budget. Snowfall can increase snowpack cold content (Jennings et al., 2018a), refresh surface albedo (Clow et al., 2016; Painter et al., 2012; United States Army Corps of Engineers, 1956), and provide dry pore space that must be filled with liquid water before melt can begin (Bengtsson, 1982b; Seligman et al., 2014). Rainfall, conversely, can advect heat to the snowpack (Marks et al., 1998), infiltrate and run off (Harr, 1986, 1981), or be refrozen in the snowpack if there is cold content to be satisfied. In this context, the precipitation phase methods that produced more rainfall affected snow cover evolution not just through reduced frozen mass but also through changes to the snowpack energy budget.

In addition to affecting snow cover evolution, rain-on-snow events are also responsible for high snowmelt rates and floods in the Oregon Cascades and Sierra Nevada mountains (McCabe et al., 2007) and these events are expected to change in spatial extent and intensity with climate warming (Musselman et al., 2018). Previous work has shown precipitation phase can affect runoff dynamics during rain-on-snow events with a shift from solid to liquid precipitation leading to enhanced snowmelt runoff (Jennings and Jones, 2015). Therefore, the marked

uncertainty in precipitation phase produced by the different methods is likely to affect simulations of rain-on-snow events. In this study, precipitation phase method selection led to ranges in the annual number of daily rain-on-snow events (SWE > 10 mm, rainfall > 10 mm, and runoff > 10 mm) between 1 and 23 days at HJA and SSC. This corresponded to annual runoff ranges from rain-on-snow events between 41.7 mm and 679.9 mm at the two sites. Thus, the conclusions of rain-on-snow modeling studies may be affected by the choice of a precipitation phase method.

4.5.3 Assumptions and limitations

Snow modeling studies are hindered by inherent uncertainties in model structure (Essery et al., 2013; Etchevers et al., 2004; Rutter et al., 2009; Slater et al., 2001) and forcing data (Lapo et al., 2015; Raleigh et al., 2016, 2015). While the research presented herein shows that precipitation phase method should be considered another critical component of model uncertainty, our work was also likely affected by the aforementioned issues in structure and forcing data which can be seen in the variability of model performance at the different sites (Appendix 4.1). In this work, we used the well-validated, physics-based SNOWPACK model, but past research has shown there is no best snow model and that model performance varies both within and across study sites (e.g., Rutter et al., 2009). Therefore, our use of a single model may overestimate or underestimate the sensitivity of snow cover evolution to precipitation phase method at certain sites and points in time. Future research should therefore focus on how model choice affects the sensitivity of simulated snow cover evolution to precipitation phase method.

In addition to the uncertainties introduced by the SNOWPACK model, we used empirical methods to estimate T_d and T_w, which could affect rain-snow partitioning. We were satisfied with the performance of the T_d method as it strongly matched T_d observations from Johnston

Draw (Sect. 4.3.2). However, there were no observations of T_w on which to validate the Stull (2011) method, which was optimized for standard surface pressure and for a range of T_a and RH values. The figures in Stull (2011) show that pressure-induced uncertainty in T_w is generally less than 1°C when RH > 50%. Additionally, the total percentage of precipitation observations falling within the Stull (2011) T_a and RH ranges was between 94.3% and 100% at our stations. Thus, we expect only marginal uncertainty to be introduced by the empirical methods. However, precipitation phase and hydrometeor temperature are strongly related to T_w (Harder and Pomeroy, 2013), suggesting there should be enhanced monitoring of T_w at research sites.

Furthermore, our research only examined methods that partition precipitation phase using surface meteorological quantities such as T_a and RH. Atmospheric and climate models can also be used for hydroclimatic simulations either through direct coupling in earth systems models or as forcing data for land surface models. Many such models employ microphysics schemes to assign and track precipitation phase from the formation of a hydrometeor, through various atmospheric layers, to the land surface. For example, the Weather Research and Forecasting (WRF) model (Skamarock et al., 2005) has been used to simulate snow cover accumulation and ablation over large study domains in the western United States when coupled to a land surface model (Ikeda et al., 2010; Musselman et al., 2017a; Rasmussen et al., 2011). WRF has also been used to model the elevation of the rain-snow transition line in order to evaluate which basin areas are receiving solid or liquid precipitation during storm events (Minder et al., 2011). In addition, work from the 5th phase of Coupled Model Intercomparison Project (CMIP5) has shown that climate models produce different snowfall fractions due to variations in both climate and precipitation phase method (Krasting et al., 2013). In CMIP5, some models utilize microphysics schemes, while others assign precipitation phase at the land surface using methods similar to the

ones presented in this work. Therefore, understanding and quantifying the sensitivity of model output due to precipitation phase method selection is important for both hydrologic and climate modeling studies.

4.5.4 Connecting this work to large-scale LSM hydroclimate simulations

Snow exerts a primary control on various hydroclimatic processes, including streamflow generation (Barnhart et al., 2016; Berghuijs et al., 2014), soil moisture (Harpold and Molotch, 2015), soil temperature (Groffman et al., 2001; Slater et al., 2017), and land surface albedo (Groisman et al., 1994). Previous basin-scale research has shown variability in precipitation phase propagates into uncertainties in hydrologic model output, such as streamflow timing and volume (Blöschl et al., 1991; Harder and Pomeroy, 2014; Mizukami et al., 2013). In this work, we showed significant variability in the sensitivity of simulated snow accumulation and melt to the selection of a precipitation phase method at stations spanning a climatic gradient in the western United States. An ideal next step would be to leverage the results from this study and others by scaling up to gridded land surface models to better understand how precipitation phase method selection affects simulations of past, present, and future hydroclimatic conditions over large spatial extents.

Two main components of such research would be streamflow volume and timing, and land surface albedo. For the former, approximately 60 million people in the western United States (Bales et al., 2006) and nearly 2 billion globally rely on snowmelt-derived water resources (Barnett et al., 2005; Mankin et al., 2015). Knowing the timing and volume of streamflow—which are directly related to snowmelt onset and peak SWE magnitude—is essential for proper water resources management. It is therefore reasonable to assume method selection will be important to simulated streamflow given that we saw snowmelt onset ranges exceeding one

month and peak SWE magnitude differences greater than 200 mm. Our work suggests that this variability will produce the greatest impact in areas that see significant precipitation and have average winter and spring T_a between 0°C and 4°C.

Additionally, land surface albedo will be directly impacted by variability in snow cover duration due to the increased albedo of snow relative to bare ground. Previous research has shown radiative forcing has increased at the earth's surface (Flanner et al., 2011) due to decreased snow cover duration over large spatial extents (Brown, 2000; Groisman et al., 1994). Thus, the ranges we showed in snow cover duration, approaching 2 months, will have direct impacts on the planet's simulated energy balance. In this regard, the use of a spatially uniform, high T_a rain-snow threshold would lead to greater snow cover duration, higher surface albedo, and a larger proportion of incoming solar radiation reflected back to space relative to a low T_a threshold. These considerable uncertainties in both hydrologic and climatic processes are particularly important when considered in the context of continued climate warming.

4.5.5 Snow and climate warming

As noted in the introduction, the shift from snow to rain in cold and temperate regions across the globe is expected to continue with further warming. Future air temperature increases are expected to lead to reduced snowfall fractions (Klos et al., 2014; Lute et al., 2015; Safeeq et al., 2015), reduced peak SWE (Adam et al., 2009), earlier snowmelt onset (Stewart et al., 2004a), and slower snowmelt rates (Musselman et al., 2017a). Climate-driven changes in snow accumulation and ablation are associated with both impacts to water resources availability (Barnett et al., 2008) and land surface albedo (Déry and Brown, 2007). Areas with winter T_a near 0°C have been identified as most "at-risk" to reductions in snowfall fraction and snow accumulation in a warming climate (Nolin and Daly, 2006). Concerningly, our work shows it is

precisely these areas that have the greatest modeled snow cover evolution sensitivity to precipitation method selection.

Harpold et al. (2017a) showed that future changes to snowfall fraction are moderated or exacerbated by the choice of a precipitation phase method, depending on the area's relative humidity. However, how this uncertainty affects the conclusion of climate change predictions is typically not discussed. In the context of the work presented herein, there should be a focus applied to areas where the baseline variability in peak SWE, snowmelt onset, and snow cover duration due to precipitation phase method approaches or exceeds the simulated change in the associated snowpack properties with warming. In warm maritime climates, research has shown peak SWE may decrease by upwards of several hundred millimeters as warming continues (e.g., Cooper et al., 2016; Leung et al., 2004; Minder, 2010; Musselman et al., 2017b), which is near the range of peak SWE sensitivity values reported in this work. Precipitation phase method selection is also likely to impact simulations of future warm snow droughts where anomalously warm winters are associated with low peak SWE (Harpold et al., 2017b). In a relative sense, this would be particularly important in low snow years like the extreme 2015 drought experienced in the Sierra Nevada and Cascade mountains. In addition, snow cover duration variability due to precipitation phase method selection may affect simulations of the snow-albedo feedback, which is the amplification of surface warming due to reduced snow cover (Hall, 2004; Hall and Qu, 2006). As climate warming shifts new areas towards the winter and spring average T_a values (0°C–4°C) that lead to the greatest snowfall fraction standard deviation, our research suggests that uncertainty in future hydroclimatic states will be exacerbated by precipitation phase method selection.

4.6 Conclusion

In this work we simulated seasonal snow cover evolution using the SNOWPACK model forced with 12 different precipitation phase methods at 11 study sites spanning a climatic gradient. We found the choice of a precipitation phase method introduced significant uncertainty into annual snowfall fraction, peak SWE, snowmelt onset, snowmelt rate, snow-off date, and snow cover duration. However, sensitivity of snow cover evolution to method selection was not consistent across our study sites. In general, cold sites were relatively insensitive to the choice of method because all methods were simulating similar amounts of snowfall. In this context, the YOS-DAN and NWT-SDL stations exhibited the lowest sensitivity to precipitation phase method selection. Peak SWE ranges were typically less than 50 mm for these two stations, while snowmelt onset date ranges were generally less than 1 week. Conversely, the warm maritime HJA and SSC stations showed marked sensitivity to precipitation phase method selection with peak SWE ranges typically greater than 200 mm, exceeding 400 mm in some years. These sites also displayed significant sensitivity in snow cover timing metrics with snowmelt onset date ranges approaching 1 month or greater and snow cover duration ranges generally exceeding 3 weeks.

The spatially variable sensitivity of snow cover evolution was primarily a result of climatic differences between the sites. Increased DJF+MAM T_a and PPT were associated with greater peak SWE ranges across the different precipitation phase methods. This meant the maritime sites HJA and SSC with significant winter and spring PPT were most affected by precipitation phase method selection. Although YOS-DAN is still in the maritime zone, its cold winter T_a was closer to the NWT stations than to the other maritime sites, making it relatively insensitive. Overall, we found stations with DJF+MAM mean T_a greater than 0°C to be more sensitive than those with mean T_a less than 0°C. This is troublesome considering climate warming is expected to push new areas in the seasonal snow zone towards winter temperatures

near 0°C and above. Thus, there is the wicked problem of the places most likely to have snow accumulation and melt impacted by further warming are the most sensitive to precipitation phase method selection. It is therefore critical that future work examine the relationship between the climate signal and the model variability that results from precipitation phase partitioning uncertainty, particularly in areas undergoing a snow-to-rain transition.

4.7 Appendix 4.1 – Model validation

As noted in the Methods section, model setup was kept constant at all the sites, no parameter tuning was performed, and the SNOWPACK canopy module was not activated. This was done to minimize the introduction of confounding factors and to keep the simulation results as comparable as possible. Figure 4.11 displays mean bias and r^2 values for the simulations relative to observed SWE and snow depth at the different stations. Each data point in the boxplots represents one precipitation method for the 8 simulation years. Mean biases were lowest at the NWT stations and at SSC-UPR relative to SWE observations and at the JD stations and SSC-LWR relative to snow depth observations. Average r^2 values were between 0.65 and 0.91 for SWE except at NWT-SDL (0.52) and HJA-VAN (0.51), and 0.61 and 0.79 for snow depth except at JD-124 (0.46). The variability of model output at the different stations is representative of both inconsistent snow model performance (Etchevers et al., 2004; Rutter et al., 2009) and the difficulty of accounting for wind processes in point snow models (Raleigh et al., 2015).

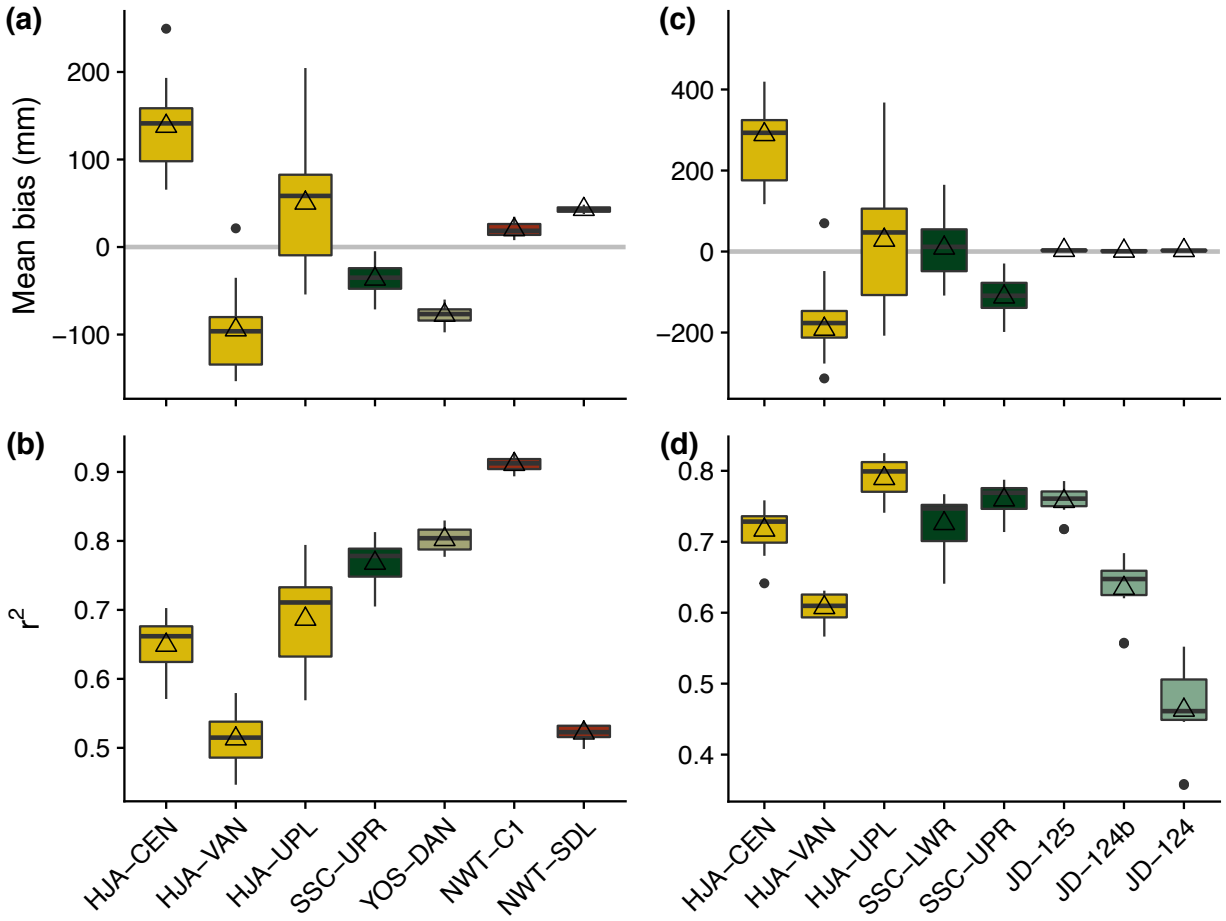

Figure 4.11. Mean bias (top row) and r^2 (bottom row) values for the SNOWPACK simulations relative to observed SWE (a,b) and snow depth (c,d). The boxplots show the median, interquartile range, minimum, maximum, and outlying values for each objective function for the different precipitation phase methods at a given station. The open triangles indicate the mean objective function value for all precipitation phase methods at that station.

Figure 4.12 shows the objective function values for SWE and snow depth for the various methods aggregated across the stations. In terms of mean bias, the binary regression models and the T_{a1} threshold provided the best performance with average values between 3.1 mm and 9.1 mm relative to observed SWE and between -1.7 mm and 6.9 mm relative to observed snow depth. Conversely, the T_{a0}, T_{a2}, T_{a3} thresholds and the T_{ar0} range provided the worst performance with T_{a2} and T_{a3} overpredicting snow accumulation and T_{a0} and T_{ar0} underpredicting snow accumulation by upwards of 100 mm relative to observed SWE and 200 mm and greater relative to observed snow depth. There was relatively little divergence in r^2 values across the methods, with only a 0.07 and 0.08 difference between the maximum and minimum average r^2 values for

SWE and snow depth, respectively. The lowest r^2 values were produced by the T_{a0} threshold and T_{ar0} range, while the highest values were produced by T_{d1}, T_{w1} and the higher T_a thresholds.

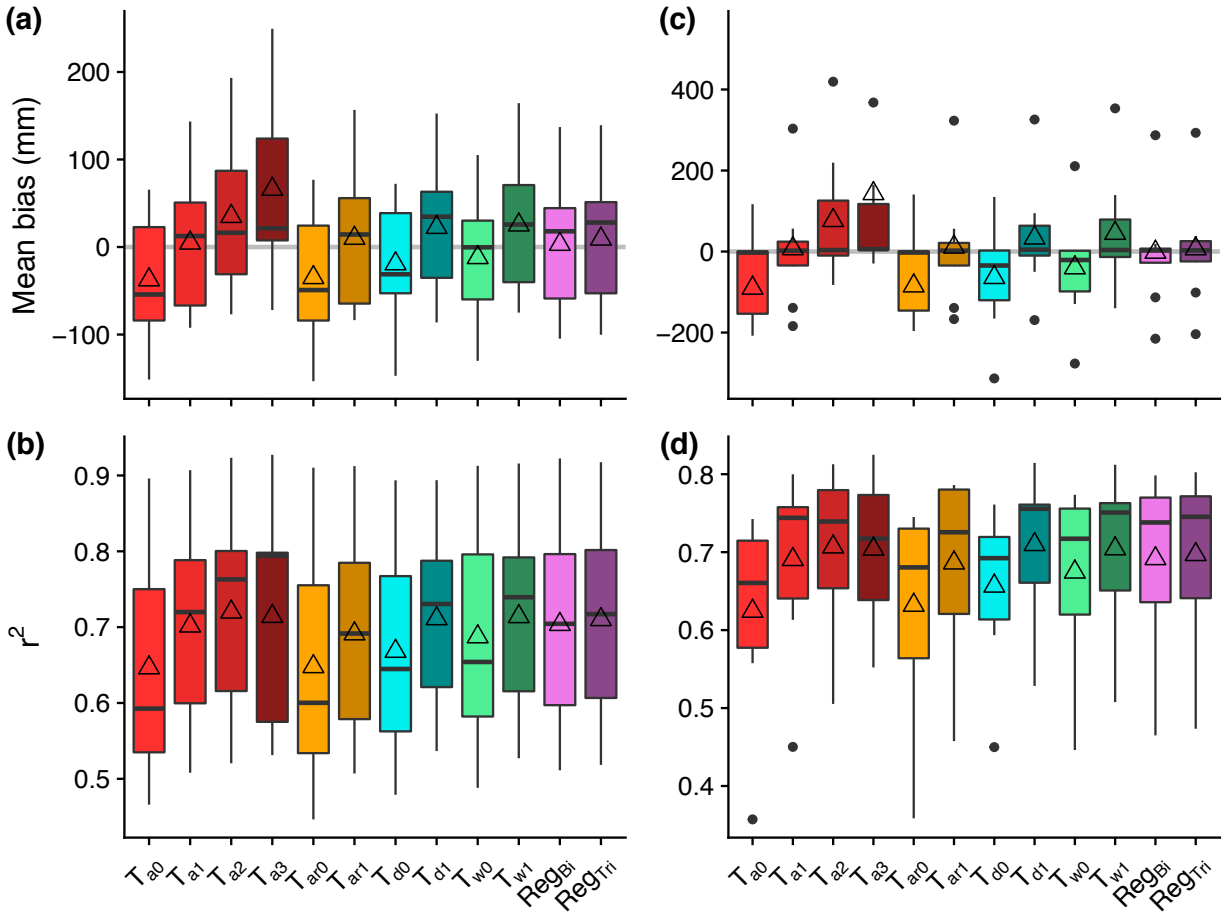

Figure 4.12. Mean bias (top row) and r^2 (bottom row) values for the SNOWPACK simulations relative to observed SWE (a,b) and snow depth (c,d). The boxplots show the median, interquartile range, minimum, maximum, and outlying values for each objective function for the different precipitation phase methods at all stations. The open triangles indicate the mean objective function value for that precipitation phase methods at all stations.

4.8 Appendix 4.2 – Instrument measurement heights

Table 4.5. Measurement heights for wind speed and other meteorological quantities at the study stations.

Station	Wind height (m)	Other measurement heights (m)
HJA-CEN	10	4.5
HJA-VAN	10	4.5
HJA-UPL	10	4.5
SSC-LWR	4	4
SSC-UPR	4	4
YOS-DAN	5	5
JD-125	3	3
JD-124b	3	3
JD-124	3	3
NWT-C1	5*	2
NWT-SDL	5	2

*The NWT-C1 anemometer is located in an unrepresentative location (open road), so observations were corrected to represent wind speed in the forest canopy (Jennings et al., 2018a).

Chapter 5

5 Conclusion

5.1 Summary of findings

The research presented in this dissertation contributed to the knowledge of snow accumulation and melt processes in a changing climate. To do this, I leveraged a combination of validation data in the form of snow pit observations and automated snow depth and SWE sensors, quality controlled and serially complete meteorological data, and the physics-based SNOWPACK model. Below are short summaries of the findings of the three projects followed by ideas for future research based on the questions that this dissertation raised but did not answer.

5.1.1 Project 1 (Chapter 2): Observations and simulations of the seasonal evolution of snowpack cold content and its relation to snowmelt and the snowpack energy budget

Observations and simulations both showed that new snowfall was the primary source of cold content development, being responsible for 84.4% and 73.0% of daily cold content gains at the alpine and subalpine sites, respectively. A negative snowpack energy balance was responsible for the remainder of daily cold content additions at the two sites, while air temperature showed little relationship to cold content development. Initial non-zero cold content values delayed snowmelt onset and damped snowmelt rates at time scales one month and less. Conversely, peak cold content magnitude was not correlated with seasonal snowmelt rate or timing, suggesting cold content magnitude has greater predictive capacity at shorter time scales.

5.1.2 Project 2 (Chapter 3): Evaluating the differential response of an alpine and subalpine snowpack to changes in climate

We simulated a differential response to climate warming at our study sites, with the colder, higher alpine site being less sensitive to air temperature increases than the subalpine site. This

was due to three physical reasons: 1) Snowfall fraction decreased less rapidly with warming than in the subalpine; 2) Significant cold content was still added to the alpine snowpack throughout the snow season, preventing mid-winter melt events; 3) Changes to snowmelt rate were non-significant because increases to the turbulent fluxes balanced decreases in the radiative fluxes with earlier melt onset. As opposed to the differential response to warming, changes to total precipitation led to relatively consistent results at the alpine and subalpine sites with later melt onset and faster snowmelt rates being associated with increased precipitation. Changes to precipitation seasonality had a near-negligible impact on snow cover properties at both sites.

5.1.3 Project 3 (Chapter 4): The sensitivity of modeled snow accumulation and melt to precipitation phase methods across a climatic gradient in the western United States

There was marked spatial variability in the sensitivity of simulated snow cover evolution to precipitation phase method selection. The three sites with average winter air temperatures less than -5°C expressed minimal sensitivity to the different methods, suggesting that method selection matters little at cold, high-elevation sites where the vast majority of annual precipitation falls as snow. Conversely, at the remaining warmer sites, precipitation phase method selection introduced significant uncertainty with ranges in annual snowfall fraction exceeding 30%. This significant uncertainty propagated into sensitivity in simulated snow cover evolution with peak SWE ranges approaching 500 mm and snow cover duration ranges nearing one month or more. Overall, sites with warmer winter and spring temperatures and greater precipitation were most sensitive to precipitation phase method selection in terms of the variability in snow cover evolution.

5.2 Future research

Snow is irreplaceable to the economy and water resources of the western United States and to many other cold and temperate regions across the globe (Bales et al., 2006; Barnett et al., 2005; Mankin et al., 2015; Sturm et al., 2017). Thus, near-certain future air temperature increases and declines in snow cover (IPCC, 2013; USGCRP, 2017) stand to have a large impact on humans, ecosystems, and regional hydroclimate. Now more than ever there is the need for research into snow accumulation and melt processes across spatial and temporal scales using a combination of ground observations, model output, and remote sensing data. Standing in the way is the fact that snow research is inherently difficult due to challenging field conditions (Marr, 1967), pronounced spatial variability (Blöschl, 1999; Clark et al., 2011), limited representativeness of point measurements (Molotch and Bales, 2006), and difficulties in observing quantities of interest. The last point is particularly salient to my work moving forward in the following ways:

1. It was noted in the introduction to Project 1 that the primary reason for a lack of cold content research is that cold content is difficult to observe. Cold content is a linear function of snowpack mass and temperature, but observations of internal snowpack temperature are scarce relative to those of snow depth and SWE. The Niwot Ridge LTER offered a unique opportunity for evaluating how cold content accumulated in seasonal snowpacks thanks to long-term snow pit and meteorological datasets. Unfortunately, due to their time-intensive nature, snow pit records from other sites are typically short, inconsistent, or non-existent. Thus, we know little about how cold content develops in other climates as there are few measurements to analyze or to employ as validation data.

   Although thermistor arrays used to monitor snowpack temperature have their own drawbacks, they offer a useful alternative to snow pits. They provide automated measurements at different vertical levels and can be used to calculate depth-weighted

snowpack temperature. These observations can then be used to compute cold content when combined with automated mass readings from a snow pillow or regular manual depth and density measurements. Moving forward I hope to collaborate with other researchers to explore their existing observations and develop strategies to incorporate automated snowpack temperature measurements at more field sites. I particularly want to focus on areas where cold content is low due to warm internal snowpack temperatures (e.g., California's Sierra Nevada mountains). Project 2 showed that a marked increase in winter melt occurred when seasonal snowpack cold content neared the daily net flux magnitude, meaning areas with low cold content could express a greater sensitivity to warming. Thus, better quantifying cold content development in such areas could further understanding into how snow accumulation and melt processes are evolving in a changing climate.

2. In addition to improving our knowledge of cold content development processes, measurements of snowpack temperature can also be used to better constrain the surface energy budget, which is notoriously difficult to close in winter over snow-covered surfaces (e.g., Blanken et al., 2009; Helgason and Pomeroy, 2011; Turnipseed et al., 2002). Project 2 showed how quantifying the snowpack energy balance is essential to understanding the differential response of mountain snowpacks to climate warming. However, most current physics-based models employ energy balance formulations that are decades old, which is particularly troublesome for the turbulent fluxes whose uncertainty is sometimes greater than their magnitude (Etchevers et al., 2004). Lapo et al. (2015) showed that monitoring snow surface temperature can improve energy balance simulations through better partitioning of the turbulent and radiative fluxes. In this

context, automated measurements of internal snowpack temperature could further constrain the snowpack energy balance as changes to internal energy are reflective of the incoming and outgoing fluxes.

In future work, I aim to improve model simulations of the energy budget through enhanced monitoring in mountain environments and development of physical relationships between surface fluxes and changes in internal snowpack energy. I hope to focus on a selection of sites that have existing research infrastructure and span a climatic gradient similar to the sites in Project 3. In the ideal scenario, each study site would have an intensive array of monitoring equipment that extends from the snow-soil interface to 5 m above the ground. Measurements would cover the full snowpack energy balance through the use of pyranometers, pyrgeometers, eddy flux instruments, ground heat flux plates, snowpack thermistors, and an infrared thermometer to measure snow surface temperature. Precipitation mass and phase, snow depth, snow mass, and snowmelt would also be measured to cover the mass balance. The observations could then be used to inform improved treatments of the snowpack energy balance in physics-based snow models.

3. Despite being visible to the human eye, precipitation phase is difficult to observe and properly quantify at air temperatures near freezing. Visual observer reports are time-intensive, include a degree of subjectivity, and do not enable quantification of rain-snow proportions in mixed-phased events. Snow boards and snow depth sensors can also be used to infer precipitation phase, but the former require manual measurements and the latter rely on depth-change algorithms to estimate phase. Laser disdrometers, although expensive, can accurately measure precipitation phase and report the solid-liquid ratio

during mixed-phase storms, thus offering a promising way forward (Wayand et al., 2016; Yuter et al., 2006). For future research, I hope to install disdrometers collocated with existing meteorological and snow observation stations that are part of the CZO, LTER, and SNOTEL networks. This work will be used to improve how precipitation phase is represented in snow, hydrologic, and land surface models by evaluating the surface controls on phase partitioning in mountain areas with diverse climatic conditions.

Furthermore, Project 3 covers only how precipitation phase method choice leads to snow cover evolution uncertainty, meaning there is much more to unpack from a hydroclimate perspective. As previously mentioned, snowpacks serve myriad roles in the global hydrologic cycle and climate system, making it essential that land and earth systems models accurately simulate precipitation phase. To this end, I am actively working with other researchers to take the information produced in Project 3 at the point scale to land surface model runs across large spatial extents. As it stands, this work will entail the forcing of a land surface model with different precipitation phase methods as in Project 3 with the aim of quantifying the uncertainty in simulated streamflow timing and magnitude as well as land surface albedo. The simulations will be done for both historic and future climatic conditions in order to evaluate how precipitation phase method selection affects the conclusions of climate change research. Such work is particularly topical given that climate warming is expected to push cold areas with currently sub-freezing winter temperatures to near- and above-freezing values, thus likely increasing the uncertainty in precipitation phase partitioning.

4. All of the work presented in this dissertation was performed at the point scale, but point measurements do not fully represent the spatial variability of snow accumulation and

melt processes (Elder et al., 1991; Molotch and Bales, 2006). Previous work has shown that such processes can vary over short distances due to the effects of wind redistribution and variations in the snowpack energy balance (e.g., Marks and Winstral, 2001; Pomeroy et al., 2003). In general, a lack of spatially distributed snowpack data has limited the validation of snowpack models to a small collection of automated snow depth and SWE monitoring sites. Thus, there has not been much well-constrained work done on how the snowpack energy balance and snowmelt rate and timing vary in space over large spatial extents. To that end, I am currently using the Alpine3D model (Lehning et al., 2006) in conjunction with distributed snow depth data from NASA's Airborne Snow Observatory (ASO).

ASO has revolutionized the way mountain snowpacks are observed through its fusion of airborne lidar and an imaging spectrometer (Painter et al., 2016). In the Tuolumne River Basin on the west side of California's Sierra Nevada mountains, their spatially distributed depth product has increased the number of validation points from a handful of automated sensors to nearly a half-million pixels. For my work, I am using one lidar snow depth scene per year to scale the precipitation input to better match how snow is distributed across the landscape (e.g., Brauchli et al., 2017; Vögeli et al., 2016), while the remaining scenes are used for model validation. Once the baseline simulations are finished, the next step of the project will be to assess how climate warming affects the snowpack energy balance to determine if certain physiographic areas are more sensitive than others in terms of the timing and rate of their meltwater deliveries. Ultimately, it will be the fusion of advanced remote sensing observations, enhanced *in situ* measurements,

and physics-based models that will make possible future advancements in understanding snow accumulation and melt processes in a changing climate.

6 References

Abatzoglou, J.T., 2011. Influence of the PNA on declining mountain snowpack in the Western United States. Int. J. Climatol. 31, 1135–1142.

Adam, J.C., Hamlet, A.F., Lettenmaier, D.P., 2009. Implications of global climate change for snowmelt hydrology in the twenty-first century. Hydrol. Process. 23, 962–972.

Albert, M.R., McGilvary, W.R., 1992. Thermal effects due to air flow and vapor transport in dry snow. J. Glaciol. 38, 273–281.

Alduchov, O.A., Eskridge, R.E., 1996. Improved Magnus form approximation of saturation vapor pressure. J. Appl. Meteorol. 35, 601–609.

Anderson, E.A., 1976. A point of energy and mass balance model of snow cover. NOAA Tech Rep NWS 19, 1–150.

Anderson, E.A., 1968. Development and testing of snow pack energy balance equations. Water Resour. Res. 4, 19–37.

Andreadis, K.M., Storck, P., Lettenmaier, D.P., 2009. Modeling snow accumulation and ablation processes in forested environments. Water Resour. Res. 45. https://doi.org/10.1029/2008WR007042

Angström, A.K., 1915. A study of the radiation of the atmosphere: based upon observations of the nocturnal radiation during expeditions to Algeria and to California. Smithsonian Institution.

Armstrong, R.L., Armstrong, B.R., 1987. Snow and avalanche climates of the western United States: a comparison of maritime, intermountain and continental conditions. IAHS Publ 162, 281–294.

Armstrong, R.L., Brun, E., 2008. Snow and climate: physical processes, surface energy exchange and modeling. Cambridge University Press.

Auer Jr, A.H., 1974. The rain versus snow threshold temperatures. Weatherwise 27, 67–67.

Avanzi, F., De Michele, C., Ghezzi, A., 2014. Liquid-solid partitioning of precipitation along an altitude gradient and its statistical properties: An Italian case study. Am. J. Clim. Change 2014.

Bales, R.C., Molotch, N.P., Painter, T.H., Dettinger, M.D., Rice, R., Dozier, J., 2006. Mountain hydrology of the western United States. Water Resour. Res. 42.

Barnett, T.P., Adam, J.C., Lettenmaier, D.P., 2005. Potential impacts of a warming climate on water availability in snow-dominated regions. Nature 438, 303–309.

Barnett, T.P., Pierce, D.W., 2009. Sustainable water deliveries from the Colorado River in a changing climate. Proc. Natl. Acad. Sci. 106, 7334–7338. https://doi.org/10.1073/pnas.0812762106

Barnett, T.P., Pierce, D.W., Hidalgo, H.G., Bonfils, C., Santer, B.D., Das, T., Bala, G., Wood, A.W., Nozawa, T., Mirin, A.A., others, 2008. Human-induced changes in the hydrology of the western United States. science 319, 1080–1083.

Barnhart, T.B., Molotch, N.P., Livneh, B., Harpold, A.A., Knowles, J.F., Schneider, D., 2016. Snowmelt rate dictates streamflow. Geophys. Res. Lett. 43, 8006–8016.

Bartelt, P., Lehning, M., 2002. A physical SNOWPACK model for the Swiss avalanche warning: Part I: numerical model. Cold Reg. Sci. Technol. 35, 123–145.

Bavay, M., Egger, T., 2014. MeteoIO 2.4.2: a preprocessing library for meteorological data. Geosci. Model Dev. 7, 3135–3151. https://doi.org/10.5194/gmd-7-3135-2014

Bavay, M., Grünewald, T., Lehning, M., 2013. Response of snow cover and runoff to climate change in high Alpine catchments of Eastern Switzerland. Adv. Water Resour. 55, 4–16.

Bengtsson, L., 1982a. Percolation of meltwater through a snowpack. Cold Reg. Sci. Technol. 6, 73–81.

Bengtsson, L., 1982b. The importance of refreezing on the diurnal snowmelt cycle with application to a northern Swedish catchment. Hydrol. Res. 13, 1–12.

Beniston, M., Keller, F., Koffi, B., Goyette, S., 2003. Estimates of snow accumulation and volume in the Swiss Alps under changing climatic conditions. Theor. Appl. Climatol. 76, 125–140.

Berg, N.H., 1986. Blowing snow at a Colorado alpine site: measurements and implications. Arct. Alp. Res. 147–161.

Berghuijs, W.R., Woods, R.A., Hrachowitz, M., 2014. A precipitation shift from snow towards rain leads to a decrease in streamflow. Nat Clim Change 4, 583–586.

Berghuijs, W.R., Woods, R.A., Hutton, C.J., Sivapalan, M., 2016. Dominant flood generating mechanisms across the United States: Flood Mechanisms Across the U.S. Geophys. Res. Lett. 43, 4382–4390. https://doi.org/10.1002/2016GL068070

Bintanja, R., Andry, O., 2017. Towards a rain-dominated Arctic. Nat. Clim. Change 7, 263–267.

Blanken, P.D., Williams, M.W., Burns, S.P., Monson, R.K., Knowles, J., Chowanski, K., Ackerman, T., 2009. A comparison of water and carbon dioxide exchange at a windy alpine tundra and subalpine forest site near Niwot Ridge, Colorado. Biogeochemistry 95, 61–76.

Blöschl, G., 1999. Scaling issues in snow hydrology. Hydrol. Process. 13, 2149–2175.

Blöschl, G., Gutknecht, D., Kirnbauer, R., 1991. Distributed snowmelt simulations in an alpine catchment: 2. Parameter study and model predictions. Water Resour. Res. 27, 3181–3188.

Blöschl, G., Kirnbauer, R., 1991. Point snowmelt models with different degrees of complexity—internal processes. J. Hydrol. 129, 127–147.

Boone, A., Etchevers, P., 2001. An intercomparison of three snow schemes of varying complexity coupled to the same land surface model: Local-scale evaluation at an Alpine site. J. Hydrometeorol. 2, 374–394.

Brauchli, T., Trujillo, E., Huwald, H., Lehning, M., 2017. Influence of Slope-Scale Snowmelt on Catchment Response Simulated With the Alpine3D Model. Water Resour. Res. 53, n/a-n/a. https://doi.org/10.1002/2017WR021278

Brooks, P.D., Williams, M.W., 1999. Snowpack controls on nitrogen cycling and export in seasonally snow-covered catchments. Hydrol. Process. 13, 2177–2190.

Brown, R.D., 2000. Northern hemisphere snow cover variability and change, 1915-97. J. Clim. 13, 2339–2355.

Burns, S.P., Molotch, N.P., Williams, M.W., Knowles, J.F., Seok, B., Monson, R.K., Turnipseed, A.A., Blanken, P.D., 2014. Snow Temperature Changes within a Seasonal Snowpack and Their Relationship to Turbulent Fluxes of Sensible and Latent Heat. J. Hydrometeorol. 15, 117–142. https://doi.org/10.1175/JHM-D-13-026.1

Caine, N., 1996. Streamflow patterns in the alpine environment of North Boulder Creek, Colorado Front Range. Z. Geomorphol. Suppl. 27–42.

Cayan, D.R., Dettinger, M.D., Kammerdiener, S.A., Caprio, J.M., Peterson, D.H., 2001. Changes in the onset of spring in the western United States. Bull. Am. Meteorol. Soc. 82, 399–415.

Cayan, D.R., Peterson, D.H., 1989. The influence of North Pacific atmospheric circulation on streamflow in the west. Asp. Clim. Var. Pac. West. Am. 375–397.

Cherkauer, K.A., Bowling, L.C., Lettenmaier, D.P., 2003. Variable infiltration capacity cold land process model updates. Glob. Planet. Change 38, 151–159. https://doi.org/10.1016/S0921-8181(03)00025-0

Christensen, N.S., Wood, A.W., Voisin, N., Lettenmaier, D.P., Palmer, R.N., 2004. The effects of climate change on the hydrology and water resources of the Colorado River basin. Clim. Change 62, 337–363.

Clark, M.P., Hendrikx, J., Slater, A.G., Kavetski, D., Anderson, B., Cullen, N.J., Kerr, T., Örn Hreinsson, E., Woods, R.A., 2011. Representing spatial variability of snow water equivalent in hydrologic and land-surface models: A review. Water Resour. Res. 47, W07539. https://doi.org/10.1029/2011WR010745

Clark, M.P., Nijssen, B., Luce, C.H., 2017. An analytical test case for snow models. Water Resour. Res. 53, 909–922. https://doi.org/10.1002/2016WR019672

Cline, D.W., 1997. Snow surface energy exchanges and snowmelt at a continental, midlatitude Alpine site. Water Resour. Res. 33, 689–701.

Clow, D.W., 2010. Changes in the timing of snowmelt and streamflow in Colorado: a response to recent warming. J. Clim. 23, 2293–2306.

Clow, D.W., Williams, M.W., Schuster, P.F., 2016. Increasing aeolian dust deposition to snowpacks in the Rocky Mountains inferred from snowpack, wet deposition, and aerosol chemistry. Atmos. Environ., Acid Rain and its Environmental Effects: Recent Scientific AdvancesPapers from the Ninth International Conference on Acid Deposition 146, 183–194. https://doi.org/10.1016/j.atmosenv.2016.06.076

Colbeck, S.C., 1989a. Air movement in snow due to windpumping. J. Glaciol. 35, 209–213.

Colbeck, S.C., 1989b. Snow-crystal growth with varying surface temperatures and radiation penetration. J. Glaciol. 35, 23–29.

Cooper, M.G., Nolin, A.W., Safeeq, M., 2016. Testing the recent snow drought as an analog for climate warming sensitivity of Cascades snowpacks. Environ. Res. Lett. 11, 084009. https://doi.org/10.1088/1748-9326/11/8/084009

Crawford, T.M., Duchon, C.E., 1999. An improved parameterization for estimating effective atmospheric emissivity for use in calculating daytime downwelling longwave radiation. J. Appl. Meteorol. 38, 474–480.

Dadic, R., Mott, R., Lehning, M., Carenzo, M., Anderson, B., Mackintosh, A., 2013. Sensitivity of turbulent fluxes to wind speed over snow surfaces in different climatic settings. Adv. Water Resour. 55, 178–189.

Dai, A., 2008. Temperature and pressure dependence of the rain-snow phase transition over land and ocean. Geophys. Res. Lett. 35.

Dai, A., 2001. Global Precipitation and Thunderstorm Frequencies. Part I: Seasonal and Interannual Variations. J. Clim. 14, 1092–1111. https://doi.org/10.1175/1520-0442(2001)014<1092:GPATFP>2.0.CO;2

Deems, J.S., Painter, T.H., Barsugli, J.J., Belnap, J., Udall, B., 2013. Combined impacts of current and future dust deposition and regional warming on Colorado River Basin snow dynamics and hydrology. Hydrol. Earth Syst. Sci. Katlenburg-Lindau 17, 4401. http://dx.doi.org.colorado.idm.oclc.org/10.5194/hess-17-4401-2013

Déry, S.J., Brown, R.D., 2007. Recent Northern Hemisphere snow cover extent trends and implications for the snow-albedo feedback. Geophys. Res. Lett. 34, L22504. https://doi.org/10.1029/2007GL031474

DeWalle, D.R., Rango, A., 2008. Principles of snow hydrology. Cambridge University Press.

Dickerson-Lange, S.E., Gersonde, R.F., Hubbart, J.A., Link, T.E., Nolin, A.W., Perry, G.H., Roth, T.R., Wayand, N.E., Lundquist, J.D., 2017. Snow disappearance timing is dominated by forest effects on snow accumulation in warm winter climates of the Pacific Northwest, United States. Hydrol. Process. 31, 1846–1862. https://doi.org/10.1002/hyp.11144

Dilley, A.C., O'Brien, D.M., 1998. Estimating downward clear sky long-wave irradiance at the surface from screen temperature and precipitable water. Q. J. R. Meteorol. Soc. 124, 1391–1401.

Ding, B., Yang, K., Qin, J., Wang, L., Chen, Y., He, X., 2014. The dependence of precipitation types on surface elevation and meteorological conditions and its parameterization. J. Hydrol. 513, 154–163.

Easterling, D.R., Kunkel, K.E., Arnold, J.R., Knutson, T., LeGrande, A.N., Leung, L.R., Vose, R.S., Waliser, D.E., Wehner, M.F., 2017. Precipitation change in the United States, in: Wuebbles, D.J., Fahey, D.W., Hibbard, K.A., Dokken, D.J., Stewart, B.C., Maycock, T.K. (Eds.), Climate Science Special Report: Fourth National Climate Assessment, Volume I. U.S. Global Change Research Program, Washington, DC, USA, pp. 207–230. https://doi.org/10.7930/J0H993CC

Elder, K., Dozier, J., Michaelsen, J., 1991. Snow accumulation and distribution in an Alpine Watershed. Water Resour. Res. 27, 1541–1552. https://doi.org/10.1029/91WR00506

Erickson, T.A., Williams, M.W., Winstral, A., 2005. Persistence of topographic controls on the spatial distribution of snow in rugged mountain terrain, Colorado, United States. Water Resour. Res. 41.

Essery, R., Morin, S., Lejeune, Y., B Ménard, C., 2013. A comparison of 1701 snow models using observations from an alpine site. Adv. Water Resour., Snow–Atmosphere Interactions and Hydrological Consequences 55, 131–148. https://doi.org/10.1016/j.advwatres.2012.07.013

Etchevers, P., Martin, E., Brown, R., Fierz, C., Lejeune, Y., Bazile, E., Boone, A., Dai, Y.-J., Essery, R., Fernandez, A., others, 2004. Validation of the energy budget of an alpine snowpack simulated by several snow models (SnowMIP project). Ann. Glaciol. 38, 150–158.

Fassnacht, S.R., Soulis, E.D., 2002. Implications during transitional periods of improvements to the snow processes in the land surface scheme-hydrological model WATCLASS. Atmosphere-Ocean 40, 389–403.

Fassnacht, S.R., Venable, N.B.H., Khishigbayar, J., Cherry, M.L., 2013. The probability of precipitation as snow derived from daily air temperature for high elevation areas of Colorado, United States. IAHS-AISH Publ. 65–70.

Feiccabrino, J., Graff, W., Lundberg, A., Sandström, N., Gustafsson, D., 2015. Meteorological Knowledge Useful for the Improvement of Snow Rain Separation in Surface Based Models. Hydrology 2, 266–288. https://doi.org/10.3390/hydrology2040266

Flanner, M.G., Shell, K.M., Barlage, M., Perovich, D.K., Tschudi, M.A., 2011. Radiative forcing and albedo feedback from the Northern Hemisphere cryosphere between 1979 and 2008. Nat. Geosci. 4, 151–155. https://doi.org/10.1038/ngeo1062

Flerchinger, G.N., Xaio, W., Marks, D., Sauer, T.J., Yu, Q., 2009. Comparison of algorithms for incoming atmospheric long-wave radiation. Water Resour. Res. 45. https://doi.org/10.1029/2008WR007394

Förster, K., Meon, G., Marke, T., Strasser, U., 2014. Effect of meteorological forcing and snow model complexity on hydrological simulations in the Sieber catchment (Harz Mountains, Germany). Hydrol. Earth Syst. Sci. 18, 4703–4720.

Froidurot, S., Zin, I., Hingray, B., Gautheron, A., 2014. Sensitivity of Precipitation Phase over the Swiss Alps to Different Meteorological Variables. J. Hydrometeorol. 15, 685–696. https://doi.org/10.1175/JHM-D-13-073.1

Gjertsen, U., Ødegaard, V., 2005. The water phase of precipitation—a comparison between observed, estimated and predicted values. Atmospheric Res., Precipitation in Urban Areas 77, 218–231. https://doi.org/10.1016/j.atmosres.2004.10.030

Gleason, K., Nolin Anne W., Roth Travis R., 2013. Charred forests increase snowmelt: Effects of burned woody debris and incoming solar radiation on snow ablation. Geophys. Res. Lett. 40, 4654–4661. https://doi.org/10.1002/grl.50896

Gleason, K.E., Nolin, A.W., 2016. Charred forests accelerate snow albedo decay: parameterizing the post-fire radiative forcing on snow for three years following fire. Hydrol. Process. 30, 3855–3870. https://doi.org/10.1002/hyp.10897

Godsey, S.E., Marks, D., Kormos, P.R., Seyfried, M.S., Enslin, C.L., Winstral, A.H., McNamara, J.P., Link, T.E., 2018. Eleven years of mountain weather, snow, soil moisture and stream flow data from the rain-snow transition zone—the Johnston Draw catchment, Reynolds Creek Experimental Watershed and Critical Zone Observatory, USA. Earth Syst. Sci. Data 10, 1207–1216. https://doi.org/10.5194/essd-10-1207-2018

Greenland, D., 1989. The climate of Niwot Ridge, front range, Colorado, USA. Arct. Alp. Res. 380–391.

Groffman, P.M., Driscoll, C.T., Fahey, T.J., Hardy, J.P., Fitzhugh, R.D., Tierney, G.L., 2001. Colder soils in a warmer world: a snow manipulation study in a northern hardwood forest ecosystem. Biogeochemistry 56, 135–150.

Groffman, P.M., Hardy, J.P., Driscoll, C.T., Fahey, T.J., 2006. Snow depth, soil freezing, and fluxes of carbon dioxide, nitrous oxide and methane in a northern hardwood forest. Glob. Change Biol. 12, 1748–1760. https://doi.org/10.1111/j.1365-2486.2006.01194.x

Groisman, P.Y., Karl, T.R., Knight, R.W., 1994. Observed Impact of Snow Cover on the Heat Balance and the Rise of Continental Spring Temperatures. Science 263, 198–200. https://doi.org/10.1126/science.263.5144.198

Hall, A., 2004. The Role of Surface Albedo Feedback in Climate. J. Clim. 17, 1550–1568. https://doi.org/10.1175/1520-0442(2004)017<1550:TROSAF>2.0.CO;2

Hall, A., Qu, X., 2006. Using the current seasonal cycle to constrain snow albedo feedback in future climate change. Geophys. Res. Lett. 33, L03502. https://doi.org/10.1029/2005GL025127

Hamlet, A.F., Mote, P.W., Clark, M.P., Lettenmaier, D.P., 2005. Effects of temperature and precipitation variability on snowpack trends in the Western United States*. J. Clim. 18, 4545–4561.

Hammond, J., Saavedra Freddy A., Kampf Stephanie K., 2018. How Does Snow Persistence Relate to Annual Streamflow in Mountain Watersheds of the Western U.S. With Wet Maritime and Dry Continental Climates? Water Resour. Res. 0. https://doi.org/10.1002/2017WR021899

Harder, P., Pomeroy, J., 2013. Estimating precipitation phase using a psychrometric energy balance method. Hydrol. Process. 27, 1901–1914. https://doi.org/10.1002/hyp.9799

Harder, P., Pomeroy, J.W., 2014. Hydrological model uncertainty due to precipitation-phase partitioning methods. Hydrol. Process. 28, 4311–4327.

Harpold, A., Brooks, P., Rajagopal, S., Heidbuchel, I., Jardine, A., Stielstra, C., 2012. Changes in snowpack accumulation and ablation in the intermountain west. Water Resour. Res. 48, 1–11. https://doi.org/10.1029/2012WR011949

Harpold, A.A., Brooks, P.D., 2018. Humidity determines snowpack ablation under a warming climate. Proc. Natl. Acad. Sci. 201716789. https://doi.org/10.1073/pnas.1716789115

Harpold, A.A., Crews, J.B., Rajagopal, S., Winchell, T., Schumer, R., 2017a. Relative Humidity Has Uneven Effects on Shifts From Snow to Rain Over the Western U.S. Geophys. Res. Lett. 44, 2017GL075046. https://doi.org/10.1002/2017GL075046

Harpold, A.A., Dettinger, M., Rajagopal, S., 2017b. Defining snow drought and why it matters. EOS-Earth Space Sci. News 98.

Harpold, A.A., Kaplan, M., Klos, P.Z., Link, T., McNamara, J.P., Rajagopal, S., Schumer, R., Steele, C.M., 2017c. Rain or snow: hydrologic processes, observations, prediction, and research needs. Hydrol Earth Syst Sci 21, 1–22.

Harpold, A.A., Molotch, N.P., 2015. Sensitivity of soil water availability to changing snowmelt timing in the western US. Geophys. Res. Lett. 42, 8011–8020.

Harr, R.D., 1986. Effects of clearcutting on rain-on-snow runoff in western Oregon: A new look at old studies. Water Resour. Res. 22, 1095–1100.

Harr, R.D., 1981. Some characteristics and consequences of snowmelt during rainfall in western Oregon. J. Hydrol. 53, 277–304.

Helgason, W., Pomeroy, J., 2011. Problems Closing the Energy Balance over a Homogeneous Snow Cover during Midwinter. J. Hydrometeorol. 13, 557–572. https://doi.org/10.1175/JHM-D-11-0135.1

Henn, B., Raleigh, M.S., Fisher, A., Lundquist, J.D., 2012. A Comparison of Methods for Filling Gaps in Hourly Near-Surface Air Temperature Data. J. Hydrometeorol. 14, 929–945. https://doi.org/10.1175/JHM-D-12-027.1

Hock, R., 2003. Temperature index melt modelling in mountain areas. J. Hydrol. 282, 104–115. https://doi.org/10.1016/S0022-1694(03)00257-9

Hood, E., Williams, M., Cline, D., 1999. Sublimation from a seasonal snowpack at a continental, mid-latitude alpine site. Hydrol. Process. 13, 1781–1797.

Hunsaker, C.T., Whitaker, T.W., Bales, R.C., 2012. Snowmelt runoff and water yield along elevation and temperature gradients in California's southern Sierra Nevada. JAWRA J. Am. Water Resour. Assoc. 48, 667–678.

Ikeda, K., Rasmussen, R., Liu, C., Gochis, D., Yates, D., Chen, F., Tewari, M., Barlage, M., Dudhia, J., Miller, K., 2010. Simulation of seasonal snowfall over Colorado. Atmospheric Res. 97, 462–477.

IPCC, 2013. Climate Change 2013: The Physical Science Basis. Contribution of Working Group I to the Fifth Assessment Report of the Intergovernmental Panel on Climate Change. Cambridge University Press Cambridge, UK, and New York.

Jennings, K.S., Jones, J.A., 2015. Precipitation-snowmelt timing and snowmelt augmentation of large peak flow events, western Cascades, Oregon. Water Resour. Res. 51, 7649–7661. https://doi.org/10.1002/2014WR016877

Jennings, K.S., Kittel, T.G.F., Molotch, N.P., 2018a. Observations and simulations of the seasonal evolution of snowpack cold content and its relation to snowmelt and the snowpack energy budget. The Cryosphere 12, 1595–1614. https://doi.org/10.5194/tc-12-1595-2018

Jennings, K.S., Kittel, T.G.F., Molotch, N.P., 2017. Infilled climate data for C1, Saddle, D1 from 1990-1-1 to 2013-12-31, hourly.

Jennings, K.S., Winchell, T.S., Livneh, B., Molotch, N.P., 2018b. Spatial variation of the rain-snow temperature threshold across the Northern Hemisphere. Nat. Commun. 9. https://doi.org/10.1038/s41467-018-03629-7

Jepsen, S.M., Molotch, N.P., Williams, M.W., Rittger, K.E., Sickman, J.O., 2012. Interannual variability of snowmelt in the Sierra Nevada and Rocky Mountains, United States: Examples from two alpine watersheds. Water Resour. Res. 48. https://doi.org/10.1029/2011WR011006

Kampf, S.K., Lefsky, M.A., 2016. Transition of dominant peak flow source from snowmelt to rainfall along the Colorado Front Range: Historical patterns, trends, and lessons from the 2013 Colorado Front Range floods. Water Resour. Res.

Kapnick, S., Hall, A., 2012. Causes of recent changes in western North American snowpack. Clim. Dyn. 38, 1885–1899.

Karl, T.R., Kukla George, Razuvayev Vyacheslav N., Changery Michael J., Quayle Robert G., Heim Richard R., Easterling David R., Fu Cong Bin, 1991. Global warming: Evidence for asymmetric diurnal temperature change. Geophys. Res. Lett. 18, 2253–2256. https://doi.org/10.1029/91GL02900

Kienzle, S.W., 2008. A new temperature based method to separate rain and snow. Hydrol. Process. 22, 5067–5085. https://doi.org/10.1002/hyp.7131

Kirchner, J.W., 2006. Getting the right answers for the right reasons: Linking measurements, analyses, and models to advance the science of hydrology. Water Resour. Res. 42.

Kittel, T.G.F., Williams, M.W., Chowanski, K., Hartman, M., Ackerman, T., Losleben, M., Blanken, P.D., 2015. Contrasting long-term alpine and subalpine precipitation trends in a mid-latitude North American mountain system, Colorado Front Range, USA. Plant Ecol. Divers. 8, 607–624. https://doi.org/10.1080/17550874.2016.1143536

Kittel, Timothy, 2009. The Development and Analysis of Climate Datasets for National Park Science and Management: A Guide to Methods for Making Climate Records Useful and Tools to Explore Critical Questions.

Klos, P.Z., Link, T.E., Abatzoglou, J.T., 2014. Extent of the rain-snow transition zone in the western US under historic and projected climate. Geophys. Res. Lett. 41, 4560–4568.

Knowles, J.F., Blanken, P.D., Williams, M.W., Chowanski, K.M., 2012. Energy and surface moisture seasonally limit evaporation and sublimation from snow-free alpine tundra. Agric. For. Meteorol. 157, 106–115. https://doi.org/10.1016/j.agrformet.2012.01.017

Knowles, J.F., Harpold, A.A., Cowie, R., Zeliff, M., Barnard, H.R., Burns, S.P., Blanken, P.D., Morse, J.F., Williams, M.W., 2015. The relative contributions of alpine and subalpine ecosystems to the water balance of a mountainous, headwater catchment. Hydrol. Process. 29, 4794–4808. https://doi.org/10.1002/hyp.10526

Knowles, J.F., Lestak, L.R., Molotch, N.P., 2017. On the use of a snow aridity index to predict remotely sensed forest productivity in the presence of bark beetle disturbance. Water Resour. Res. 53, 4891–4906.

Knowles, J.F., Molotch Noah P., Trujillo Ernesto, Litvak Marcy E., 2018. Snowmelt□Driven Trade□Offs Between Early and Late Season Productivity Negatively Impact Forest Carbon Uptake During Drought. Geophys. Res. Lett. 45, 3087–3096. https://doi.org/10.1002/2017GL076504

Knowles, N., Dettinger, M.D., Cayan, D.R., 2006. Trends in snowfall versus rainfall in the western United States. J. Clim. 19, 4545–4559.

Krasting, J.P., Broccoli, A.J., Dixon, K.W., Lanzante, J.R., 2013. Future Changes in Northern Hemisphere Snowfall. J. Clim. 26, 7813–7828. https://doi.org/10.1175/JCLI-D-12-00832.1

Lapo, K.E., Hinkelman, L.M., Raleigh, M.S., Lundquist, J.D., 2015. Impact of errors in the downwelling irradiances on simulations of snow water equivalent, snow surface temperature, and the snow energy balance. Water Resour. Res. 51, 1649–1670.

Leavesley, G.H., Stannard, L.G., Singh, V.P., others, 1995. The precipitation-runoff modeling system-PRMS. Comput. Models Watershed Hydrol. 281–310.

Lehning, M., Bartelt, P., Brown, B., Fierz, C., 2002a. A physical SNOWPACK model for the Swiss avalanche warning: Part III: Meteorological forcing, thin layer formation and evaluation. Cold Reg. Sci. Technol. 35, 169–184.

Lehning, M., Bartelt, P., Brown, B., Fierz, C., Satyawali, P., 2002b. A physical SNOWPACK model for the Swiss avalanche warning: Part II. Snow microstructure. Cold Reg. Sci. Technol. 35, 147–167.

Lehning, M., Fierz, C., Lundy, C., 2001. An objective snow profile comparison method and its application to SNOWPACK. Cold Reg. Sci. Technol., ISSW 2000:International Snow Science Workshop 33, 253–261. https://doi.org/10.1016/S0165-232X(01)00044-1

Lehning, M., Völksch, I., Gustafsson, D., Nguyen, T.A., Stähli, M., Zappa, M., 2006. ALPINE3D: a detailed model of mountain surface processes and its application to snow hydrology. Hydrol. Process. 20, 2111–2128.

Leung, L.R., Qian, Y., Bian, X., Washington, W.M., Han, J., Roads, J.O., 2004. Mid-century ensemble regional climate change scenarios for the western United States. Clim. Change 62, 75–113.

Li, D., Wrzesien, M.L., Durand, M., Adam, J., Lettenmaier, D.P., 2017. How much runoff originates as snow in the western United States, and how will that change in the future? Geophys. Res. Lett. 44, 6163–6172. https://doi.org/10.1002/2017GL073551

Liston, G.E., Elder, K., 2006. A meteorological distribution system for high-resolution terrestrial modeling (MicroMet). J. Hydrometeorol. 7, 217–234.

Litaor, M.I., Williams, M., Seastedt, T.R., 2008. Topographic controls on snow distribution, soil moisture, and species diversity of herbaceous alpine vegetation, Niwot Ridge, Colorado. J. Geophys. Res. Biogeosciences 113.

Livneh, B., Deems, J.S., Buma, B., Barsugli, J.J., Schneider, D., Molotch, N.P., Wolter, K., Wessman, C.A., 2015. Catchment response to bark beetle outbreak and dust-on-snow in the Colorado Rocky Mountains. J. Hydrol. 523, 196–210. https://doi.org/10.1016/j.jhydrol.2015.01.039

Livneh, B., Xia, Y., Mitchell, K.E., Ek, M.B., Lettenmaier, D.P., 2010. Noah LSM Snow Model Diagnostics and Enhancements. J. Hydrometeorol. 11, 721–738. https://doi.org/10.1175/2009JHM1174.1

Luce, C., Lopez-Burgos, V., Holden, Z., 2014. Sensitivity of snowpack storage to precipitation and temperature using spatial and temporal analog models. Water Resour. Res. 50, 9447–9462. https://doi.org/10.1002/2013WR014844

Lundquist, J.D., Dickerson-Lange, S.E., Lutz, J.A., Cristea, N.C., 2013. Lower forest density enhances snow retention in regions with warmer winters: A global framework developed from plot-scale observations and modeling: Forests and Snow Retention. Water Resour. Res. 49, 6356–6370. https://doi.org/10.1002/wrcr.20504

Lundquist, J.D., Roche, J.W., Forrester, H., Moore, C., Keenan, E., Perry, G., Cristea, N., Henn, B., Lapo, K., McGurk, B., Cayan, D.R., Dettinger, M.D., 2016. Yosemite Hydroclimate Network: Distributed stream and atmospheric data for the Tuolumne River watershed and surroundings. Water Resour. Res. 52, 7478–7489. https://doi.org/10.1002/2016WR019261

Lundy, C.C., Brown, R.L., Adams, E.E., Birkeland, K.W., Lehning, M., 2001. A statistical validation of the SNOWPACK model in a Montana climate. Cold Reg. Sci. Technol. 33, 237–246.

Lute, A.C., Abatzoglou, J.T., Hegewisch, K.C., 2015. Projected changes in snowfall extremes and interannual variability of snowfall in the western United States. Water Resour. Res. 51, 960–972. https://doi.org/10.1002/2014WR016267

Lynch-Stieglitz, M., 1994. The development and validation of a simple snow model for the GISS GCM. J. Clim. 7, 1842–1855.

Lytle, D.A., Poff, N.L., 2004. Adaptation to natural flow regimes. Trends Ecol. Evol. 19, 94–100. https://doi.org/10.1016/j.tree.2003.10.002

Mankin, J.S., Viviroli, D., Singh, D., Hoekstra, A.Y., Diffenbaugh, N.S., 2015. The potential for snow to supply human water demand in the present and future. Environ. Res. Lett. 10, 114016. https://doi.org/10.1088/1748-9326/10/11/114016

Marks, D., Dozier, J., 1992. Climate and energy exchange at the snow surface in the alpine region of the Sierra Nevada: 2. Snow cover energy balance. Water Resour. Res. 28, 3043–3054.

Marks, D., Dozier, J., Davis, R.E., 1992. Climate and Energy Exchange at the Snow Surface in the Alpine Region of the Sierra Nevada 1. Meteorological Measurements and Monitoring. Water Resour. Res. 28, 3029–3042.

Marks, D., Kimball, J., Tingey, D., Link, T., 1998. The sensitivity of snowmelt processes to climate conditions and forest cover during rain-on-snow: a case study of the 1996 Pacific Northwest flood. Hydrol. Process. 12, 1569–1587.

Marks, D., Link, T., Winstral, A., Garen, D., 2001. Simulating snowmelt processes during rain-on-snow over a semi-arid mountain basin. Ann. Glaciol. 32, 195–202.

Marks, D., Winstral, A., 2001. Comparison of snow deposition, the snow cover energy balance, and snowmelt at two sites in a semiarid mountain basin. J. Hydrometeorol. 2, 213–227.

Marks, D., Winstral, A., Flerchinger, G., Reba, M., Pomeroy, J., Link, T., Elder, K., 2008. Comparing simulated and measured sensible and latent heat fluxes over snow under a pine canopy to improve an energy balance snowmelt model. J. Hydrometeorol. 9, 1506–1522.

Marks, D., Winstral, A., Reba, M., Pomeroy, J., Kumar, M., 2013. An evaluation of methods for determining during-storm precipitation phase and the rain/snow transition elevation at the surface in a mountain basin. Adv. Water Resour. 55, 98–110. https://doi.org/10.1016/j.advwatres.2012.11.012

Marr, J.W., 1967. Data on mountain environments: I. Front Range, Colorado, sixteen sites, 1952-1953. Univ. Colo. Press.

Marty, C., Schlögl, S., Bavay, M., Lehning, M., 2017. How much can we save? Impact of different emission scenarios on future snow cover in the Alps. The Cryosphere 11, 517.

Mazurkiewicz, A.B., Callery, D.G., McDonnell, J.J., 2008. Assessing the controls of the snow energy balance and water available for runoff in a rain-on-snow environment. J. Hydrol. 354, 1–14.

McCabe, G.J., Hay, L.E., Clark, M.P., 2007. Rain-on-snow events in the western United States. Bull. Am. Meteorol. Soc. 88, 319–328.

McGuire, C.R., Nufio, C.R., Bowers, M.D., Guralnick, R.P., 2012. Elevation-Dependent Temperature Trends in the Rocky Mountain Front Range: Changes over a 56- and 20-Year Record. PLoS ONE 7, e44370. https://doi.org/10.1371/journal.pone.0044370

Meek, D.W., Hatfield, J.L., 1994. Data quality checking for single station meteorological databases. Agric. For. Meteorol. 69, 85–109.

Meromy, L., Molotch, N.P., Williams, M.W., Musselman, K.N., Kueppers, L.M., 2015. Snowpack-climate manipulation using infrared heaters in subalpine forests of the Southern Rocky Mountains, USA. Agric. For. Meteorol. 203, 142–157. https://doi.org/10.1016/j.agrformet.2014.12.015

Milly, P.C.D., Betancourt, J., Falkenmark, M., Hirsch, R.M., Kundzewicz, Z.W., Lettenmaier, D.P., Stouffer, R.J., 2008. Stationarity is dead: Whither water management? Science 319, 573–574.

Minder, J.R., 2010. The Sensitivity of Mountain Snowpack Accumulation to Climate Warming. J. Clim. 23, 2634–2650. https://doi.org/10.1175/2009JCLI3263.1

Minder, J.R., Durran, D.R., Roe, G.H., 2011. Mesoscale Controls on the Mountainside Snow Line. J. Atmospheric Sci. 68, 2107–2127. https://doi.org/10.1175/JAS-D-10-05006.1

Mizukami, N., Koren, V., Smith, M., Kingsmill, D., Zhang, Z., Cosgrove, B., Cui, Z., 2013. The impact of precipitation type discrimination on hydrologic simulation: Rain–snow partitioning derived from HMT-West radar-detected brightband height versus surface temperature data. J. Hydrometeorol. 14, 1139–1158.

Molotch, N.P., Bales, R.C., 2006. SNOTEL representativeness in the Rio Grande headwaters on the basis of physiographics and remotely sensed snow cover persistence. Hydrol. Process. 20, 723–739.

Molotch, N.P., Bales, R.C., 2005. Scaling snow observations from the point to the grid element: Implications for observation network design. Water Resour. Res. 41.

Molotch, N.P., Barnard, D.M., Burns, S.P., Painter, T.H., 2016. Measuring spatiotemporal variation in snow optical grain size under a subalpine forest canopy using contact spectroscopy. Water Resour. Res. https://doi.org/10.1002/2016WR018954

Molotch, N.P., Blanken, P.D., Williams, M.W., Turnipseed, A.A., Monson, R.K., Margulis, S.A., 2007. Estimating sublimation of intercepted and sub-canopy snow using eddy covariance systems. Hydrol. Process. 21, 1567–1575.

Molotch, N.P., Brooks, P.D., Burns, S.P., Litvak, M., Monson, R.K., McConnell, J.R., Musselman, K., 2009. Ecohydrological controls on snowmelt partitioning in mixed-conifer sub-alpine forests. Ecohydrology 2, 129–142.

Monson, R.K., Lipson, D.L., Burns, S.P., Turnipseed, A.A., Delany, A.C., Williams, M.W., Schmidt, S.K., 2006. Winter forest soil respiration controlled by climate and microbial community composition. Nature 439, 711.

Mosier, T.M., Hill, D.F., Sharp, K.V., 2016. How much cryosphere model complexity is just right? Exploration using the conceptual cryosphere hydrology framework. The Cryosphere 10, 2147–2171. https://doi.org/10.5194/tc-10-2147-2016

Mote, P.W., Hamlet, A.F., Clark, M.P., Lettenmaier, D.P., 2005. Declining mountain snowpack in western North America*. Bull. Am. Meteorol. Soc. 86, 39–49.

Mote, P.W., Li, S., Lettenmaier, D.P., Xiao, M., Engel, R., 2018. Dramatic declines in snowpack in the western US. Npj Clim. Atmospheric Sci. 1, 2. https://doi.org/10.1038/s41612-018-0012-1

Musselman, K.N., Clark, M.P., Liu, C., Ikeda, K., Rasmussen, R., 2017a. Slower snowmelt in a warmer world. Nat. Clim. Change 7, 214–219. https://doi.org/10.1038/nclimate3225

Musselman, K.N., Lehner, F., Ikeda, K., Clark, M.P., Prein, A.F., Liu, C., Barlage, M., Rasmussen, R., 2018. Projected increases and shifts in rain-on-snow flood risk over western North America. Nat. Clim. Change 1. https://doi.org/10.1038/s41558-018-0236-4

Musselman, K.N., Molotch, N.P., Margulis, S.A., 2017b. Snowmelt response to simulated warming across a large elevation gradient, southern Sierra Nevada, California. The Cryosphere 11, 2847–2866. https://doi.org/10.5194/tc-11-2847-2017

Musselman, K.N., Molotch, N.P., Margulis, S.A., 2017c. Snow melt response to simulated warming across a large elevation gradient, southern Sierra Nevada, California. Cryosphere Discuss 2017, 1–47. https://doi.org/10.5194/tc-2017-123

Nayak, A., Marks, D., Chandler, D.G., Seyfried, M., 2010. Long-term snow, climate, and streamflow trends at the Reynolds Creek Experimental Watershed, Owyhee Mountains, Idaho, United States: CLIMATE TRENDS AT RCEW. Water Resour. Res. 46, n/a-n/a. https://doi.org/10.1029/2008WR007525

Nolin, A.W., Daly, C., 2006. Mapping “at risk” snow in the Pacific Northwest. J. Hydrometeorol. 7, 1164–1171.

Obled, C., Rosse, B., 1977. Mathematical models of a melting snowpack at an index plot. J. Hydrol. 32, 139–163. https://doi.org/10.1016/0022-1694(77)90123-8

O’Gorman, P.A., 2014. Contrasting responses of mean and extreme snowfall to climate change. Nature 512, 416–418. https://doi.org/10.1038/nature13625

Oyler, J.W., Dobrowski, S.Z., Ballantyne, A.P., Klene, A.E., Running, S.W., 2015. Artificial amplification of warming trends across the mountains of the western United States. Geophys. Res. Lett. 42, 153–161. https://doi.org/10.1002/2014GL062803

Painter, T.H., Berisford, D.F., Boardman, J.W., Bormann, K.J., Deems, J.S., Gehrke, F., Hedrick, A., Joyce, M., Laidlaw, R., Marks, D., others, 2016. The Airborne Snow Observatory: Fusion of scanning lidar, imaging spectrometer, and physically-based modeling for mapping snow water equivalent and snow albedo. Remote Sens. Environ. 184, 139–152.

Painter, T.H., Deems, J.S., Belnap, J., Hamlet, A.F., Landry, C.C., Udall, B., 2010. Response of Colorado River runoff to dust radiative forcing in snow. Proc. Natl. Acad. Sci. 107, 17125–17130.

Painter, T.H., Skiles S. McKenzie, Deems Jeffrey S., Brandt W. Tyler, Dozier Jeff, 2017. Variation in Rising Limb of Colorado River Snowmelt Runoff Hydrograph Controlled by Dust Radiative Forcing in Snow. Geophys. Res. Lett. 45, 797–808. https://doi.org/10.1002/2017GL075826

Painter, T.H., Skiles, S.M., Deems, J.S., Bryant, A.C., Landry, C.C., 2012. Dust radiative forcing in snow of the Upper Colorado River Basin: 1. A 6 year record of energy balance, radiation, and dust concentrations. Water Resour. Res. 48, W07521. https://doi.org/10.1029/2012WR011985

Pederson, G.T., Betancourt, J.L., McCabe, G.J., 2013. Regional patterns and proximal causes of the recent snowpack decline in the Rocky Mountains, US. Geophys. Res. Lett. 40, 1811–1816.

Pederson, G.T., Gray, S.T., Ault, T., Marsh, W., Fagre, D.B., Bunn, A.G., Woodhouse, C.A., Graumlich, L.J., 2011a. Climatic controls on the snowmelt hydrology of the northern Rocky Mountains. J. Clim. 24, 1666–1687.

Pederson, G.T., Gray, S.T., Woodhouse, C.A., Betancourt, J.L., Fagre, D.B., Littell, J.S., Watson, E., Luckman, B.H., Graumlich, L.J., 2011b. The unusual nature of recent snowpack declines in the North American Cordillera. Science 333, 332–335.

Pepin, N., Losleben, M., 2002. Climate change in the Colorado Rocky Mountains: free air versus surface temperature trends. Int. J. Climatol. 22, 311–329.

Perkins, R.M., Jones, J.A., 2008. Climate variability, snow, and physiographic controls on storm hydrographs in small forested basins, western Cascades, Oregon. Hydrol. Process. 22, 4949–4964.

Pomeroy, J.W., Toth, B., Granger, R.J., Hedstrom, N.R., Essery, R.L.H., 2003. Variation in surface energetics during snowmelt in a subarctic mountain catchment. J. Hydrometeorol. 4, 702–719.

Rajagopal, S., Harpold, A.A., 2016. Testing and Improving Temperature Thresholds for Snow and Rain Prediction in the Western United States. JAWRA J. Am. Water Resour. Assoc.

Raleigh, M.S., Livneh, B., Lapo, K., Lundquist, J.D., 2016. How Does Availability of Meteorological Forcing Data Impact Physically Based Snowpack Simulations? J. Hydrometeorol. 17, 99–120. https://doi.org/10.1175/JHM-D-14-0235.1

Raleigh, M.S., Lundquist, J.D., 2012. Comparing and combining SWE estimates from the SNOW-17 model using PRISM and SWE reconstruction. Water Resour. Res. 48, W01506. https://doi.org/10.1029/2011WR010542

Raleigh, M.S., Lundquist, J.D., Clark, M.P., 2015. Exploring the impact of forcing error characteristics on physically based snow simulations within a global sensitivity analysis framework. Hydrol. Earth Syst. Sci. 19, 3153–3179. https://doi.org/10.5194/hess-19-3153-2015

Rasmus, S., Räisänen, J., Lehning, M., 2004. Estimating snow conditions in Finland in the late 21st century using the SNOWPACK model with regional climate scenario data as input. Ann. Glaciol. 38, 238–244. https://doi.org/10.3189/172756404781814843

Rasmussen, R., Baker, B., Kochendorfer, J., Meyers, T., Landolt, S., Fischer, A.P., Black, J., Thériault, J.M., Kucera, P., Gochis, D., others, 2012. How well are we measuring snow: The NOAA/FAA/NCAR winter precipitation test bed. Bull. Am. Meteorol. Soc. 93, 811–829.

Rasmussen, R., Liu, C., Ikeda, K., Gochis, D., Yates, D., Chen, F., Tewari, M., Barlage, M., Dudhia, J., Yu, W., 2011. High-resolution coupled climate runoff simulations of seasonal snowfall over Colorado: a process study of current and warmer climate. J. Clim. 24, 3015–3048.

Regonda, S.K., Rajagopalan, B., Clark, M., Pitlick, J., 2005. Seasonal cycle shifts in hydroclimatology over the western United States. J. Clim. 18, 372–384.

Rice, R., Bales, R.C., Painter, T.H., Dozier, J., 2011. Snow water equivalent along elevation gradients in the Merced and Tuolumne River basins of the Sierra Nevada. Water Resour. Res. 47, W08515. https://doi.org/10.1029/2010WR009278

Roth, T.R., Nolin, A.W., 2017. Forest impacts on snow accumulation and ablation across an elevation gradient in a temperate montane environment. Hydrol Earth Syst Sci 21, 5427–5442. https://doi.org/10.5194/hess-21-5427-2017

Rutter, N., Essery, R., Pomeroy, J., Altimir, N., Andreadis, K., Baker, I., Barr, A., Bartlett, P., Boone, A., Deng, H., others, 2009. Evaluation of forest snow processes models (SnowMIP2). J. Geophys. Res. Atmospheres 114. https://doi.org/doi/10.1029/2008JD011063/

Safeeq, M., Shukla, S., Arismendi, I., Grant, G.E., Lewis, S.L., Nolin, A., 2015. Influence of winter season climate variability on snow–precipitation ratio in the western United States. Int. J. Climatol.

Schlögl, S., Marty, C., Bavay, M., Lehning, M., 2016. Sensitivity of Alpine3D modeled snow cover to modifications in DEM resolution, station coverage and meteorological input quantities. Environ. Model. Softw. 83, 387–396. https://doi.org/10.1016/j.envsoft.2016.02.017

Schmucki, E., Marty, C., Fierz, C., Lehning, M., 2014. Evaluation of modelled snow depth and snow water equivalent at three contrasting sites in Switzerland using SNOWPACK simulations driven by different meteorological data input. Cold Reg. Sci. Technol. 99, 27–37.

Seligman, Z.M., Harper, J.T., Maneta, M.P., 2014. Changes to Snowpack Energy State from Spring Storm Events, Columbia River Headwaters, Montana. J. Hydrometeorol. 15, 159–170. https://doi.org/10.1175/JHM-D-12-078.1

Serreze, M.C., Clark, M.P., Armstrong, R.L., McGinnis, D.A., Pulwarty, R.S., 1999. Characteristics of the western United States snowpack from snowpack telemetry (SNOTEL) data. Water Resour. Res. 35, 2145–2160.

Sexstone, G.A., Clow, D.W., Stannard, D.I., Fassnacht, S.R., 2016. Comparison of methods for quantifying surface sublimation over seasonally snow-covered terrain. Hydrol. Process. 30, 3373–3389. https://doi.org/10.1002/hyp.10864

Skamarock, W.C., Klemp, J.B., Dudhia, J., Gill, D.O., Barker, D.M., Wang, W., Powers, J.G., 2005. A description of the advanced research WRF version 2. National Center For Atmospheric Research Boulder Co Mesoscale and Microscale Meteorology Div.

Skiles, S.M., Painter, T.H., Deems, J.S., Bryant, A.C., Landry, C.C., 2012. Dust radiative forcing in snow of the Upper Colorado River Basin: 2. Interannual variability in radiative forcing and snowmelt rates. Water Resour. Res. 48, W07522. https://doi.org/10.1029/2012WR011986

Slater, A.G., Lawrence, D.M., Koven, C.D., 2017. Process-level model evaluation: a snow and heat transfer metric. The Cryosphere 11, 989–996. https://doi.org/10.5194/tc-11-989-2017

Slater, A.G., Schlosser, C.A., Desborough, C.E., Pitman, A.J., Henderson-Sellers, A., Robock, A., Vinnikov, K.Y., Entin, J., Mitchell, K., Chen, F., others, 2001. The representation of snow in land surface schemes: Results from PILPS 2 (d). J. Hydrometeorol. 2, 7–25.

Sospedra-Alfonso, R., Melton, J.R., Merryfield, W.J., 2015. Effects of temperature and precipitation on snowpack variability in the Central Rocky Mountains as a function of elevation: CLIMATE DRIVEN ALPINE SNOWPACK. Geophys. Res. Lett. 42, 4429–4438. https://doi.org/10.1002/2015GL063898

Stewart, I.T., 2009. Changes in snowpack and snowmelt runoff for key mountain regions. Hydrol. Process. 23, 78–94.

Stewart, I.T., Cayan, D.R., Dettinger, M.D., 2005. Changes toward earlier streamflow timing across western North America. J. Clim. 18, 1136–1155.

Stewart, I.T., Cayan, D.R., Dettinger, M.D., 2004a. Changes in snowmelt runoff timing in western North America under a “business as usual” climate change scenario. Clim. Change 62, 217–232.

Stewart, I.T., Cayan, D.R., Dettinger, M.D., 2004b. Changes in snowmelt runoff timing in western North America under abusiness as usual’climate change scenario. Clim. Change 62, 217–232.

Stull, R., 2011. Wet-bulb temperature from relative humidity and air temperature. J. Appl. Meteorol. Climatol. 50, 2267–2269.

Sturm, M., Goldstein, M.A., Parr, C., 2017. Water and life from snow: A trillion dollar science question. Water Resour. Res. n/a-n/a. https://doi.org/10.1002/2017WR020840

Sturm, M., Holmgren, J., König, M., Morris, K., 1997. The thermal conductivity of seasonal snow. J. Glaciol. 43, 26–41.

Sturm, M., Holmgren, J., Liston, G.E., 1995. A seasonal snow cover classification system for local to global applications. J. Clim. 8, 1261–1283.

Tarboton, D.G., Luce, C.H., 1996. Utah energy balance snow accumulation and melt model (UEB). Citeseer.

Tennant, C.J., Harpold, A.A., Lohse, K.A., Godsey, S.E., Crosby, B.T., Larsen, L.G., Brooks, P.D., Van Kirk, R.W., Glenn, N.F., 2017. Regional sensitivities of seasonal snowpack to elevation, aspect, and vegetation cover in western North America. Water Resour. Res. 53, 6908–6926. https://doi.org/10.1002/2016WR019374

Trenberth, K.E., 2011. Changes in precipitation with climate change. Clim. Res. 47, 123.

Trujillo, E., Molotch, N.P., 2014. Snowpack regimes of the Western United States. Water Resour. Res. 50, 5611–5623. https://doi.org/10.1002/2013WR014753

Trujillo, E., Molotch, N.P., Goulden, M.L., Kelly, A.E., Bales, R.C., 2012. Elevation-dependent influence of snow accumulation on forest greening. Nat. Geosci. 5, 705.

Turnipseed, A.A., Blanken, P.D., Anderson, D.E., Monson, R.K., 2002. Energy budget above a high-elevation subalpine forest in complex topography. Agric. For. Meteorol. 110, 177–201.

Udall, B., Overpeck, J., 2017. The twenty-first century Colorado River hot drought and implications for the future. Water Resour. Res. 53, 2404–2418.

United States Army Corps of Engineers, 1956. Snow hydrology. US Army North Pac. Div. Portland Or.

United States Geological Survey, 2005. Changes in Streamflow Timing in the Western United States in Recent Decades. Fact Sheet 2005-3018.

Unsworth, M.H., Monteith, J.L., 1975. Long-wave radiation at the ground I. Angular distribution of incoming radiation. Q. J. R. Meteorol. Soc. 101, 13–24.

USGCRP, 2017. Climate Science Special Report: Fourth National Climate Assessment, Volume I. U.S. Global Change Research Program, Washington, DC, USA. https://doi.org/10.7930/J0J964J6

Vincent, C., Le Meur, E., Six, D., Funk, M., Hoelzle, M., Preunkert, S., 2007. Very high-elevation Mont Blanc glaciated areas not affected by the 20th century climate change. J. Geophys. Res. Atmospheres 112.

Viviroli, D., Dürr, H.H., Messerli, B., Meybeck, M., Weingartner, R., 2007. Mountains of the world, water towers for humanity: Typology, mapping, and global significance. Water Resour. Res. 43.

Vögeli, C., Lehning, M., Wever, N., Bavay, M., 2016. Scaling precipitation input to spatially distributed hydrological models by measured snow distribution. Front. Earth Sci. 4, 108.

Vose, R.S., Easterling, D.R., Kunkel, K.E., LeGrande, A.N., Wehner, M.F., 2017. Temperature changes in the United States, in: Wuebbles, D.J., Fahey, D.W., Hibbard, K.A., Dokken, D.J., Stewart, B.C., Maycock, T.K. (Eds.), Climate Science Special Report: Fourth National Climate Assessment, Volume I. U.S. Global Change Research Program, Washington, DC, USA, pp. 185–206. https://doi.org/10.7930/J0N29V45

Walker, D.A., Halfpenny, J.C., Walker, M.D., Wessman, C.A., 1993. Long-term studies of snow-vegetation interactions. BioScience 43, 287–301.

Walker, M.D., Webber, P.J., Arnold, E.H., Ebert-May, D., 1994. Effects of interannual climate variation on aboveground phytomass in alpine vegetation. Ecology 75, 393.

Wayand, N.E., Clark, M.P., Lundquist, J.D., 2017. Diagnosing snow accumulation errors in a rain-snow transitional environment with snow board observations. Hydrol. Process. 31, 349–363. https://doi.org/10.1002/hyp.11002

Wayand, N.E., Stimberis, J., Zagrodnik, J.P., Mass, C.F., Lundquist, J.D., 2016. Improving simulations of precipitation phase and snowpack at a site subject to cold air intrusions: Snoqualmie Pass, WA. J. Geophys. Res. Atmospheres 121, 9929–9942.

Webb, R., Fassnacht, S.R., Gooseff, M., 2018a. Hydrologic flow path development varies by aspect during spring snowmelt in complex subalpine terrain. The Cryosphere 12, 287–300. https://doi.org/10.5194/tc-12-287-2018

Webb, R., Williams, M., Erickson, T.A., 2018b. The Spatial and Temporal Variability of Meltwater Flow Paths: Insights From a Grid of Over 100 Snow Lysimeters. Water Resour. Res. 54, 1146–1160. https://doi.org/10.1002/2017WR020866

Wen, L., Nagabhatla, N., Lü, S., Wang, S.-Y., 2013. Impact of rain snow threshold temperature on snow depth simulation in land surface and regional atmospheric models. Adv. Atmospheric Sci. 30, 1449–1460. https://doi.org/10.1007/s00376-012-2192-7

Wigmosta, M.S., Vail, L.W., Lettenmaier, D.P., 1994. A distributed hydrology-vegetation model for complex terrain. Water Resour. Res. 30, 1665–1679.

Williams, M., 2016. Snow cover profile data for Niwot Ridge, Green Lakes Valley from 1993/2/26 - ongoing, weekly to biweekly.

Williams, M.W., Bardsley, T., Rikkers, M., 1998. Overestimation of snow depth and inorganic nitrogen wetfall using NADP data, Niwot Ridge, Colorado. Atmos. Environ. 32, 3827–3833.

Williams, M.W., Cline, D., Hartman, M., Bardsley, T., 1999. Data for snowmelt model development, calibration, and verification at an alpine site, Colorado Front Range. Water Resour. Res. 35, 3205–3209.

Williams, M.W., Losleben, M., Caine, N., Greenland, D., 1996. Changes in climate and hydrochemical responses in a high-elevation catchment in the Rocky Mountains, USA. Limnol. Oceanogr. 41, 939–946.

Winchell, T.S., Barnard, D.M., Monson, R.K., Burns, S.P., Molotch, N.P., 2016. Earlier snowmelt reduces atmospheric carbon uptake in midlatitude subalpine forests. Geophys. Res. Lett. 43, 8160–8168.

Yang, D., Goodison, B.E., Metcalfe, J.R., Louie, P., Leavesley, G., Emerson, D., Hanson, C.L., Golubev, V.S., Elomaa, E., Gunther, T., others, 1999. Quantification of precipitation measurement discontinuity induced by wind shields on national gauges. Water Resour. Res. 35, 491–508.

Ye, H., Cohen, J., Rawlins, M., 2013. Discrimination of Solid from Liquid Precipitation over Northern Eurasia Using Surface Atmospheric Conditions*. J. Hydrometeorol. 14, 1345–1355.

Yuter, S.E., Kingsmill, D.E., Nance, L.B., Löffler-Mang, M., 2006. Observations of Precipitation Size and Fall Speed Characteristics within Coexisting Rain and Wet Snow. J. Appl. Meteorol. Climatol. 45, 1450–1464. https://doi.org/10.1175/JAM2406.1

Zhang, Z., Glaser, S., Bales, R., Conklin, M., Rice, R., Marks, D., 2017. Insights into mountain precipitation and snowpack from a basin-scale wireless-sensor network. Water Resour. Res. 53, 6626–6641. https://doi.org/10.1002/2016WR018825